Improving preoperative imaging for the localisation of parathyroid adenomas

MSc Thesis Technical Medicine

Robin Johannes Antonius Duteweert

November 2024

Prof. dr. I. Sechopoulos
Dr. F. Intema
Drs. J.P. Krol
Dr. M.L.E. Bernsen
Drs. L. Deden
Drs. R.J. Lambers
Dr. M.L. Groot Koerkamp

UNIVERSITY OF TWENTE.

Rijnstate

Abstract

Introduction

Primary hyperparathyroidism (PHPT) is the enlargement of one or more parathyroid glands, also known as parathyroid adenomas (PAs), resulting in the overproduction of the parathyroid hormone. The only curative treatment for PHPT is minimally invasive surgical excision of the PAs, so knowing the exact location and number of PAs is essential. Currently, the Rijnstate Hospital does not have an unambiguous imaging protocol for patients with a suspected PA. The goal of this research was to develop the optimal localisation protocol for patients with a suspected PA in terms of the number of examinations, the lowest possible total radiation dose and the highest localisation accuracy.

Method

A multireader, multicase (MRMC) study involving thirteen radiologists determined whether the number of CT phases in the four-dimensional CT (4DCT) protocol can be reduced, resulting in a lower radiation exposure to the patient. In addition, a map was created to provide information on the level of contrast enhancement in the PA in a single image to help the radiologist locate the PAs. Finally, a pilot study compared the newly developed ^{18}F-Choline PET/4DCT protocol as a 'one-stop shop' with the 4DCT and ^{18}F-Choline PET/CT protocols in terms of image quality and radiation dose.

Results

The MRMC study demonstrated that it is possible to reduce the number of phases in the 4DCT protocol from four to three while maintaining localisation accuracy. For experienced 4DCT radiologists, the number of phases could be further reduced to a two-phase 4DCT protocol. The enhancement map was developed to increase the detectability of PAs, but despite a promising quantitative analysis and promising feedback from the radiologists, no increased detectability of PAs was observed during the MRMC study to date. Finally, the ^{18}F-Choline PET/4DCT protocol has proven to be a promising 'one-stop shop' alternative to the currently used imaging protocols in terms of image quality and radiation dose.

Conclusion

The patient benefits from the proposed 4DCT protocols, since the radiation dose can be reduced compared to the currently used four-phase 4DCT protocol. The ^{18}F-Choline PET/4DCT protocol may further improve patient comfort, since less hospital visits are required to localise the PA. In the future, when the radiation dose of the ^{18}F-Choline PET/4DCT protocol has been optimised, an MRMC study should determine the performance of PA localisation with the ^{18}F-Choline PET/4DCT protocol, compared to the other imaging protocols.

Table of contents

List of Abbreviations

Abbreviation	Definition
4DCT	Four-dimensional Computed Tomography
4DMRI	Four-dimensional Magnetic Resonance Imaging
AUC	Area Under the Curve
BMI	Body Mass Index
BNE	Bilateral neck exploration
CI	Confidence interval
CNR	Contrast-to-Noise Ratio
$CTDI_{vol}$	Computed Tomography Dose Index Volume
DECT	Dual-energy Computed Tomography
DLP	Dose Length Product
HU	Hounsfield units
ICRP	International Commission on Radiological Protection
IMR	Iterative Model Reconstruction
IQR	Interquartile range
MIPS	Minimally invasive parathyroid surgery
MRMC	Multireader, multicase
PA	Parathyroid adenoma
PHPT	Primary hyperparathyroidism
PTH	Parathyroid hormone
ROC	Receiver Operating Characteristic
ROI	Region of interest
SAFIRE	Sinogram-Affirmed Iterative Reconstruction
SNR	Signal-to-Noise Ratio
Tc-MIBI	^{99m}Tc-Sestamibi SPECT
US	Ultrasonography
VNC	Virtual non-contrast

1 General Introduction

Primary hyperparathyroidism (PHPT) is a disorder of the parathyroid glands characterised by excessive secretion of the parathyroid hormone (PTH) and hypercalcaemia [1]. PHPT is the third most common endocrine disorder after diabetes mellitus and thyroid diseases [2]. PHPT is caused by a single enlarged adenoma in 85-90% of the cases, or by multiple adenomas in the remaining 10-15% [3]. Parathyroid carcinoma is the cause of PHPT in less than 1% of the cases. The risk of PHPT increases with age, with the peak age group between 50 and 60, and is about four times higher in women (1 in 500) than in men (1 in 2000) [4]. Patients with PHPT usually present with non-specific symptoms, like renal colic, bone pain, weakness and psychiatric problems. Laboratory blood tests show elevated levels of PTH and calcium [1]. Over time, PHPT is associated with an increased risk of cardiovascular disease, cerebrovascular disease, renal disease, osteoporosis and all-cause mortality [5].

Intervention is recommended for people with clear symptoms or complications. The only curative treatment for PHPT is surgical excision of the abnormal parathyroid gland [6]. This can be performed by a bilateral neck exploration (BNE) or by minimally invasive parathyroid surgery (MIPS) [5]. In both procedures, PTH levels are monitored intraoperatively at 0, 5, and 10 minutes after tissue resection to confirm complete removal of hyperfunctioning parathyroid tissue [7]. Nowadays, MIPS is the preferred method because of shorter operating times, shorter hospital stays, lower costs, and smaller incisions, while still achieving the same high cure rate of >95% as with BNE. However, the same high cure rate can only be achieved with accurate and precise preoperative imaging of the parathyroid adenoma (PA). This implies that the radiologist must provide the surgeon with essential information about the exact location and the number of PAs [6].

Localising the parathyroid glands is not straightforward, because of their small size and variable location (Figure 1). Most commonly, there are four parathyroid glands: two superior and two inferior [7]. The embryological origin of the parathyroid glands guides the search for both orthotopic and ectopic parathyroid tissue. The superior parathyroid glands derive from the fourth parapharyngeal pouch and have a relatively fixed position in the neck due to their limited embryological migration. They are most commonly found dorsal to the superior pole of the thyroid gland. The inferior parathyroid glands derive from the third parapharyngeal pouch and are more variable in location

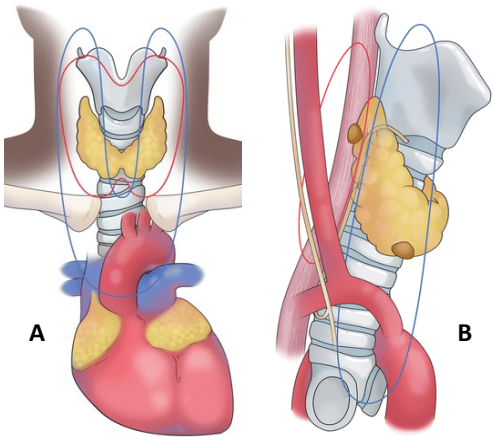

Figure 1: Potential anatomic sites of superior (red outline) and inferior (blue outline) parathyroid glands on frontal (A) and lateral (B) views.

due to their relatively long migration, ranging from the angle of the mandible to the pericardium [5]. Nevertheless, the inferior parathyroid glands are most commonly found close to the inferior pole of the thyroid gland. Overall, approximately 16% of both superior and inferior parathyroid glands are ectopic, with the most common locations being mediastinal, intrathyroidal, intra-thymic or in the tracheoesophageal groove [8], [9].

Traditional modalities for parathyroid imaging in the first stage of localisation are cervical ultrasonography (US) and ^{99m}Tc-Sestamibi SPECT (Tc-MIBI) [10]. Cervical US is an accessible, inexpensive imaging technique that can be used to visualise PAs without the use of ionising radiation. PAs are described on cervical US as an elongated or ovoid, hypoechoic structure with an echogenic capsule and a large amount of vascularisation [11]. Normal parathyroid glands are much more difficult to identify. In some cases, the parathyroid gland has a recognisable feeding vessel that makes it easier to locate, known as the polar vessel sign [12]. However, lymph nodes also have a feeding vessel, which sometimes makes it difficult to distinguish the PA from lymph nodes on cervical US. Therefore, cervical US is rarely the only preoperative imaging examination performed and should not be relied upon in isolation as the usual standard of care [11]. As a result, cervical US is often combined with Tc-MIBI to increase the sensitivity of PA localisation to approximately 65-97% [13], [14]. Tc-MIBI is a functional, non-invasive imaging technique to visualise the parathyroid glands. The uptake of Tc-MIBI per gram of PA is usually greater than the uptake per gram of thyroid tissue [15]. In addition, Tc-MIBI usually washes out faster from the thyroid compared to the PA. Therefore, a dual-phase protocol is often used to locate the PA. To further increase sensitivity, dual-phase, dual-isotope subtraction scintigraphy can be used, combining ^{99m}Tc-Sestamibi with ^{123}I, which is only taken up by thyroid tissue [16]. However, if the combination of cervical US and Tc-MIBI has a negative or contrary result, further imaging is required [17]. In addition, in challenging clinical situations, such as multiple adenomas or ectopic adenomas, the combination of cervical US and Tc-MIBI is less sufficient.

Four-dimensional computed tomography (4DCT) or ^{18}F-Choline PET/CT are commonly used in the second stage of localisation in cases where the primary imaging techniques appear to be inadequate [18], [19]. Whether 4DCT or ^{18}F-Choline PET/CT is used depends on local experience and availability. ^{18}F-Choline PET/CT has gained interest in recent years due to its high spatial resolution, short scan time compared to Tc-MIBI, and relatively low radiation dose to the patient [11]. An example of a ^{18}F-Choline PET/CT image with a PA is shown in Figure 2. The uptake of ^{18}F-Choline is increased by the upregulation of choline kinase and is related to the secretion of PTH in PAs [20]. The sensitivity of ^{18}F-Choline PET/CT is the highest of all parathyroid imaging techniques ranging from 85-97% [19], [21], [22]. This may raise the question why ^{18}F-Choline PET/CT is not used in the first stage of parathyroid localisation. The main

reasons are the high cost and limited availability of ^{18}F-Choline PET/CT [23]. The other second stage localisation technique, 4DCT, uses both morphological and enhancement patterns to differentiate the PA from lymph nodes, normal thyroid tissue and thyroid nodules [10], [12], [24]. The fourth dimension derives information from imaging in two or more contrast-enhanced phases over time [10]. The reported sensitivity of 4DCT varies from 75 to 97% [5], [24], [25]. This relatively wide range may be caused by large differences in expertise of radiologists with 4DCT, as well as large variability in 4DCT protocols used. However, it still outperforms the combination of cervical US and Tc-MIBI [25], [26]. The main disadvantage of 4DCT is the high radiation dose to the thyroid, which is about 50 times higher with 4DCT compared to Tc-MIBI [23], [27]. Therefore, it is important to investigate the possibility of reducing the radiation dose to the patient.

Figure 2: ^{18}F-Choline PET/CT image of a patient with a parathyroid adenoma, which is denoted by a red arrow [28].

The radiation dose of 4DCT can be reduced by limiting the number of contrast phases. It has been introduced as a four-phase protocol with a non-contrast phase, an arterial phase, a venous phase and a delayed (venous) phase [26]. This is based on the enhancement pattern of a PA. In the non-contrast phase, the PA has a low attenuation compared to the thyroid, due to the intrinsic iodine content of the thyroid (Figure 3A) [29]. In the second phase, rapid wash-in of the iodinated contrast agent is seen in the PA and the thyroid (Figure 3B). In the third phase, a rapid wash-out of the contrast agent is observed in the PA compared to the thyroid (Figure 3C). In the fourth phase, further washout is seen (Figure 3D). The enhancement patterns varied somewhat between individuals, as Bahl et al. demonstrated three different attenuation patterns of the PA relative to the thyroid [24]. The PA showed either higher attenuation than thyroid tissue on the arterial phase (type A), no higher attenuation on the arterial phase but lower attenuation on the venous phase (type B), or neither higher attenuation on the arterial phase nor lower attenuation on the venous phase (type C). This heterogeneity in the attenuation pattern sometimes makes it difficult to localise PAs on 4DCT images. It is currently unknown if, and which, contrast phases of the 4DCT protocol can be reduced without loss of sensitivity.

Previously, multiple studies have attempted to optimise the number of phases in the 4DCT protocol. Nevertheless, there is no clear consensus in the literature as to which phases are necessary to detect the PA [30], [31]. A large meta-analysis from 2017 by Kluijfhout et al. concluded that a non-contrast phase together with two post-contrast phases is optimal [25]. However, in many studies, 4DCT images were read by a small number of neuroradiologists, with a high level of 4DCT experience. In many hospitals, there is little to no experience with 4DCT, which may result in a different number of phases needed to localise the PA. Ultimately, the main goal is to find the right compromise between radiation exposure and sensitivity for PA localisation.

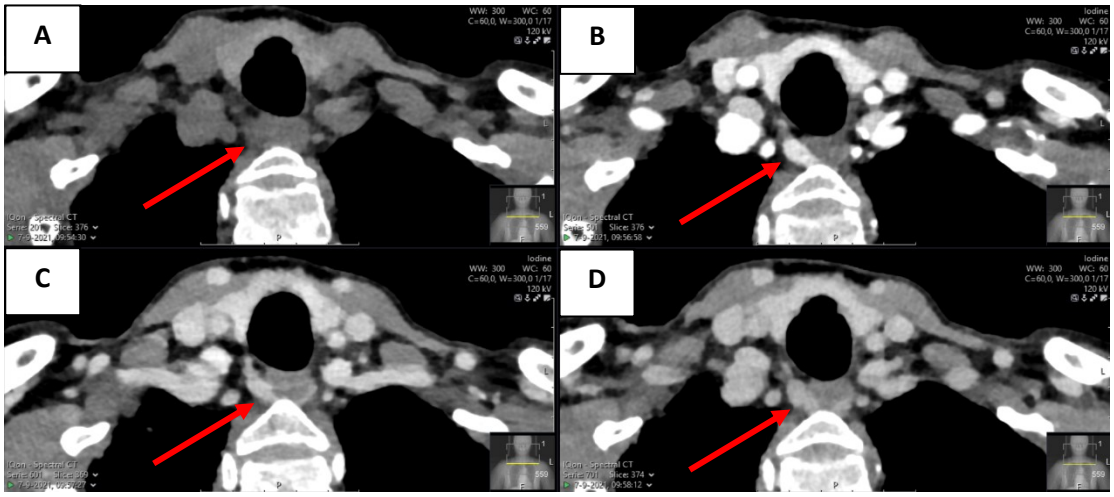

Figure 3: Classic parathyroid adenoma (PA) appearance at 4DCT, denoted by a red arrow. A: Non-contrast phase with hypoattenuation of the PA relative to the thyroid. B: Arterial phase with hyperattenuation of the PA and the thyroid. C: Venous phase with hypoattenuation of the PA relative to the thyroid due to rapid wash-out of the contrast agent. D: Delayed (venous) phase with further washout of the contrast agent.

2 Goal of this research

Currently, the Rijnstate Hospital does not have an unambiguous protocol for patients with a suspected PA. The first-stage imaging techniques, cervical US and Tc-MIBI, and the second-stage imaging techniques, 4DCT and ^{18}F-Choline PET/CT, are performed in various orders, depending on the requesting endocrinologist. The goal of this research is to develop the optimal localisation protocol for patients with a suspected PA in terms of the number of examinations, the lowest possible total radiation dose and the highest localisation accuracy. Firstly, a map to assist the radiologist in locating PAs was investigated. Secondly, a multireader, multicase (MRMC) study with a large number of readers with different levels of 4DCT experience, will provide insight into a possible reduction in the number of 4DCT phases. Currently, the Rijnstate Hospital uses a four-phase protocol. The goal of the MRMC study is to reduce the radiation exposure to the patient by reducing the number of phases and to achieve PA localisation that is not inferior to the current protocol. Thirdly, the use of 4DCT and ^{18}F-Choline PET/CT integrated into a single ^{18}F-Choline PET/4DCT examination in patients with PHPT will be investigated, to see if this 'one-stop shop' could be a promising alternative to the current imaging techniques.

3 The enhancement map

3.1 Introduction

In addition to the existing non-contrast, arterial, venous and delayed (venous) phases, the Rijnstate Hospital recently created a subtraction map to show arterial enhancement as a colour scale (Figure 4) [17]. The subtraction map was created by subtracting the non-contrast phase from the arterial phase. The aim of the subtraction map is to assist the radiologist in finding the parathyroid adenomas (PAs), since it should be easier to differentiate between the PA and thyroid tissue. An important advantage of the subtraction map is that it provides information about the level of enhancement in a single image without the need for increased radiation dose. However, as shown by Bahl et al, there are three different attenuation patterns of the PA relative to the thyroid [24]. The subtraction map is only useful when the attenuation of the PA is higher than thyroid tissue on the arterial phase (type A adenomas as described by Bahl et al. [24]). For adenomas with other attenuation patterns, it is very difficult to distinguish between the PA and thyroid tissue on the subtraction map. The arterial enhancement of these adenomas is not large enough, resulting in a subtraction value of the PA that is equal to or less than the subtraction value of the thyroid. Unfortunately, the prevalence of type A adenomas is the lowest at only 20%, compared to 57% for type B adenomas and 22% for type C adenomas. The subtraction map would therefore only be useful in a few patients with a PA. In addition, the usefulness of the subtraction map is limited by several artefacts and by misalignment between the non-contrast and arterial phase images, often due to patient movement and breathing, which may result in small PAs being missed. Therefore, we aimed to develop a more robust colour scale to better visualise the enhancement differences between the PA and the thyroid.

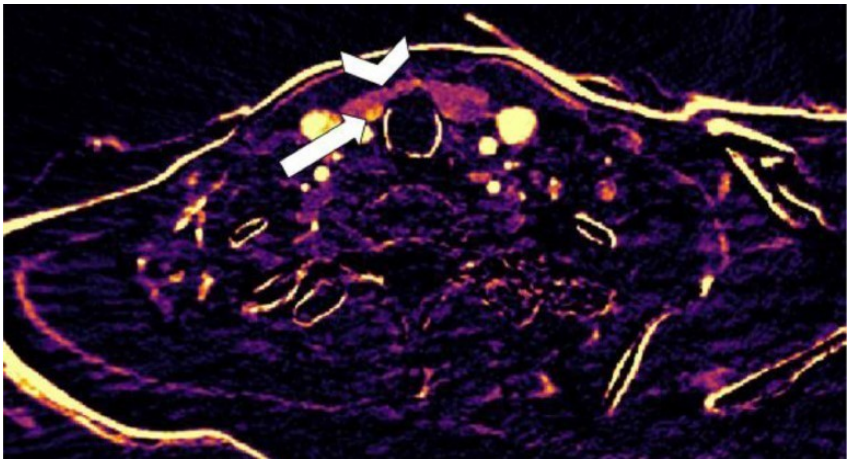

Figure 4: Subtraction map that shows a lesion with high arterial contrast enhancement compared to the thyroid gland (arrowhead). The arrow points to the lesion with increased arterial enhancement just dorsal to the right thyroid gland lobe. This turned out to be the parathyroid adenoma after surgery. The inferno colour map was used for the subtraction map. [17]

3.2 Materials and Methods

3.2.1 Creating the enhancement map

An alternative to the subtraction map was sought and found in the form of the enhancement map. The enhancement map is the relative percentual increase in arterial enhancement from the non-contrast phase calculated for each voxel. The enhancement map takes advantage of the fact that the attenuation of the PA in the non-contrast phase is usually less than the attenuation of thyroid tissue. As a result, the enhancement difference between the PA and thyroid tissue is increased on the enhancement map, potentially adding value to the localisation of the PA.

In order to make the enhancement map useful in a clinical setting, a number of optimisation steps had to be performed (Figure 5). The first step was to register the non-contrast phase image to the arterial phase image to align the two images. This is necessary because breathing and movement of the patient can cause misregistration between the non-contrast and arterial phase images, which could result in small PAs being missed. Therefore, the open-source tool Elastix was used to align the two images and the parameter set was selected based on the modality (3D CT monomodal) and content (head and neck) [32]. This resulted in a rigid transformation with an advanced mean square metric, followed by a B-spline transformation with a normalised cross-correlation metric. The second step was then performed by calculating the relative percentual increase for each voxel (Eq. 1).

$$Relative\ percentual\ increase = \frac{Arterial\ phase - Non\ contrast\ phase}{Non\ contrast\ phase} \times 100\% \quad (Eq. 1)$$

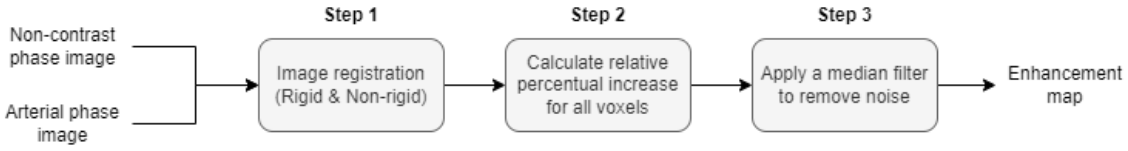

Figure 5: Workflow of how the enhancement map was created out of non-contrast and arterial phase images.

The third and final step was to apply a three-dimensional median filter (3 x 3 x 3) to remove noise from the enhancement map. This noise can be described as salt and pepper noise, since it appears as sparsely occurring white and black pixels [33]. Removal of salt and pepper noise is necessary because it makes it difficult for radiologists to evaluate the enhancement map. The noise occurs because the non-contrast and arterial phase images are not fully aligned. A slight mismatch between the pixels of two images can result in extreme pixel values on the enhancement map. This occurs when one of the corresponding pixels in the non-contrast or arterial phase image has a very high or low pixel value.

Extreme pixel values on the enhancement map can also be observed when the pixel value in the non-contrast phase image is close to zero.

3.2.2 Comparison of the subtraction map and the enhancement map

To compare the contrast between the PA and the thyroid on the subtraction map with the contrast on the enhancement map, non-contrast and arterial phase images were retrospectively selected from May 2020 to March 2023 to create a dataset consisting of twenty-seven patients with primary hyperparathyroidism (PHPT). All patients were scanned on the IQon dual-energy CT scanner (Philips Healthcare, Best, The Netherlands) with a slice thickness of 0.9 mm, a tube voltage of 120 kVp and a tube current-exposure time product value between 27 and 88 mAs. The non-contrast phase was followed by the injection of 90-120 mL of iodinated intravenous contrast agent (Xenetix 300, Guerbet, Villepinte, France) at a flow rate of 3.5-5.0 mL/sec. Bolus tracking in the proximal part of the descending aorta is used to monitor when a threshold of 150 Hounsfield units (HU) is reached. The arterial phase was acquired 10 seconds after the threshold was reached.

In the Sectra PACS environment (Sectra AB, Linköping, Sweden), regions of interest (ROIs) with a diameter of 5 mm were delineated in the thyroid gland and the PA on the non-contrast and arterial phase images. The ROIs were reviewed and validated by J.K., a radiology resident with five years of experience. The mean HU value was noted for each ROI.

For the subtraction map, thyroid and PA enhancement were calculated by subtracting the mean HU value on the non-contrast phase from the mean HU value on the arterial phase. A difference of more than +15 HU between PA enhancement and thyroid enhancement was considered sufficient to distinguish between the two structures on the subtraction map. For the enhancement map, the relative percentual increase from the non-contrast phase to the arterial phase was calculated for the thyroid and the PA. A difference in the relative percentual increase between the PA and thyroid tissue of more than 30 was considered sufficient to distinguish between the two structures on the enhancement map.

3.3 Results

3.3.1 Creating the enhancement map

Figure 6 shows the result of aligning the non-contrast and arterial phase images. While the PA is not visible in the unaligned image, it becomes visible in the aligned image. Figure 7 shows the result of applying a median image filter to remove noise from the enhancement map. The result is a final enhancement map that is less noisy and easier for the radiologist to evaluate.

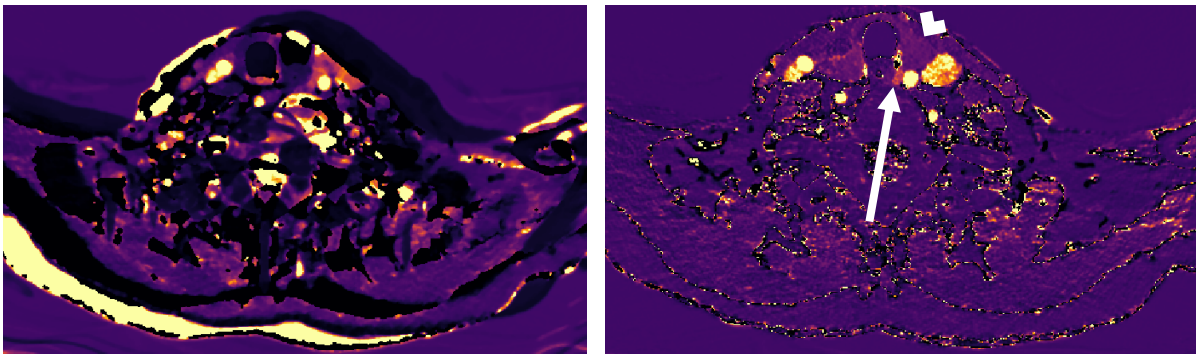

Figure 6: Left: The enhancement map of one patient where the non-contrast and arterial phase images were not aligned. Right: The enhancement map of the same patient with alignment of the non-contrast and arterial phase images. The arrowhead is pointing to the thyroid gland and the arrow points to the parathyroid adenoma dorsal to the left thyroid gland lobe.

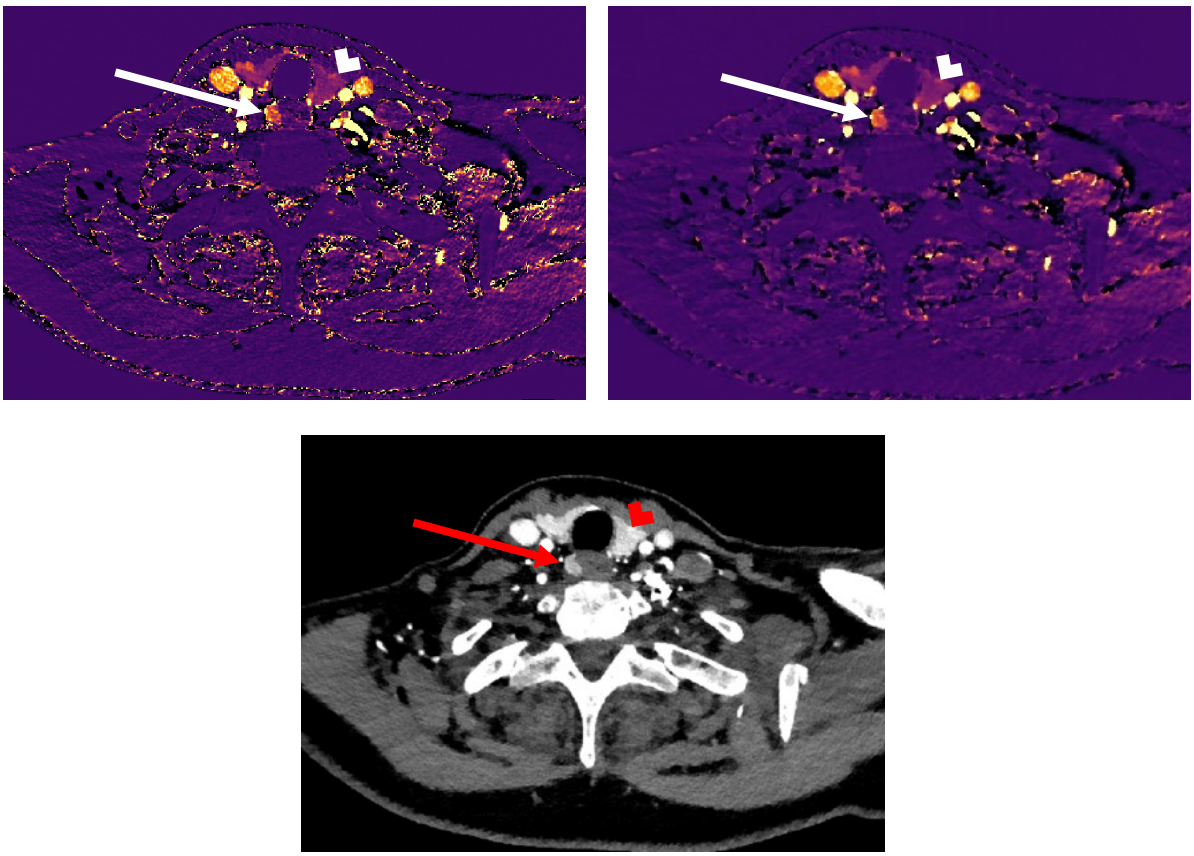

Figure 7: Left: The enhancement map of one patient where noise is present that complicates the ability to evaluate the image. Right: Final result of the enhancement map. Bottom: Arterial phase image of this patient for anatomical reference. The arrowhead is pointing to the thyroid and the arrow points to the parathyroid adenoma dorsal to the right thyroid gland lobe.

3.3.2 Comparison of the subtraction map and the enhancement map

The median contrast on the subtraction map between the PA enhancement and thyroid enhancement was 0 HU (IQR: -50, 19). In only 30% of the patients the contrast was greater than +15 HU. The enhancement map showed a median difference of 114 (IQR: 35, 182) in the relative percentual increase

between the PA and thyroid tissue. In 78% of the patients the difference in the relative percentual increase was greater than 30. An example of a patient where the enhancement map would be preferred to the subtraction map is shown in Figure 8. The contrast between the PA and the thyroid for this patient is clearly greater on the enhancement map than on the subtraction map. The contrast on the subtraction map and the contrast on the enhancement map for each patient are shown in Appendix A.

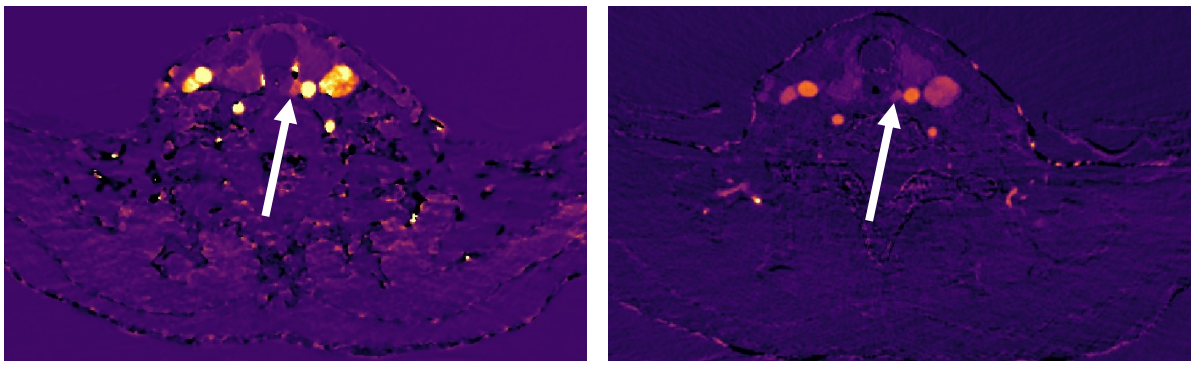

Figure 8: Comparison of the enhancement map (left) with the subtraction map (right) of one patient. For both maps, the non-contrast phase and the arterial phase were aligned. The arrow points to the parathyroid adenoma dorsal to the left thyroid gland lobe.

Figure 9 shows the mean HU values for both the PA and thyroid tissue for each included patient and the median HU value over all included patients. The difference between the median HU value of the PA and the thyroid over all included patients on the subtraction map was very small at only 2 HU (Figure 9A). The difference between the median HU value of the PA and the thyroid over all included patients on the enhancement map was significantly higher at 101 (Figure 9B).

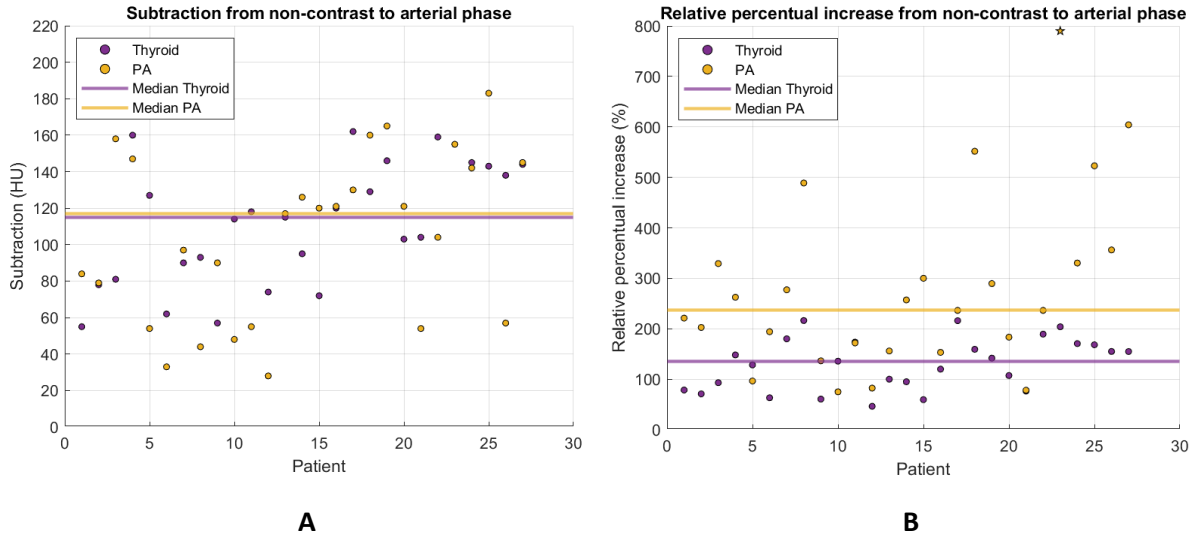

Figure 9: Mean HU values for both the PA and thyroid tissue and the median HU value over all included patients. The median values over all twenty-seven patients for both structures are shown with horizontal lines. (A) Subtraction of the non-contrast phase from the arterial phase for thyroid and PA. (B) Relative percentual increase from the non-contrast phase to the arterial phase for thyroid and PA. The yellow star in patient 23 has a value of 1550 and has been marked as an outlier for visualisation purposes.

3.4 Discussion

The ability to detect the PA based on the contrast with the thyroid gland increased from 30% on the subtraction map to 78% on the enhancement map. In the remaining 22% of the patients with insufficient contrast between the PA and thyroid tissue, weak enhancement in the PA or a relatively high attenuation in the non-contrast phase, or both, was observed. These adenomas will always be difficult to locate on four-dimensional CT (4DCT) scans.

Despite the ability to detect the PA based on the contrast with the thyroid gland in 78% of the patients, there are several reasons why the PA may still be difficult to locate. The main reason for this is artefacts present in the non-contrast and arterial phase images and therefore also on the enhancement map. The beam hardening artefact present in these images causes dark bands to appear behind structures with a high attenuation coefficient [34]. Only higher energy photons are left to contribute to the beam, increasing the mean beam energy. The clavicle is one of the structures that causes the beam hardening artefact to appear on the non-contrast and arterial phase images. The contrast agent administered to the patient also causes the beam hardening artefact to appear on the arterial phase images. If the PA is within the dark bands of the artefact, it may be difficult to locate the PA on the arterial phase image and also on the enhancement map (Figure 10).

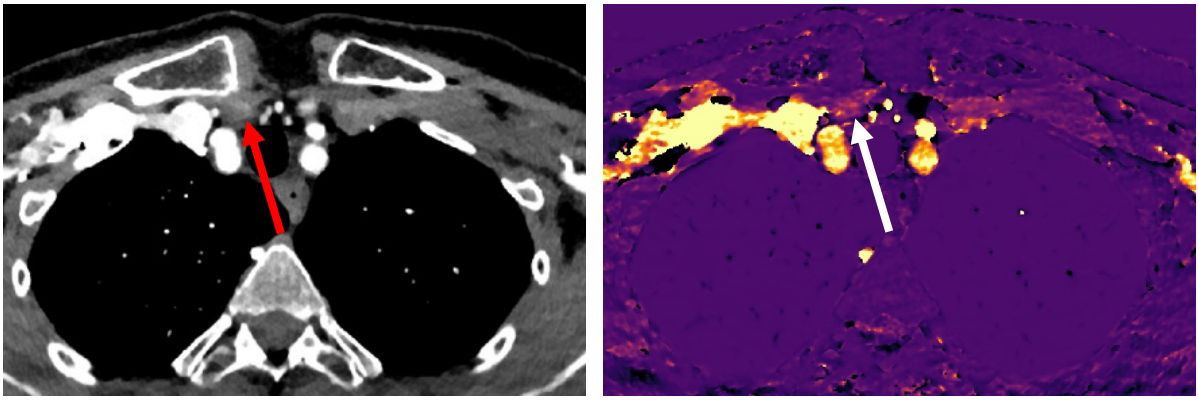

Figure 10: Example of a patient where it is difficult to locate the PA on both the arterial phase image (left) and the enhancement map (right) due to the beam hardening artefact. The arrow points to the parathyroid adenoma near the sternohyoid muscle.

The beam hardening artefact can be reduced by increasing the mean beam energy [35]. However, the disadvantage of increasing the mean beam energy is that the photons will penetrate through the PA more easily. Another way to reduce the beam hardening artefact is to reduce the amount of contrast agent administered to the patient [36]. This would not only improve image quality, but would also result in less possibility of damage to the patient's kidneys. Following evaluation of the current contrast administration protocol for 4DCT parathyroid adenoma scans, the contrast administration protocol was modified (Table 1). Visually, the first five patients scanned with the new contrast protocol showed no

major differences in contrast between the PA and thyroid tissue, according to J.K., a radiology resident with five years of experience.

Table 1: Modifications to the contrast administration protocol for 4DCT parathyroid adenoma scans.

Weight (kg)	Volume IV contrast / NaCl (mL)		Flow (mL/s)
	Old contrast protocol	New contrast protocol	
<60	90 / 30	50 / 30	3.5
60 - 80	100 / 30	60 / 30	4
80 - 100	110 / 30	70 / 30	4.5
100+	120 / 30	75 / 30	5

Besides beam hardening artefacts, heterogeneous arterial enhancement of thyroid tissue may complicate PA localisation and could be misinterpreted as a PA (Figure 11). Therefore, it is recommended to always interpret the enhancement map together with the non-contrast and arterial phase images. The multireader, multicase (MRMC) study investigating the potential reduction in the number of 4DCT phases also examined the enhancement map in its current state to calculate several performance metrics of PA localisation using the enhancement map.

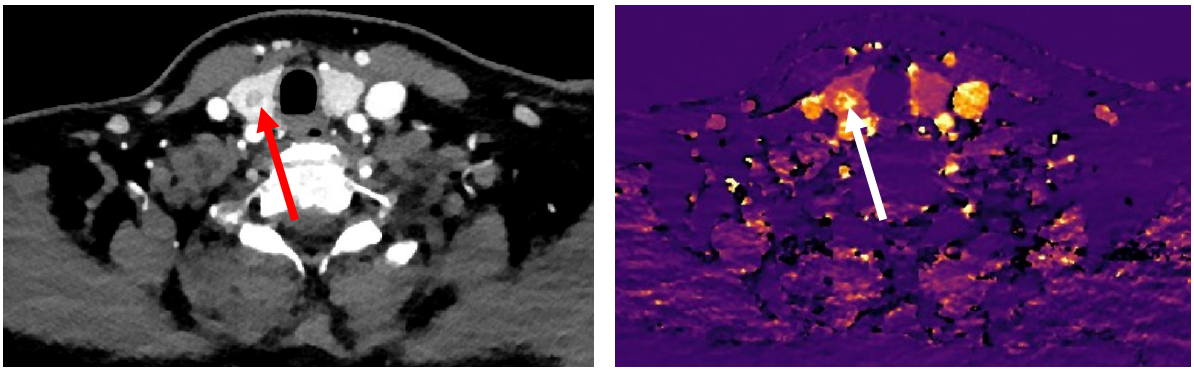

Figure 11: Example of a patient where heterogeneous arterial enhancement could be misinterpreted as a PA. The arrow points to a thyroid nodule, which shows hypoattenuation on the arterial phase image (left) and is visible as a bright spot on the enhancement map (right).

3.5 Conclusion

In conclusion, an alternative to the subtraction map was found in the form of the enhancement map. The ability to detect the PA on the enhancement map was significantly higher than on the subtraction map. However, beam hardening artefacts and heterogeneous arterial enhancement of thyroid tissue may still complicate PA localisation on the enhancement map. The multireader, multicase study will provide insight into the performance of PA localisation using the enhancement map.

4 Reducing the number of four-dimensional CT phases

4.1 Introduction

In many hospitals, four-dimensional CT (4DCT) is currently used as a secondary imaging technique to localise a parathyroid adenoma (PA). However, some hospitals have successfully used 4DCT as a primary imaging technique in patients with a suspected PA [37], [38]. The main reason for this success is the high sensitivity of 4DCT as a first-line imaging modality, which can be attributed to a higher spatial resolution compared to cervical ultrasonography (US) and ^{99m}Tc-Sestamibi SPECT (Tc-MIBI).

At the Rijnstate Hospital, cervical US and Tc-MIBI were almost always followed by four-phase 4DCT and/or ^{18}F-Choline PET/CT imaging to confirm the findings of cervical US and/or Tc-MIBI with greater certainty. Performing only 4DCT as first-line imaging would likely be more time and cost efficient [39]. In addition, it would likely be more beneficial for the patient, since fewer hospital visits would be required to confirm the location of any PA. However, the main disadvantage of 4DCT is the relatively high radiation dose, which limits its use as the primary imaging modality in every hospital [27]. Therefore, it is important to investigate a potential reduction in radiation exposure.

Multiple studies have attempted to reduce the radiation exposure by reducing the number of phases in the 4DCT protocol. Raghavan et al. concluded that adequate diagnostic accuracy for PA localisation could be achieved with only the arterial phase provided to the radiologist [30]. However, this is one of many studies using a small number of readers with a high level of experience in interpreting 4DCT scans [25].

This study aims to compare several combinations of 4DCT phases and the previously described enhancement map with a large number of readers with different levels of experience with 4DCT. This multireader, multicase (MRMC) study will determine whether the number of phases can be reduced, resulting in less radiation exposure to the patient. It will also determine whether experience with 4DCT has an impact on the required number of phases and whether the enhancement map can assist the radiologist in locating the PA.

4.2 Materials and Methods

4.2.1 Data acquisition and characteristics of the dataset

4DCT data were retrospectively selected from May 2020 to March 2023, resulting in a dataset of thirty patients, constructed to reflect clinical practice in terms of the number and location of PAs (Table 2). In twenty-seven patients with primary hyperparathyroidism (PHPT), the 4DCT scan showed evidence of a PA together with a confirmatory PET scan and histopathological confirmation of a PA after surgery. In

three patients, the 4DCT scan showed no clear evidence of a PA, and another cause for their elevated parathyroid hormone (PTH) levels was later found (gastric bypass, medication, renal failure). The characteristics of each patient are given in Appendix B.

Table 2: Characteristics of the dataset.

Patient characteristics (n = 30)	
Age (years), mean (SD)	61 (11)
Female, n (%)	25 (83.3)
Weight (kg), mean (SD)	72.5 (17.5)
Size of adenoma (mm), mean (SD)	12.6 (8.8)
Number of adenomas	
Single adenoma, n (%)	24 (80)
Double adenoma, n (%)	3 (10)
No adenoma, n (%)	3 (10)
Location of adenomas	
Upper left, n (%)	3 (11.1)
Bottom left, n (%)	10 (37.0)
Upper right, n (%)	1 (3.7)
Bottom right, n (%)	7 (25.9)
Ectopic, n (%)	3 (11.1)
Bottom left & bottom right, n (%)	2 (7.4)
Upper left & bottom right, n (%)	1 (3.7)
PTH blood level (pmol/L)	
PTH pre-operative, mean (SD)	25.5 (19.7)
PTH post-operative, mean (SD)	5.0 (5.3)

All patients were scanned on the IQon dual-energy CT scanner (Philips Healthcare, Best, The Netherlands) with a slice thickness of 0.9 mm, a tube voltage of 120 kVp and a tube current-exposure time product value between 27 and 88 mAs. The 4DCT protocol at the Rijnstate Hospital consists of a non-contrast phase followed by the injection of 90-120 mL of iodinated intravenous contrast agent (Xenetix 300, Guerbet, Villepinte, France) at a flow rate of 3.5-5.0 mL/sec (Table 3). Bolus tracking in the proximal part of the descending aorta is used to monitor when a threshold of 150 Hounsfield units (HU) is reached. The arterial, venous and delayed venous phases were acquired at 10, 40 and 85 seconds post-threshold delay, respectively.

Table 3: Contrast protocol used for all enrolled patients who underwent a 4DCT scan.

Weight (kg)	Volume IV contrast / NaCl (mL)	Flow (mL/s)
<60	90 / 30	3.5
60 - 80	100 / 30	4
80 - 100	110 / 30	4.5
100+	120 / 30	5

4.2.2 Structure of the MRMC study

Thirteen radiologists from the Rijnstate Hospital, with different levels of experience in interpreting 4DCT scans, evaluated the case set five times with different combinations of 4DCT phases in each round. In the first round, the radiologists received only the arterial phase image to locate the PA, after which they received more images and therefore more information in each round. The fifth round represents the currently used protocol with all four 4DCT phases. In each round, the anonymised cases appeared in a randomised order, with a washout period of at least four weeks between each round. The different combinations of phases in each round are shown in Figure 12. The 4DCT scans were evaluated by the radiologists in the Sectra PACS environment (Sectra AB, Linköping, Sweden) with preset layouts. In each round, the axial images were displayed on the left screen and the coronal images on the right screen. In the third round, the enhancement map was added to the non-contrast and arterial phase images. A PowerPoint with instructions and eighteen test cases in PACS was provided to the radiologists, since they had no experience in assessing the enhancement map.

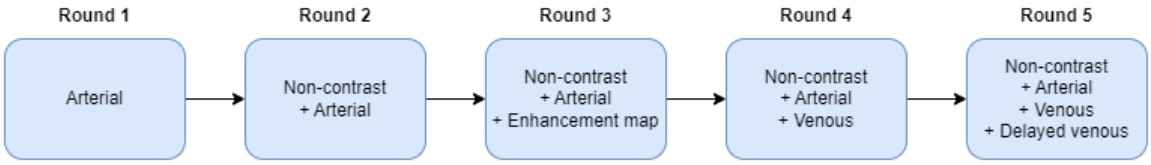

Figure 12: The different combinations of phases that were provided to the radiologists in each round. The wash-out period between each round is set at a minimum of four weeks.

For each patient, the radiologists were asked in a form to assess whether a PA was present and in which of the four thyroid quadrants (upper left, lower left, upper right, lower right) or ectopic they located the adenoma (Figure 13). This location in relation to the thyroid gland is usually written in the conclusion of the radiology report and is used by the surgeon to describe the location. The radiologists were also asked to mark the PA with an arrow in PACS, since this is usually also included in their radiology report. If the arrow did not match the location in relation to the thyroid, the principal investigators used the location of the arrow for the radiologist's answer, which was compared to the ground truth. The ground truth was determined by the location of the PA according to the surgical report and pathology report. In cases where the ground truth was on a boundary between two quadrants, the principal investigators attempted to reach a consensus on the

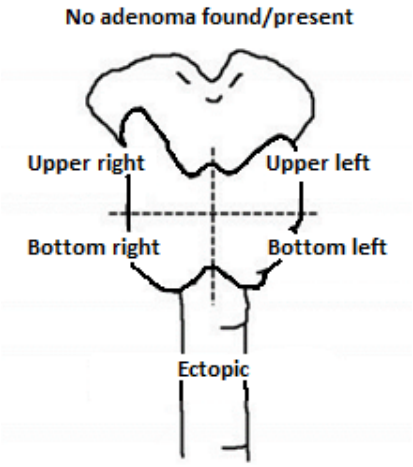

Figure 13: Locations that the radiologists were able to depict for the parathyroid adenoma.

location of the PA. Finally, for each case and each designated adenoma, the radiologists were asked for their level of confidence. The level of confidence was divided into four parts: 0-25%, 25-50%, 50-75% and 75-100% confidence.

4.2.3 Data analysis

Each patient case was divided into five cases, based on the possible locations of the PA relative to the thyroid, to increase the sample size. The result is thirty patients multiplied by five possible locations of the PA in relation to the thyroid, which equates to 150 cases assessed by the radiologist during each round. A true positive result is a case where the radiologist has correctly identified the PA, according to the ground truth. However, a true positive result is also given if the radiologist pointed to a lymph node in the same location in relation to the thyroid gland as the confirmed PA. This decision is based on the clinical implications. The surgeon will begin by making an incision at the location where the radiologist has placed the arrow in relation to the thyroid. The likelihood that the surgeon will still be able to identify the actual PA when inspecting this site, despite the radiologist pointing to a lymph node, is probably about the same as if the PA had been correctly identified earlier in the preoperative imaging. This is because the location of the PA on preoperative imaging is often slightly different from the actual intraoperative location of the PA. Also, in most cases, the surgeon is able to distinguish the PA from a lymph node. The principal investigators therefore felt that it was most important for the radiologist to place the arrow in the correct location in relation to the thyroid. In the end, the sensitivity, specificity and the area under the receiver operating characteristic (ROC) curve (AUC) were calculated for each reader with 95% confidence interval (CI) for all the investigated combinations of 4DCT phases. ROC curves were constructed to visualise the results.

The AUC was calculated because it represents a trade-off between sensitivity and specificity, and because the level of confidence can be incorporated into the analysis and linked to the radiologists' responses. The AUC was used to analyse whether the investigated combinations of phases were statistically significantly non-inferior to the current protocol (round 5). A non-inferiority design is chosen because the investigated combinations of phases do not necessarily have to perform better than the current protocol, but at least not worse. The non-inferiority margin (δ) was set at 0.05. Non-inferiority to the current protocol was concluded if the mean difference in AUC with the investigated combination of phases, and the lower bound of the 95% CI was greater than -0.05. If the null hypothesis was not rejected, the investigated combination of phases may be inferior to the current protocol.

$$H_0: \quad \theta_{Round\ X} - \theta_{Round\ 5} = -\delta$$

$$H_1: \quad \theta_{Round\ X} - \theta_{Round\ 5} > -\delta$$

To obtain the mean AUC across all radiologists, the publicly available iMRMC software was used for analysis [40]. As described by Chen et al, the p-value for a non-inferiority test is equal to:

$$p = 2\left(1 - F(t;\ df_0|H_0)\right) \qquad (Eq.2)$$

Where $F(t;\ df_0|H_0)$ is the cumulative distribution function of the test statistic t under the null hypothesis [41]. An investigated combination of 4DCT phases may have a higher AUC than the currently used protocol. In this case, a superiority test is performed to determine whether superiority over the current protocol can be inferred [41]. An investigated combination of 4DCT phases was considered superior if the p-value was less than 0.05.

In a subanalysis, the radiologists were divided into two groups, based on their level of experience with 4DCT. The radiologists were asked about their level of experience with 4DCT before the first round of the study was assessed. This resulted in one group with a high level of experience with 4DCT, mainly consisting of neuroradiologists. The other group of radiologists had little to no experience with 4DCT, and consisted mostly of radiologists from other specialties within the field of radiology. The mean sensitivity, specificity, and AUC were calculated for both groups. The non-inferiority test was performed to determine whether the level of experience with 4DCT affected the number of 4DCT phases required. The AUCs of both groups were then compared at each round, to determine if the groups were significantly different using Student's t-test. A significant difference between the two groups was considered if the p-value was less than 0.05. All statistical calculations were performed using statistical software (R version 4.0.3; R foundation for Statistical Computing).

In an additional analysis, the mean sensitivity and specificity were calculated using MATLAB R2023b (The Mathworks, Natick, MA, USA) based on each PA identified by the radiologist, rather than calculating the mean sensitivity and specificity based on the possible locations of the PA relative to the thyroid. This method, based on each PA identified by the radiologist, limits statistical power and is therefore not suitable for a non-inferiority analysis. However, comparing the mean sensitivity and specificity with the main and subanalysis may provide useful additional insight.

4.2.4 Radiologists' view on the enhancement map

In the third round, the enhancement map was introduced in the MRMC study. In addition to locating the PA in all cases, radiologists in this round were also asked to complete a form about the enhancement map (Figure 14). This form was created because the enhancement map was new to all radiologists and it was thought that the performance metrics of this round might differ from the opinion of the radiologists. Furthermore, the opinion of the radiologists can be used to further develop the enhancement map. The questions put to the radiologists are listed on the next page.

1. To what extent did you use the different phases in the third round to locate the PA?	Never	Rarely	Sometimes	Often	Always
a. Non-contrast	○	○	○	○	○
b. Arterial	○	○	○	○	○
c. Enhancement map	○	○	○	○	○

2. The enhancement map gives me … in localizing the PA.	More uncertainty									More certainty
	1	2	3	4	5	6	7	8	9	10

3. What is your opinion about the following aspects of the enhancement map?	Very bad	Bad	Neutral	Good	Very good
a. Image registration	○	○	○	○	○
b. Colour scale	○	○	○	○	○
c. Number of artefacts	○	○	○	○	○

4. How likely is it that you would use the enhancement map in its current state to localise the PA in daily practice?	Very unlikely									Very likely
	1	2	3	4	5	6	7	8	9	10

5. Which adjustments do you think are needed to the enhancement map in order to be able to use it in daily practice?

6. How likely is it that you would use the enhancement map after optimization to localise the PA in daily practice?	Very unlikely									Very likely
	1	2	3	4	5	6	7	8	9	10

7. How likely is it that you would recommend the enhancement map in its current state to other radiologists?	Very unlikely									Very likely
	1	2	3	4	5	6	7	8	9	10

Figure 14: The form about the enhancement map provided to the radiologists.

4.3 Results

4.3.1 Non-inferiority analysis over all radiologists

The AUC of each investigated combination of 4DCT phases was statistically non-inferior to the AUC of the current four-phase 4DCT protocol (round 5). The difference in AUC between the first four rounds and the fifth round with corresponding p-values are shown in Table 4. The highest AUC was obtained in round 4 with 0.84, which is 0.03 higher than the AUC of the four-phase 4DCT protocol. Nevertheless, superiority of the AUC of round 4 over the AUC of the four-phase 4DCT protocol could not be established ($p = 0.075$). The lowest AUC was observed in round 3 with 0.80, which is 0.01 less than the AUC of the four-phase 4DCT protocol. The average ROC curves over all radiologists in each round are shown in Figure 15A. The average ROC curves of all rounds are close together, which was expected since non-inferiority was concluded for each round. The ROC curves of individual radiologists are shown in Figure 16 and show that there is a relatively large variability between the radiologists in each round. Sensitivity, specificity and AUC in each round for each radiologist can be found in Appendix C.

4.3.2 Non-inferiority analysis for both groups of radiologists

In a subanalysis, the radiologists were divided into two groups, based on their level of experience with 4DCT assessment of PAs. For the experienced 4DCT radiologists, the AUC of the first, second and fourth rounds were statistically non-inferior to the AUC of the current four-phase 4DCT protocol. The difference in AUC between the first four rounds and the fifth round with corresponding p-values are shown in Table 4. The highest AUC for the experienced 4DCT group was obtained in round 4 with 0.86, which is 0.02 higher than the AUC of the four-phase 4DCT protocol. Nevertheless, superiority of the AUC of round 4 over the AUC of the four-phase 4DCT protocol could not be established ($p = 0.408$). The lowest AUC for this group was observed in round 3 with 0.82, which is 0.02 less than the AUC of the four-phase 4DCT protocol. The average ROC curves for the experienced 4DCT radiologists in each round are shown in Figure 15B.

For the less experienced 4DCT radiologists, only the AUC of the fourth round was statistically non-inferior to the AUC of the current four-phase 4DCT protocol. The difference in AUC between the first four rounds and the fifth round with corresponding p-values are shown in Table 4. The highest AUC for the experienced 4DCT group was obtained in round 4 with 0.82, which is 0.05 higher than the AUC of the four-phase 4DCT protocol. Nevertheless, superiority of the AUC of round 4 over the AUC of the four-phase 4DCT protocol could not be established ($p = 0.151$). The lowest AUC for this group was observed in rounds 3 and 5 with 0.77. The average ROC curves for the less experienced 4DCT radiologists in each round are shown together with the ROC curves for the experienced 4DCT radiologists in Figure 15B.

A comparison between the two groups of radiologists in each round showed that only the AUCs of the first round were statistically different between the two groups (p = 0.048). Figure 16A confirms this observation, since the average ROC curves for both groups are furthest apart in the first round. In addition, the average AUC of the experienced 4DCT group was higher than the average AUC of the less experienced 4DCT group in each round (Figure 16A-E). Furthermore, in each round, the radiologist with the lowest AUC is from the less experienced 4DCT group, and the radiologist with the highest AUC is from the experienced 4DCT group. All p-values and statistical outcomes of the comparison between the two groups of radiologists can be found in Appendix D. The ROC curves for each individual radiologist are shown in Appendix E.

Table 4: Mean sensitivity, specificity and AUC with 95% CIs shown in brackets. Non-inferiority test of each investigated combination of 4DCT phases (rounds 1-4) compared to the currently used four-phase 4DCT protocol (round 5). The non-inferiority tests are performed with all radiologists and also within the two groups.

	Round 1	Round 2	Round 3	Round 4	Round 5
	All radiologists together				
Sensitivity	0.68	0.64	0.64	0.70	0.64
Specificity	0.94	0.96	0.94	0.97	0.96
AUC	0.82 (0.76, 0.88)	0.81 (0.74, 0.87)	0.80 (0.73, 0.86)	0.84 (0.78, 0.90)	0.81 (0.75, 0.87)
ΔAUC with Round 5	0.01 (-0.03, 0.05)	0.00 (-0.04, 0.04)	-0.01 (-0.04, 0.02)	0.03 (0.00, 0.07)	
P value	0.006	0.011	0.010	<0.001	
	Experienced 4DCT group				
Sensitivity	0.73	0.69	0.68	0.73	0.69
Specificity	0.95	0.96	0.95	0.97	0.97
AUC	0.85 (0.79, 0.92)	0.83 (0.76, 0.90)	0.82 (0.75, 0.89)	0.86 (0.78, 0.93)	0.84 (0.77, 0.91)
ΔAUC with Round 5	0.01 (-0.05, 0.08)	-0.01 (-0.05, 0.04)	-0.02 (-0.06, 0.03)	0.02 (-0.03, 0.07)	
P value	0.046	0.038	0.086	0.014	
	Less experienced 4DCT group				
Sensitivity	0.62	0.58	0.60	0.66	0.58
Specificity	0.92	0.97	0.93	0.97	0.96
AUC	0.78 (0.71, 0.85)	0.78 (0.70, 0.85)	0.77 (0.70, 0.85)	0.82 (0.75, 0.89)	0.77 (0.70, 0.84)
ΔAUC with Round 5	0.01 (-0.06, 0.08)	0.01 (-0.07, 0.09)	0.00 (-0.05, 0.06)	0.05 (-0.02, 0.12)	
P value	0.076	0.128	0.061	0.017	

4.3.3 Sensitivity and specificity analysis per identified adenoma

The observed mean sensitivity and specificity for the analysis per adenoma identified by the radiologist (Table 5) were consistently lower than the mean sensitivity and specificity for the analysis based on the possible locations of the PA relative to the thyroid (Table 4). The greatest decrease in mean sensitivity between the two analyses was observed in the less experienced 4DCT group. The large decrease in specificity for both groups can be explained by the small number of negative cases (n = 3) for this analysis, compared to 120 negative cases for the analysis based on the possible locations of the PA relative to the thyroid. The lowest mean specificity was observed in the first and third rounds, with values below 0.25. The lowest mean sensitivity and specificity for both analyses was observed in the less experienced 4DCT group.

Table 5: Mean sensitivity and specificity calculated for the analysis per adenoma identified by the radiologist.

	Round 1	Round 2	Round 3	Round 4	Round 5
	All radiologists together				
Sensitivity	0.62	0.62	0.64	0.68	0.62
Specificity	0.20	0.30	0.20	0.36	0.34
	Experienced 4DCT group				
Sensitivity	0.69	0.69	0.68	0.72	0.69
Specificity	0.24	0.34	0.21	0.38	0.38
	Less experienced 4DCT group				
Sensitivity	0.54	0.54	0.59	0.63	0.56
Specificity	0.15	0.26	0.18	0.34	0.29

Figure 15: Receiver operating characteristic (ROC) curves. (A) Each ROC curve is an average over all radiologists for each round. (B) Each ROC curve is an average over a group of radiologists with high or low 4DCT experience for each round.

A

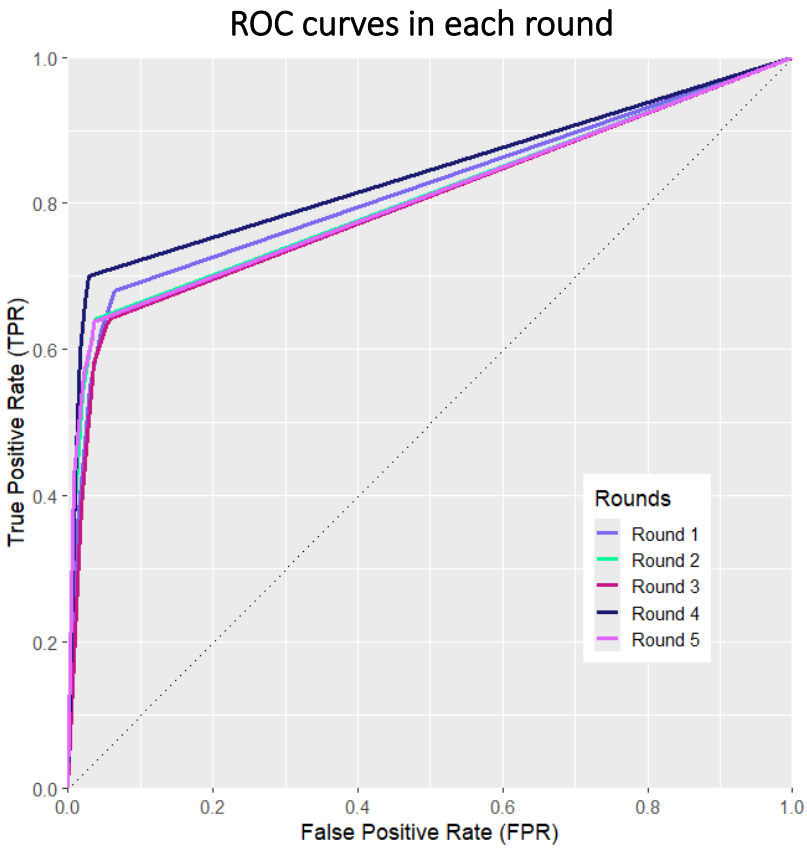

B

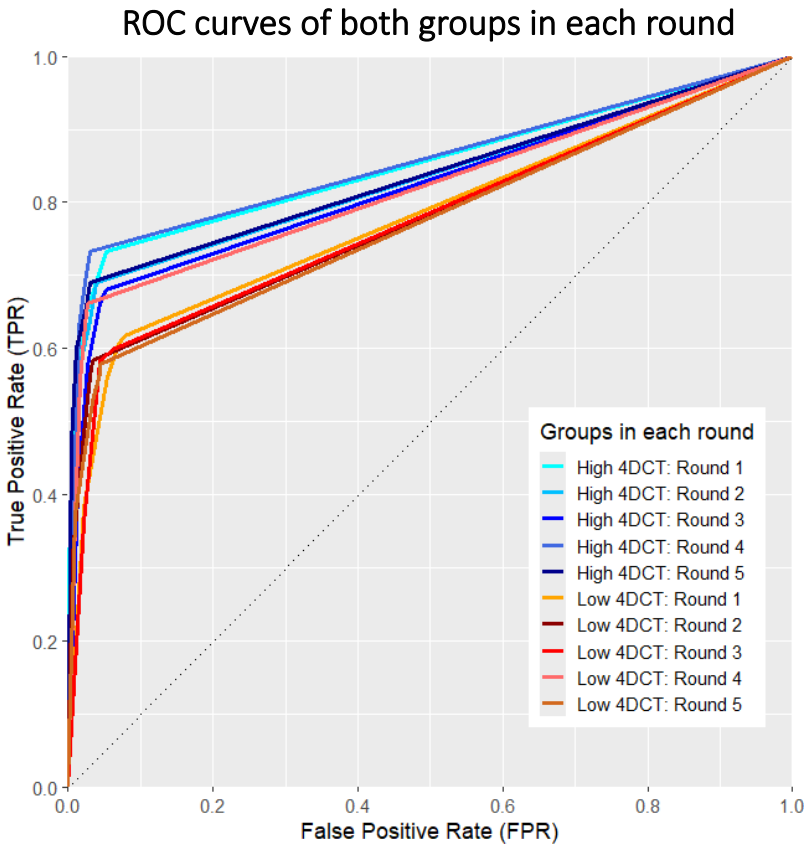

Figure 16: Individual and average receiver operating characteristic (ROC) curves for both groups of radiologists. Each ROC plot shows the results of a different round.

A

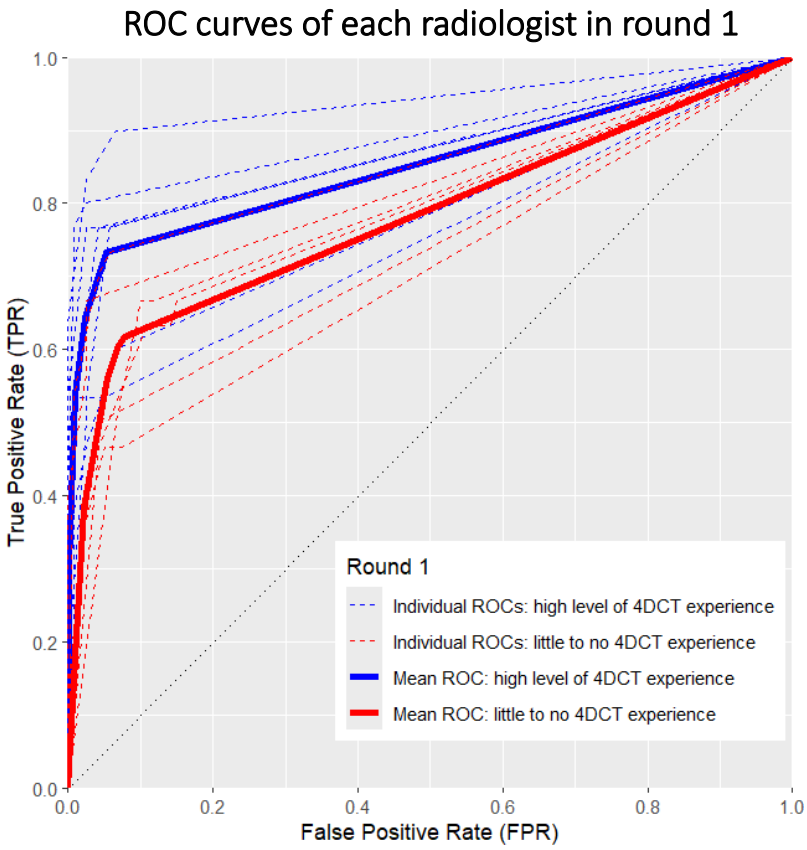

B

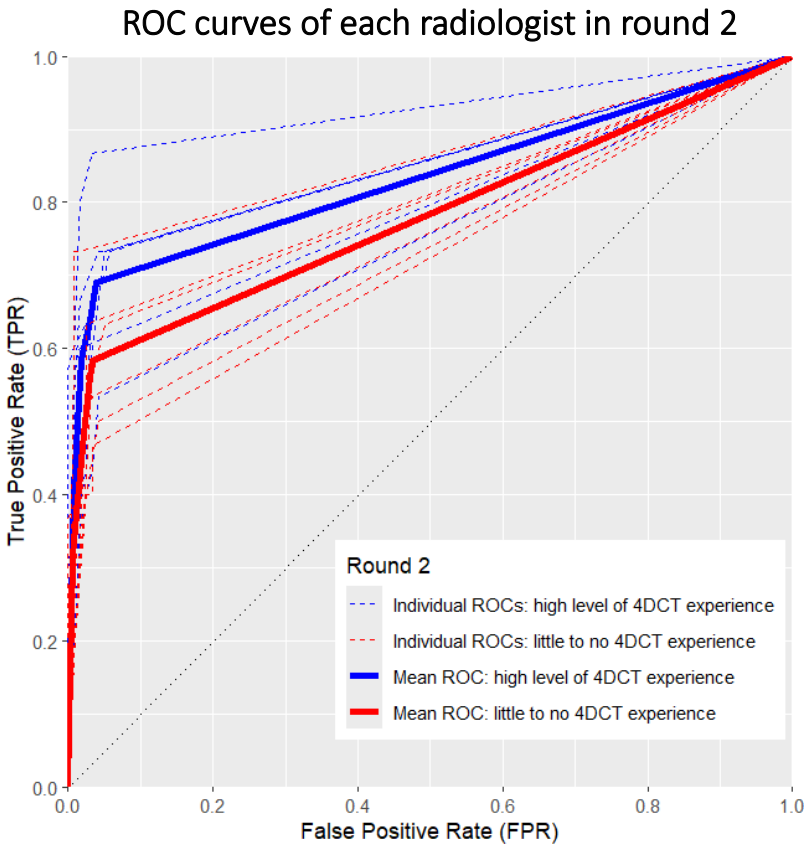

C

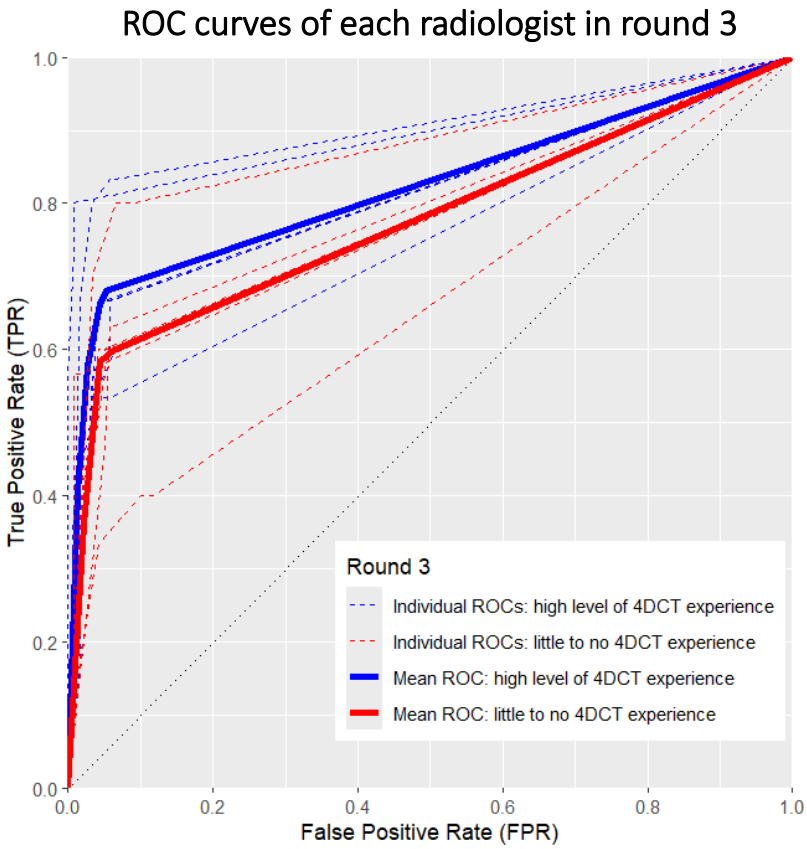
ROC curves of each radiologist in round 3
True Positive Rate (TPR)
False Positive Rate (FPR)
0.0
0.2
0.4
0.6
0.8
1.0
Round 3
Individual ROCs: high level of 4DCT experience
Individual ROCs: little to no 4DCT experience
Mean ROC: high level of 4DCT experience
Mean ROC: little to no 4DCT experience

D

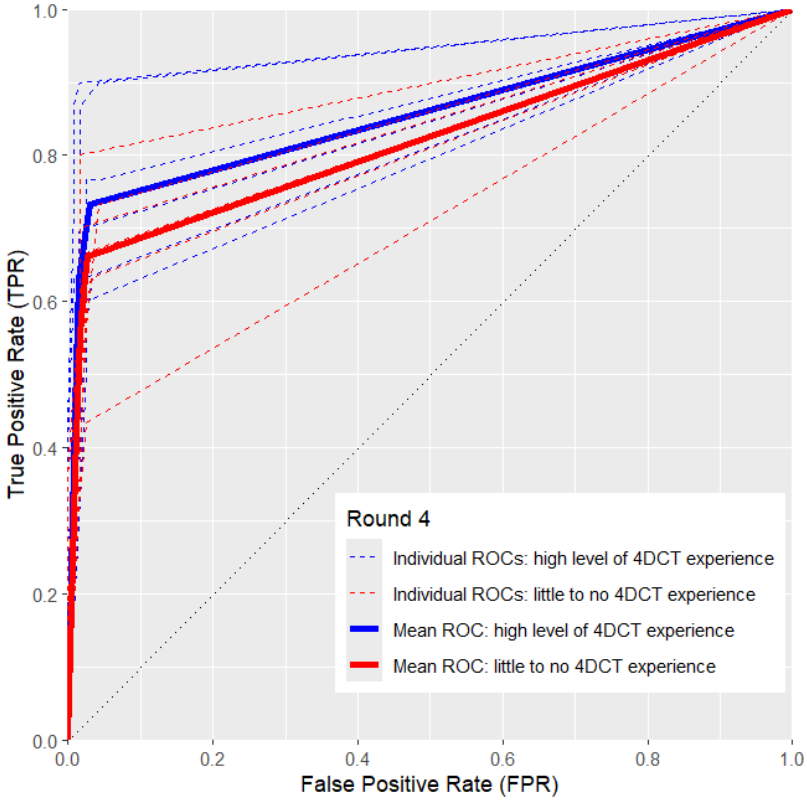
ROC curves of each radiologist in round 4
True Positive Rate (TPR)
False Positive Rate (FPR)
0.0
0.2
0.4
0.6
0.8
1.0
Round 4
Individual ROCs: high level of 4DCT experience
Individual ROCs: little to no 4DCT experience
Mean ROC: high level of 4DCT experience
Mean ROC: little to no 4DCT experience

E

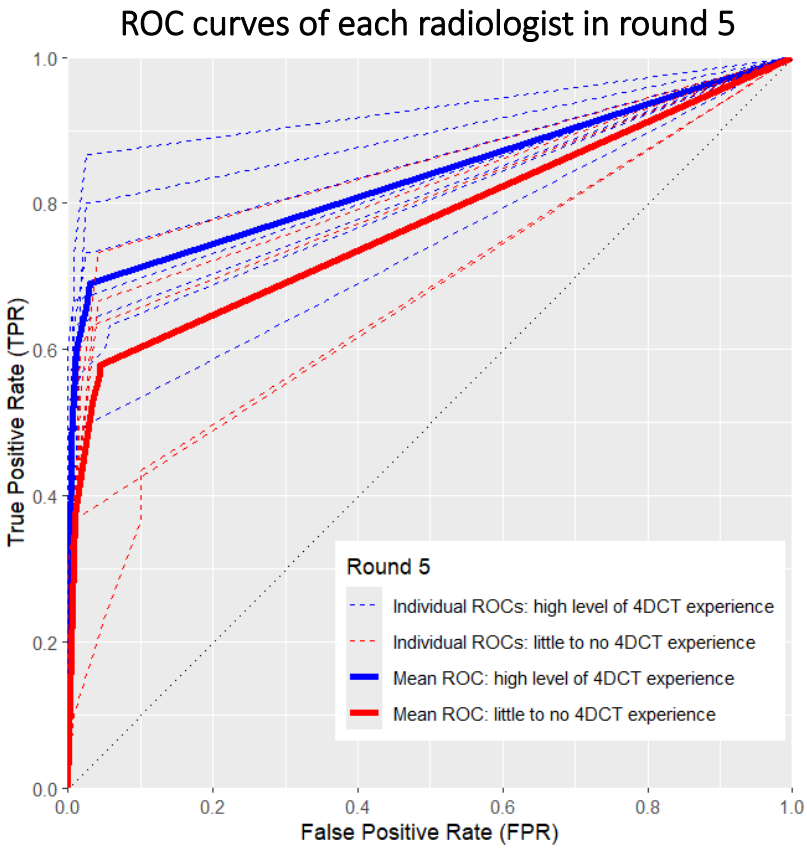
ROC curves of each radiologist in round 5
True Positive Rate (TPR)
False Positive Rate (FPR)
0.0
0.2
0.4
0.6
0.8
1.0
Round 5
Individual ROCs: high level of 4DCT experience
Individual ROCs: little to no 4DCT experience
Mean ROC: high level of 4DCT experience
Mean ROC: little to no 4DCT experience

4.3.4 Radiologists' view on the enhancement map

The radiologists' opinions of the enhancement map were collected and presented on the next page (Figure 17). The mean responses are shown as red dots and the range of the responses is shown as a red line. The first question showed that radiologists used the arterial phase the most, followed by the enhancement map, while the non-contrast phase was used the least. The second question showed that radiologists were more confident (average 7/10) in locating the PA using the enhancement map. However, some radiologists explained in the comments section that it was not necessarily more confidence, but that they used the enhancement map as a screening tool. The third question showed that radiologists were satisfied with image registration between the non-contrast and arterial phase images. The colour scale of the enhancement map was also well received by most radiologists. However, the number of artefacts was perceived as bad. The fourth question showed that the radiologists were very much willing to use the enhancement map in its current state (average 8/10). The fifth question was to obtain feedback on possible improvements to the enhancement map. The most common responses were that artefact reduction is crucial, that some would prefer the enhancement map in greyscale, and that some felt that no adjustments were necessary. The penultimate question showed that it is very likely (average 9/10) that radiologists will use the enhancement map after optimisation. The last question showed that radiologists participating in the MRMC study were likely to recommend the enhancement map to other radiologists (average 8/10).

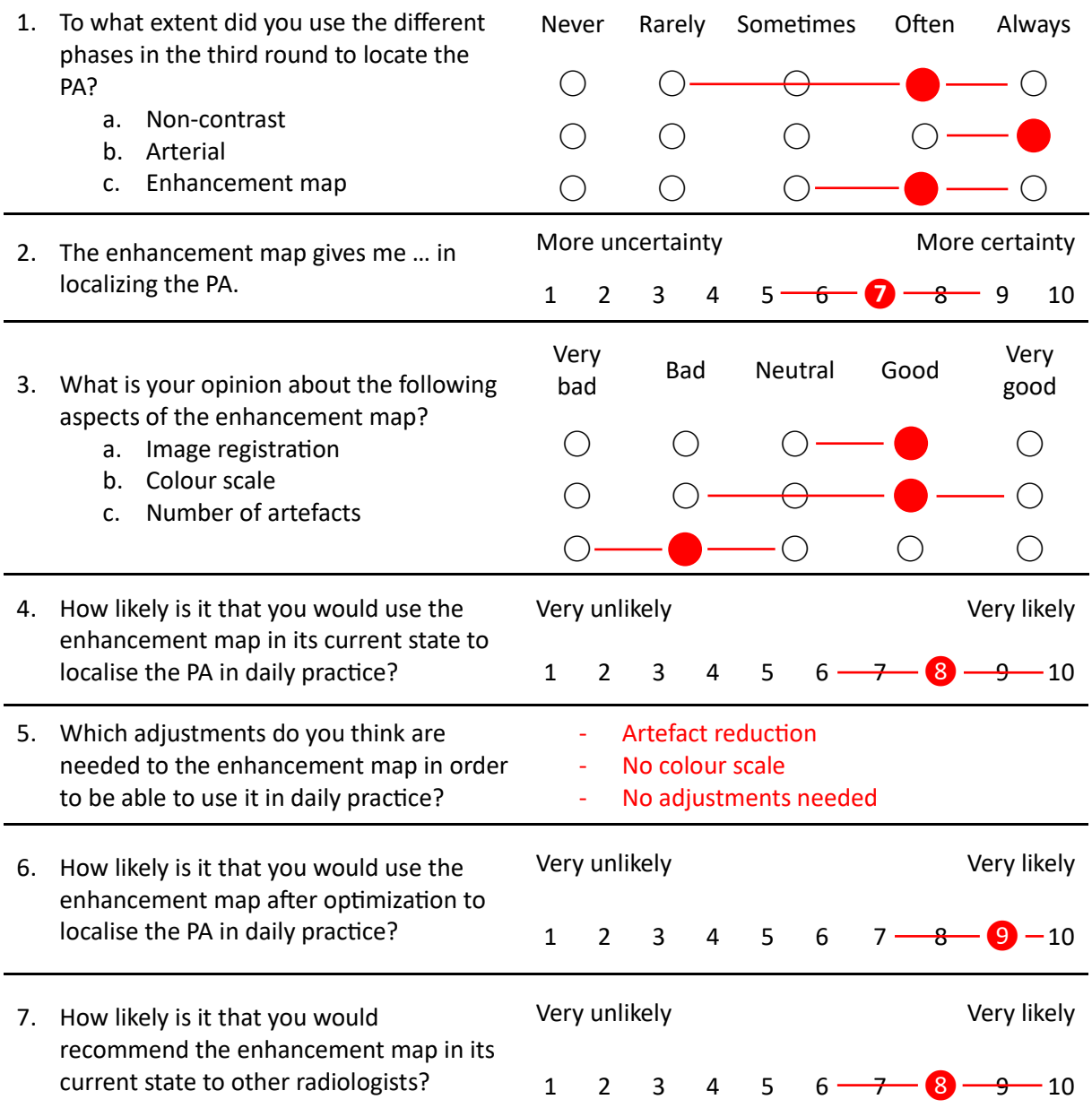

Figure 17: The radiologists' responses to the enhancement map. The mean responses are shown as red dots and the range of responses is shown as a red line.

4.4 Discussion

An increase in information did not result in better PA localisation performance, which contrasts with our initial expectations. The currently used four-phase 4DCT protocol (round 5), did not yield the best performance in this study. The 4DCT protocol consisting of three phases (non-contrast, arterial and venous phase) has been demonstrated to yield the highest values in terms of sensitivity, specificity and AUC. The radiologist's level of experience with 4DCT does not affect this, since round 4 is the best scoring round for both groups. However, it should be noted that there is a large overlap in the 95% CI of the mean AUC of all rounds. The main question of this study is whether it is possible to eliminate one or more phases from the currently used four-phase 4DCT protocol, and whether this differs for radiologists with different levels of 4DCT experience. This MRMC study has shown that a reduction from four to three 4DCT phases is strongly recommended, since removal of the delayed venous phase from the 4DCT protocol resulted in non-inferior performance to the four-phase 4DCT protocol for both groups of radiologists. Superiority of the three-phase 4DCT protocol over the four-phase 4DCT protocol could not be inferred, suggesting that it may be possible to remove more than one phase.

For radiologists with a high level of 4DCT experience, it is possible to achieve non-inferior performance to the four-phase 4DCT protocol with the non-contrast and arterial phases (round 2), and even with the arterial phase only (round 1). Nevertheless, the principal investigators of this study recommend the use of a two-phase protocol for the experienced 4DCT group, since the non-contrast phase has the ability to show attenuation differences in PAs adjacent to the thyroid gland [24], [29]. In addition, providing only the arterial phase, will increase the number of false positives due to lymph nodes being misinterpreted as PAs, which has major clinical implications. This was reflected in a low specificity in the first round, which was particularly evident in the analysis per identified adenoma. For the radiologists with little to no 4DCT experience, the investigated one- and two-phase 4DCT protocols were not non-inferior to the four-phase 4DCT protocol. Therefore, a three-phase 4DCT protocol is recommended for radiologists with less 4DCT experience.

All investigated 4DCT protocols were non-inferior to the four-phase 4DCT protocol when the radiologists were not divided into groups, indicating that the number of phases does not affect PA localisation performance. However, this study has shown that it is important to distinguish between radiologists with different levels of 4DCT experience, since it affects the required number of 4DCT phases.

The radiologists with a high level of experience in 4DCT assessment of PAs, consistently performed better than the group of radiologists who had little to no experience in 4DCT assessment of PAs. This is in line with our initial expectations that more experience with 4DCT would at least lead to better

performance and might also affect the number of phases required for both groups. The difference between the two groups was also tested statistically, which showed a statistically significant difference for the first round, where only the arterial phase was provided to the radiologists. There could be two reasons for this significant difference in the first round. Firstly, the experienced 4DCT group are familiar with assessing this type of scan, whereas the group with little to no 4DCT experience faced a learning curve which may have affected their initial performance. To minimise this effect, the radiologists were given test cases and a PowerPoint with instructions two weeks before the first round started. Secondly, locating a PA with only the arterial phase available is difficult even for experienced radiologists, let alone radiologists with little 4DCT experience.

The results showed that the sensitivity of most radiologists is relatively low. The reported sensitivity of 4DCT in the literature varies from 75 to 97%, whereas the mean sensitivity over the five rounds in our study varied from 68 to 73% for the experienced 4DCT group and from 58 to 66% for the inexperienced 4DCT group [5], [24], [25]. This difference with the literature may be explained by the large number of readers with different levels of 4DCT experience in our study, whereas most other studies have investigated a small group of highly experienced radiologists in the 4DCT assessment of PAs. In addition, the ROC curves of individual radiologists showed a large variability between radiologists in each round. This suggests that 4DCT assessment of PAs may benefit from being performed by a small group of radiologists.

The recommended 4DCT protocols do not include the enhancement map, but could there be a place for the enhancement map in the proposed 4DCT protocols since they include the non-contrast and arterial phases? In general, the radiologists were quite satisfied with the enhancement map. The initial aim of the enhancement map was to increase radiologists' confidence in 4DCT assessment of PAs. However, some radiologists used the enhancement map more as a screening tool. The form showed that they used the enhancement map frequently, were willing to use it in a clinical setting, and would recommend it to other radiologists. Despite these promising responses, the MRMC study showed that the addition of the enhancement map did not improve PA localisation performance. In both groups of radiologists, the observed mean sensitivity was quite comparable to the other rounds. However, specificity was strongly affected by radiologists incorrectly identifying structures for a PA, which was particularly evident in the analysis per identified adenoma. This was reflected in an observed mean specificity of less than 0.25 for both groups of radiologists. There are several possible reasons for the high number of false positives in the third round. Firstly, the radiologists were not familiar with the enhancement map. To minimise this effect, the radiologists were provided with test cases and a PowerPoint with instructions on the enhancement map. Secondly, the large number of cases with beam hardening artefacts could have affected the ability to locate the PAs. The radiologists responded in the

form that the number of artefacts was the most important aspect of the enhancement map to improve. Thirdly, the enhancement map may be difficult to interpret due to poor image registration between the non-contrast and arterial phase images in some cases. This idea was confirmed by a case-by-case analysis, since the cases in which the third round stood out in a negative way were mostly cases that had already been identified as difficult to read due to poor image registration. Removing these cases, improved the performance of the third round although it did not change the outcome of the recommended 4DCT protocols. The performance of PA localisation on the enhancement map may improve with more experience with the enhancement map.

The case-by-case analysis also showed that the most challenging cases for all radiologists in each round were those where the PA was adjacent to the thyroid and the enhancement pattern of the PA was atypical. The case with the highest number of false positives had a large thyroid nodule that many radiologists misinterpreted as a PA. As a result, it is likely that many radiologists did not search further and therefore did not successfully locate the actual PA. Radiologists with little 4DCT experience also had difficulty with cases containing a double PA. Removing these difficult cases did not change the outcome of the recommended 4DCT protocols. The cases with the highest number of true positives contained either a large PA, a typical enhancement pattern of the PA, a PA that was not adjacent to the thyroid, or a combination.

There are several limitations to our study. Firstly, although thirteen radiologists participated in this study - a relatively large number compared to similar studies - each group based on 4DCT experience was still relatively small, with only six and seven radiologists per group. With AUC values relatively close between groups, small changes in group composition could potentially affect the conclusions of the subanalysis. A larger number of radiologists per group would be needed to increase the reliability of our findings. Secondly, the radiologists were asked for their level of confidence for each identified PA and for each case where they did not find a PA. However, the analysis is performed based on the location in relation to the thyroid. Ideally, radiologists would have been asked for their level of confidence for each location in relation to the thyroid, thus aligning the analysis method with radiologist input. However, this was considered to be an onerous task for the radiologists, who had to assess the 4DCT scans in addition to their regular duties. Thirdly, the time spent by radiologists on each case was not measured. This is unfortunate, since this could have been helpful to gain more insight into the results. For example, in the last round where the performance was lower than expected, there is a feeling that the radiologists completed the cases quickly and reluctantly. However, it could also be the case that more information misleads the radiologists and only creates a distraction. Therefore, an indication of the time spent on each case would have been helpful in drawing conclusions. Fourthly, the empirically derived ROC curves may slightly underestimate actual performance due to limited data

in the lower specificity range. A binormal model is often used to construct smooth ROC curves to empirical points. This model was also applied to our data and the resulting ROC curves are shown in Appendix F. Although the binormal curves may slightly overestimate the performance - because the operating points don't fit the curves perfectly - the actual AUC values are likely to fall somewhere between the empirical and binormal estimates. However, it is the relative relationship between the AUC values rather than their absolute values that is of primary interest. Regardless of the approach used, the relative differences between the curves remained consistent, supporting the conclusions of the study.

Finally, an important note, and not necessarily a limitation, is the method currently used to conclude non-inferiority. This method was chosen because it takes into account the clinical implications of the radiology report. The principal investigators believed that it was most important for the radiologist to mention the correct location in relation to the thyroid gland, since the surgeon is able to distinguish the PA from other structures at this location. In addition, the non-inferiority software used is not able to assign a false negative and false positive result to the location in relation to the thyroid when a structure, most commonly a lymph node, is misinterpreted as a PA. Nevertheless, the additional analysis that was performed based on each PA identified by the radiologist, assigned one false positive and one false negative result if the radiologist identified the wrong structure, rather than a true positive result. Comparing the sensitivities of the two methods may therefore provide an insight into the consequences of the current method used to conclude non-inferiority. For the experienced 4DCT group, only the first round was affected by a decrease in mean sensitivity from 0.73 to 0.69. This actually supports our recommendation to use a two-phase 4DCT protocol instead of a one-phase 4DCT protocol. For the less experienced 4DCT group, the first round was most affected by a decrease in mean sensitivity from 0.62 to 0.54, followed by the second round with a decrease from 0.58 to 0.54. This method, based on each PA identified by the radiologist, reduced the performance of the one- and two-phase 4DCT protocols compared to the four-phase 4DCT protocol. This supports our recommendation to use a three-phase 4DCT protocol for less experienced 4DCT radiologists. Although a non-inferiority analysis could not be performed with the additional method, the principal investigators believe that the method currently used to conclude non-inferiority did not affect the proposed 4DCT protocols.

4.5 Conclusion

In conclusion, this MRMC study demonstrated that it is possible to reduce the number of phases in the 4DCT protocol, while maintaining localisation accuracy. A reduction from four to three 4DCT phases is strongly recommended for all radiologists. For experienced 4DCT radiologists, the number of phases could be further reduced to a one- or two-phase 4DCT protocol. The principal investigators recommend the use of the two-phase 4DCT protocol, because it reduces the number of false positives and makes it easier to differentiate between the PA and adjacent thyroid tissue. For radiologists with little to no 4DCT experience, a three-phase 4DCT protocol is recommended. The addition of the enhancement map did not improve localisation performance, but this may improve as radiologists gain more experience with the enhancement map. The patient will benefit from the proposed 4DCT protocols, since the radiation dose can be reduced compared to the currently used four-phase 4DCT protocol.

5 Integrated ^{18}F-Choline PET/4DCT: A pilot study

5.1 Introduction

The 4DCT MRMC study showed that it is possible to reduce the number of phases in the currently used four-phase 4DCT protocol and thus the radiation dose, while maintaining localisation accuracy. However, the localisation accuracy of 4DCT is not sufficient for many radiologists at the Rijnstate Hospital, who usually want more evidence of a PA to confirm their findings on 4DCT. Therefore, the 4DCT scan is often followed by the increasingly popular ^{18}F-Choline PET/CT scan. The sensitivity of ^{18}F-Choline PET/CT is the highest among all parathyroid imaging techniques, ranging from 85-97% [19], [21], [22]. Currently, the relatively high cost compared to the other parathyroid imaging techniques and the limited availability of PET/CT imaging systems prevent it from becoming the primary parathyroid imaging technique [23]. Therefore, ^{18}F-Choline PET/CT is mostly used as secondary parathyroid imaging technique, to confirm the findings of the used primary imaging technique.

The additional ^{18}F-Choline PET/CT scan to confirm the findings of the 4DCT scan, requires an additional hospital visit for the patient. It would be beneficial for the patient to schedule the 4DCT scan and the ^{18}F-Choline PET/CT scan on the same day, and even more so if the 4DCT and ^{18}F-Choline PET/CT could be integrated into a single ^{18}F-Choline PET/4DCT examination (Figure 18). In a systematic review, Piccardo et al. found that integrated ^{18}F-Choline PET/4DCT was superior to 4DCT, but only slightly better than ^{18}F-Choline PET/CT [42]. However, ^{18}F-Choline PET/4DCT has the advantage of having an arterial phase image, which often eases segmentation of the PA and surrounding structures. This segmentation can be used to construct 3D models to guide the surgeon in the search for the PA.

The nuclear medicine department of the Rijnstate Hospital decided to investigate ^{18}F-Choline PET/4DCT in a pilot study with non-contrast and arterial phase CT scans as a so-called ‘one-stop shop’ for PA localisation. To compare the localisation performance of 4DCT and ^{18}F-Choline PET/CT with ^{18}F-Choline PET/4DCT, a MRMC study such as the 4DCT study is needed. However, there is insufficient time to obtain histopathological confirmation of a PA, and furthermore a lot of time must again be demanded from the physicians. Therefore, the aim of this pilot study was changed to a quantitative comparison of CT images from the ^{18}F-Choline PET/4DCT protocol with CT images from the 4DCT protocol. In addition, the total radiation dose of the ^{18}F-Choline PET/4DCT protocol will be compared to the ^{18}F-Choline PET/CT and 4DCT protocols.

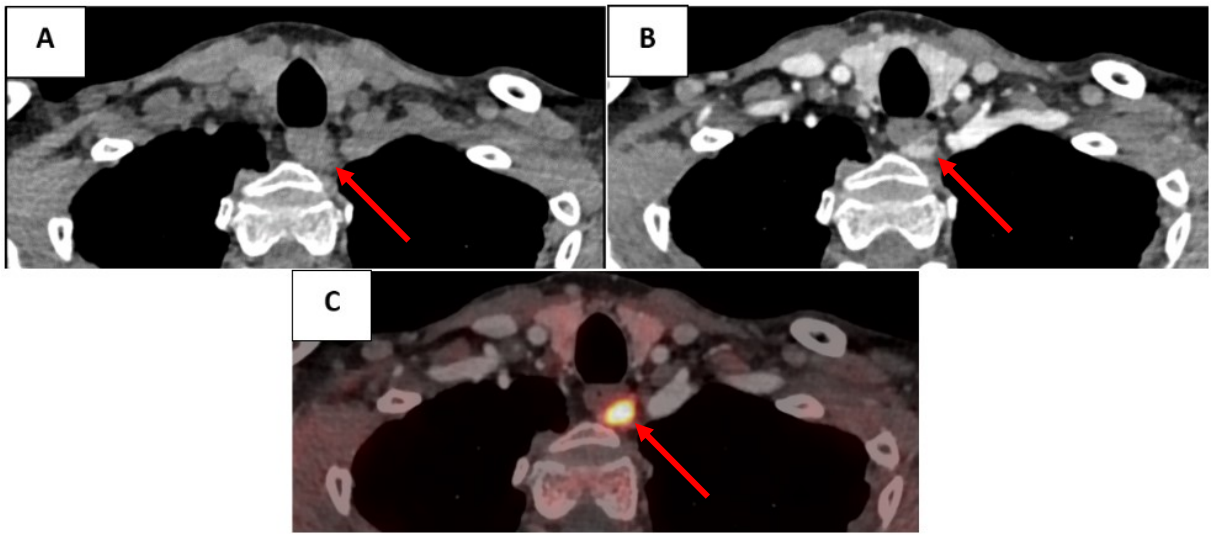

Figure 18: Example of a patient that is scanned with the ^{18}F-Choline PET/4DCT protocol. (A) Non-contrast phase image, (B) Arterial phase image and (C) Fused ^{18}F-Choline PET with the arterial phase CT image. The parathyroid adenoma is denoted by a red arrow.

5.2 Materials and Methods

5.2.1 Data acquisition

^{18}F-Choline PET/4DCT data were acquired from July 2024 to October 2024, resulting in a dataset of twenty-two patients. All ^{18}F-Choline PET/4DCT patients were scanned on the Biograph Vision 600 PET/CT scanner (Siemens Healthineers, Erlangen, Germany) with a slice thickness of 0.75 mm, and CARE Dose 4D under a tube voltage of 120 kVp and a reference tube current-exposure time product value of 116 mAs for the normal-dose CT scans. The low-dose CT scans for PET attenuation correction were acquired with a reference tube current-exposure time product value of 37 mAs.

4DCT data were retrospectively selected from May 2020 to March 2023, resulting in a dataset of thirty patients. This is the same dataset used in the 4DCT multireader multicase study. All patients were scanned on the IQon dual-energy CT (DECT) scanner (Philips Healthcare, Best, The Netherlands) with a slice thickness of 0.9 mm, a tube voltage of 120 kVp, and a reference tube current-exposure time product value of 83 mAs for the non-contrast phase images and 53 mAs for the arterial phase images.

^{18}F-Choline PET/CT data were retrospectively selected from March 2024 to July 2024, resulting in a dataset of thirty patients. All ^{18}F-Choline PET/CT patients were scanned on the Biograph Vision 600 PET/CT scanner (Siemens Healthineers, Erlangen, Germany), with the main difference from the ^{18}F-Choline PET/4DCT protocol being a slice thickness of 3.00 mm. The only CT image acquired in this ^{18}F-Choline PET/CT protocol was a low-dose, non-contrast CT scan for PET attenuation correction and anatomical reference. The reference tube current-exposure time product was slightly increased to 58 mAs for this low-dose CT scan to allow the radiologist to better recognize the contours of anatomical structures.

5.2.2 CT image quality

The first goal was to compare the image quality of CT images from the ^{18}F-Choline PET/4DCT protocol obtained using the Siemens Biograph Vision 600 PET/CT scanner with CT images from the 4DCT protocol obtained using the Philips IQon CT scanner. This comparison was made by focusing specifically on two key metrics: Signal-to-Noise Ratio (SNR) and Contrast-to-Noise Ratio (CNR). SNR measures the level of the desired signal against the background noise, while CNR measures the system's ability to distinguish between the target and surrounding tissue.

In the Sectra PACS environment (Sectra AB, Linköping, Sweden), regions of interest (ROIs) with a diameter of 5 mm were drawn on a slice of the non-contrast phase image within the thyroid gland for each patient. The thyroid gland was chosen as the target organ for calculating the SNR, since this was the most generalisable for each patient. All ROIs were reviewed and validated by J.K., a radiology resident with five years of experience. For each ROI, the mean Hounsfield units (HU) and standard deviation were noted and used to calculate the SNR for each patient (Eq. 3).

$$SNR = \frac{\bar{x}_{target}}{s_{target}} \qquad (Eq. 3)$$

Where $\overline{x}_{target}$ is equal to the mean HU and s_{target} to the standard deviation within the ROI.

To calculate the CNR, ROIs with a diameter of 3 mm were drawn in the PA. Keeping the ROIs relatively small ensures that image quality is assessed and not the physiological process of heterogeneous contrast uptake in the PA. In this study, two approaches were used to estimate the CNR. First, the CNR between the thyroid gland and the PA was calculated on the arterial phase image, referred to as $CNR_{PA\text{-}T}$. A low $CNR_{PA\text{-}T}$ does not necessarily indicate difficulty in differentiating the PA from the thyroid gland, since the adenoma is not always adjacent to the thyroid gland. Therefore, a second method was used: calculating the CNR between the PA on the arterial phase image and the PA on the non-contrast phase image, referred to as $CNR_{A\text{-}NC}$. For each ROI, the mean and standard deviation were noted and used to calculate two CNRs for each patient (Eq. 4).

$$CNR = \frac{\bar{x}_{target} - \bar{x}_{tissue}}{\sqrt{s_{target}^2 + s_{tissue}^2}} \qquad (Eq. 4)$$

Where $\overline{x}_{target}$ is equal to the mean HU and s_{target} to the standard deviation within the ROI that was drawn in the PA on the arterial phase image. $\overline{x}_{tissue}$ is equal to the mean HU and s_{tissue} to the standard deviation within the ROI that was drawn either in the thyroid gland on the arterial phase image (for $CNR_{PA\text{-}T}$) or in the PA on the non-contrast phase image (for $CNR_{A\text{-}NC}$).

5.2.3 Total radiation dose

The second goal was to compare the total radiation dose of the ^{18}F-Choline PET/4DCT protocol with the ^{18}F-Choline PET/CT protocol, both scanned on the Siemens Biograph Vision 600 PET/CT scanner, and with the 4DCT protocol scanned on the Philips IQon CT scanner. The first protocol created for the ^{18}F-Choline PET/4DCT scan included a normal-dose non-contrast CT scan from the base of the skull to halfway up the liver. This non-contrast CT scan was used for PET attenuation correction and PA localisation. This was followed by a normal-dose arterial phase CT scan from the base of the skull to the carina. The hypothesis was that the ^{18}F-Choline PET/4DCT scan should not result in more radiation exposure than a four-phase 4DCT scan because the ^{18}F-Choline PET/4DCT scan uses only non-contrast and arterial phase images.

The comparison in radiation dose was made by focusing specifically on two key metrics: Computed Tomography Dose Index Volume ($CTDI_{vol}$) and Dose Length Product (DLP). While $CTDI_{vol}$ and DLP indicate the radiation dose output of a CT scanner, it is important to note that they do not directly measure the effective dose received by the patient. $CTDI_{vol}$ represents the average radiation dose output in a single CT slice and is measured in milligrays (mGy). It provides a standardised measure for comparing dose output between different CT protocols. DLP represents the total radiation dose over the entire scan length and is calculated as the product of $CTDI_{vol}$ and the scan length. DLP is measured in milligray-centimetres (mGy*cm).

For each patient, $CTDI_{vol}$ and DLP were extracted from the dose evaluation report stored in the Sectra PACS environment. $CTDI_{vol}$ was recorded for each CT scan within the image protocol, while the total DLP was recorded as the cumulative dose over all CT scans. In addition, the body mass index (BMI) was recorded for each patient, since BMI can have a significant impact on radiation dose output; higher BMIs are often associated with increased dose requirements, since more radiation is required to penetrate a larger body mass [43].

The radiation dose of the ^{18}F-Choline PET/4DCT protocol was continuously evaluated during this pilot study and modifications to the ^{18}F-Choline PET/4DCT protocol were made if high radiation dose metrics were observed.

5.3 Results

5.3.1 CT image quality

The median SNR of the CT images obtained using the Siemens Biograph Vision 600 PET/CT scanner was 5.3 (IQR: 4.1, 8.0), which was lower than that of the Philips IQon CT scanner, with a median SNR of 12.0 (IQR: 9.5, 14.4) (Figure 19). The interquartile ranges (IQRs) were relatively similar between the two imaging systems, but there was no overlap in the IQRs.

The median CNR_{PA-T} of the CT images obtained using the Siemens Biograph Vision 600 PET/CT scanner was -1.9 (IQR: -3.3, -0.3), which was closer to zero than that of the Philips IQon CT scanner, with a median CNR_{PA-T} of -2.8 (IQR: -4.9, -1.3) (Figure 20). This closer to zero CNR on the Siemens Biograph Vision 600 PET/CT scanner suggests less contrast between the PA and the thyroid gland on the arterial phase image compared to the Philips IQon CT scanner. The IQRs of the CNR_{PA-T} were relatively similar between the two imaging systems, while there was also a large overlap in the IQRs.

The median CNR_{A-NC} of the CT images obtained using the Siemens Biograph Vision 600 PET/CT scanner was 4.7 (IQR: 2.0, 6.8), which was closer to zero than that of the Philips IQon CT scanner, with a median CNR_{A-NC} of 6.3 (IQR: 3.4, 8.6) (Figure 21). The IQRs of the CNR_{A-NC} were relatively similar between the two imaging systems, while there was also a large overlap in the IQRs.

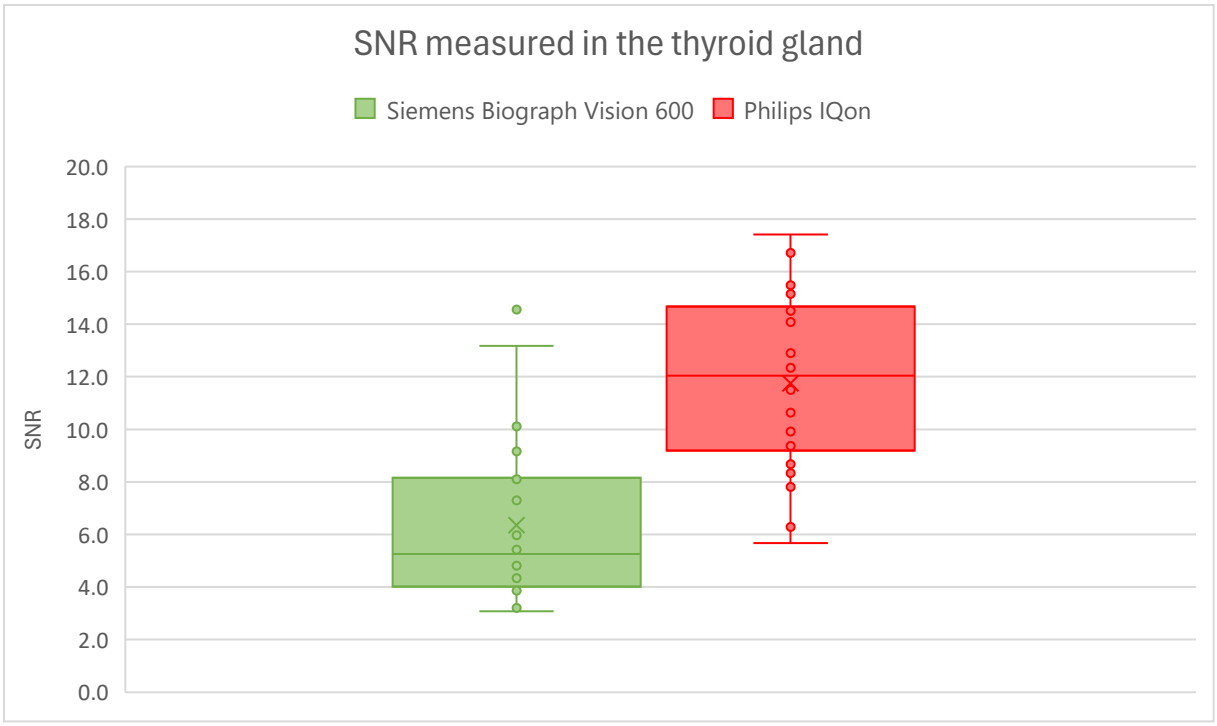

Figure 19: Signal-to-noise ratio (SNR) comparison of CT images obtained using the Siemens Biograph Vision 600 PET/CT scanner with CT images obtained using the Philips IQon CT scanner.

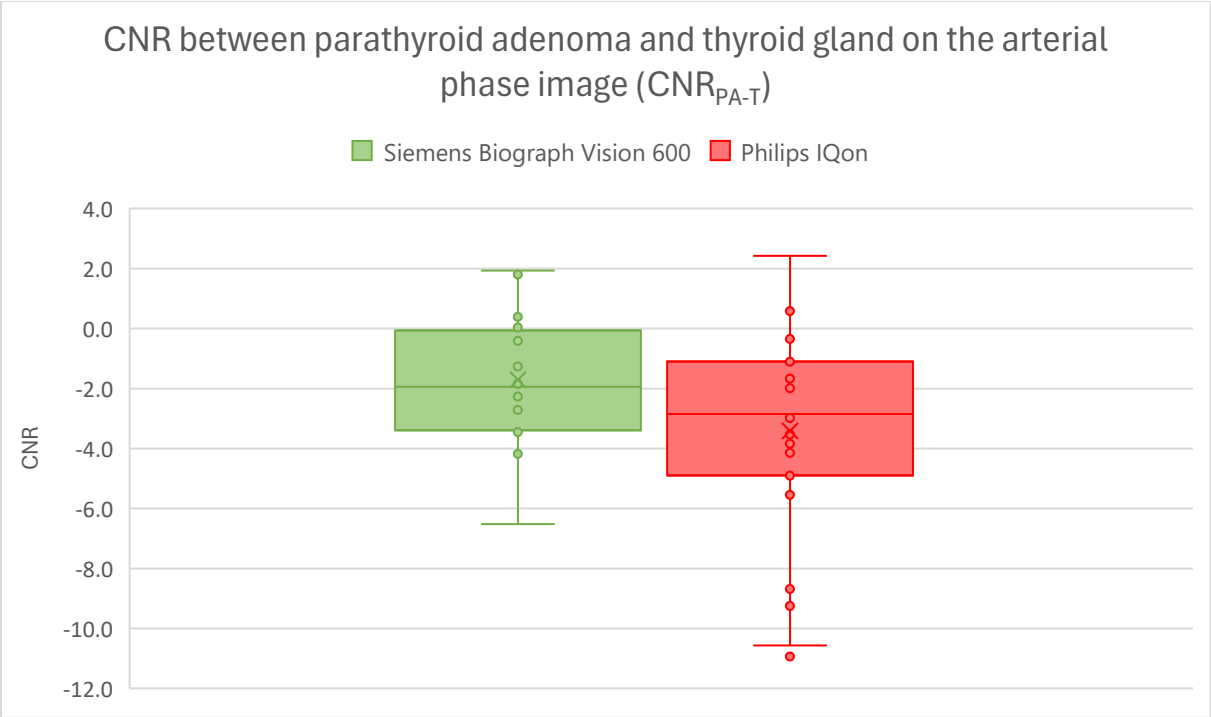

Figure 20: Contrast-to-noise ratio (CNR) comparison of CT images obtained using the Siemens Biograph Vision 600 PET/CT scanner with CT images obtained using the Philips IQon CT scanner. CNR_{PA-T} was measured between the parathyroid adenoma and the thyroid gland on the arterial phase image.

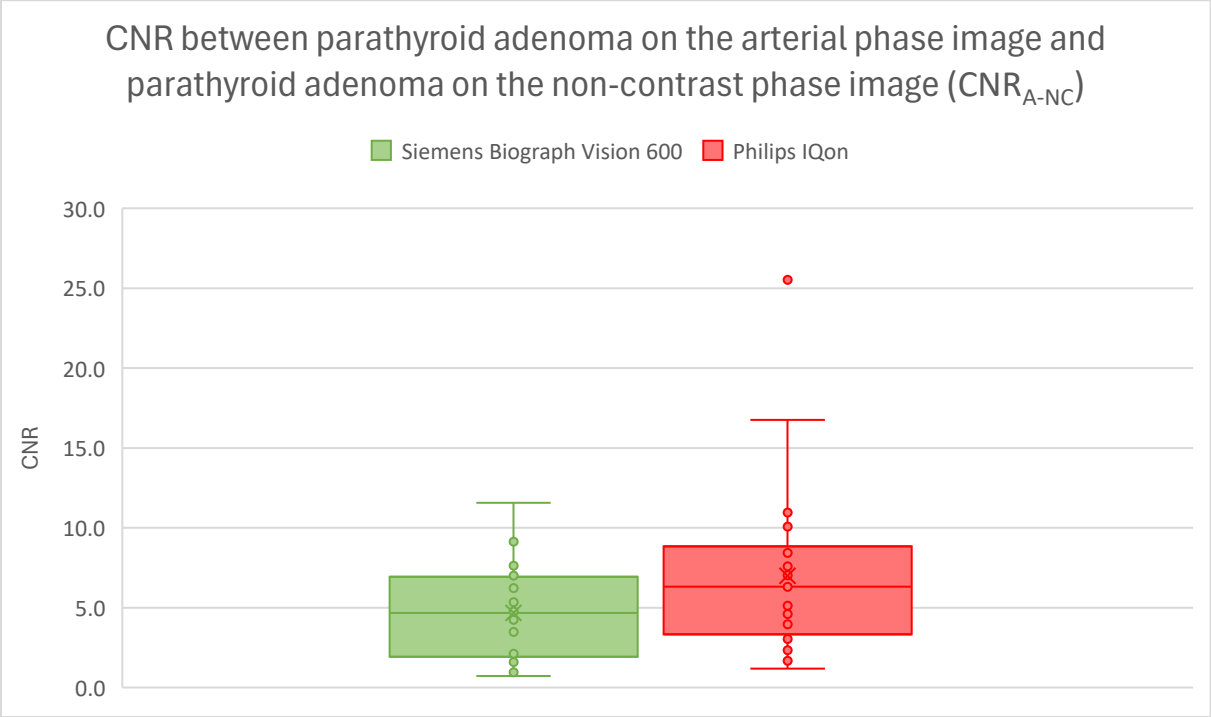

Figure 21: Contrast-to-noise ratio (CNR) comparison of CT images obtained using the Siemens Biograph Vision 600 PET/CT scanner with CT images obtained using the Philips IQon CT scanner. CNR_{A-NC} was measured between the parathyroid adenoma on the arterial phase image and the parathyroid adenoma on the non-contrast phase image.

5.3.2 Total radiation dose

Analysis of the total DLP for the first six patients scanned with the ^{18}F-Choline PET/4DCT protocol, showed that the total DLP was considerably higher for the ^{18}F-Choline PET/4DCT protocol compared to both the 4DCT and ^{18}F-Choline PET/CT protocols (Figure 22). To reduce the total DLP, the original ^{18}F-Choline PET/4DCT protocol was modified by splitting the non-contrast phase into two scans: a low-dose CT scan to halfway up the liver (for PET attenuation correction) and a normal-dose CT scan up to the carina (for PA localisation). The modification to the original ^{18}F-Choline PET/4DCT protocol is shown in Table 6.

Table 6: Modifications made to the ^{18}F-Choline PET/4DCT protocol.

	Scan 1	Scan 2	Scan 3
Protocol 1 (PT01 – PT06)	Normal-dose, non-contrast CT scan (base of skull – mid-liver)	Normal-dose, arterial CT scan (base of skull – carina)	
Protocol 2 (PT07 – PT15)	Low-dose, non-contrast CT-scan (base of skull – mid-liver)	Normal-dose, non-contrast CT scan (base of skull – carina)	Normal-dose, arterial CT scan (base of skull – carina)
Protocol 3 (PT16 – PT22)	Low-dose, non-contrast CT scan (base of skull – mid-liver)	Normal-dose, non-contrast CT scan (base of skull – carina)	Normal-dose (dose saving optimised for CTA), arterial CT scan (base of skull – carina)

Nine patients were included to confirm that the modification to the original ^{18}F-Choline PET/4DCT protocol was successful. Analysis of the total DLP of these nine patients showed that the total DLP of the ^{18}F-Choline PET/4DCT protocol was closer to the total DLP of the four-phase 4DCT protocol (Figure 22). However, the total DLP of the second ^{18}F-Choline PET/4DCT protocol was still greater than the total DLP of the four-phase 4DCT protocol, especially in patients with a higher BMI. Further analysis of the second ^{18}F-Choline PET/4DCT protocol showed that the arterial phase $CTDI_{vol}$ was on average 50% higher than the non-contrast phase $CTDI_{vol}$ (Figure 23). Therefore, a second modification to the ^{18}F-Choline PET/4DCT protocol was made by optimising the dose-saving parameter for the arterial phase image (Table 6). After this modification, the $CTDI_{vol}$ of the arterial phase images was on average similar to the DLP of the non-contrast phase images (Figure 23). This modification should result in a further reduction in total DLP for patients scanned with the third ^{18}F-Choline PET/4DCT protocol. However, this has not yet been observed in the seven patients scanned with this new protocol (Figure 22). Finally, total DLP showed greater variability in all three ^{18}F-Choline PET/4DCT protocols compared to both the 4DCT and ^{18}F-Choline PET/CT protocols.

The $CTDI_{vol}$ and total DLP data for each patient and each scan can be found in Appendix G.

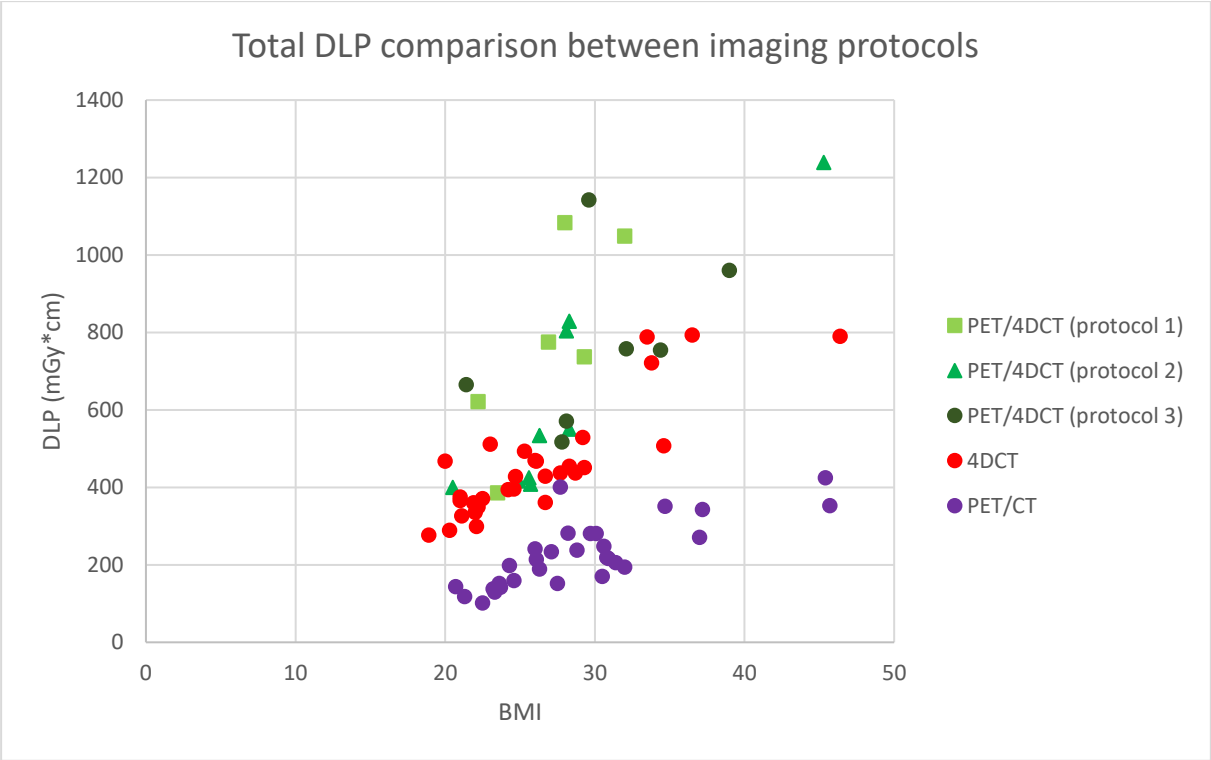

Figure 22: Comparison of the total dose length product (DLP) for all three investigated ^{18}F-Choline PET/4DCT protocols, the four-phase 4DCT protocol and the ^{18}F-Choline PET/CT protocol.

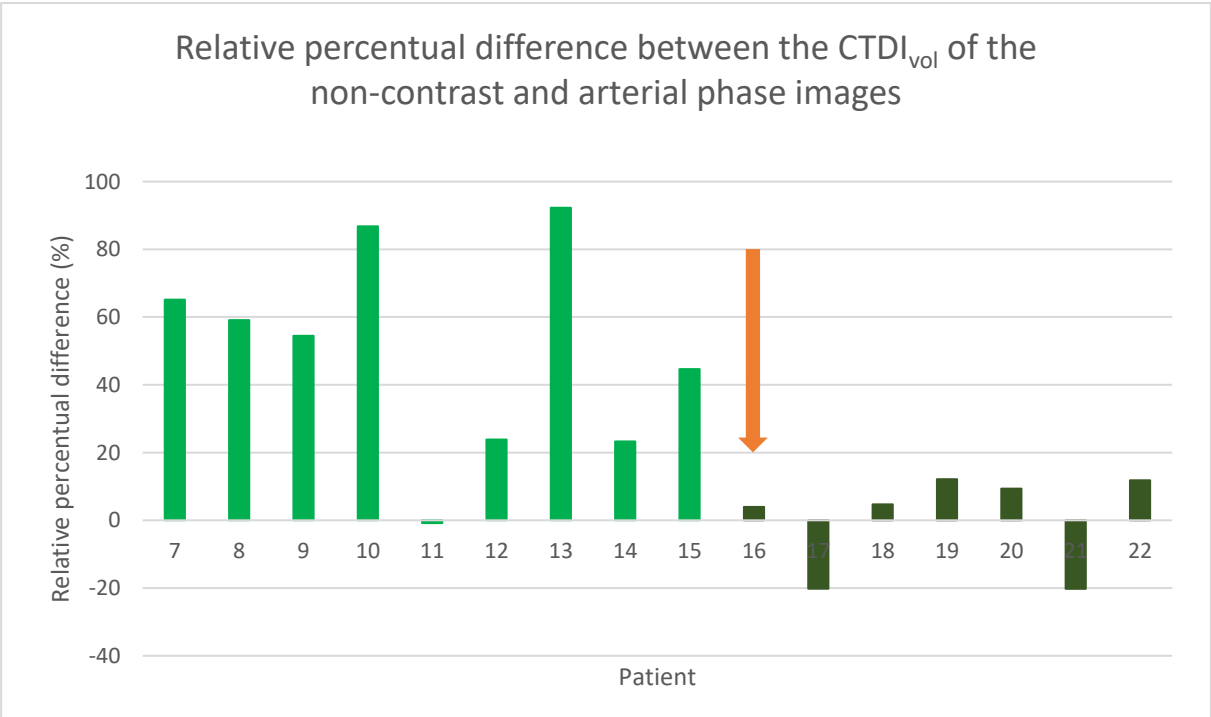

Figure 23: Relative percentual difference between the $CTDI_{vol}$ of the non-contrast and arterial phase images of the second and third ^{18}F-Choline PET/4DCT protocols scanned on the Siemens Biograph Vision 600 PET/CT scanner. The orange coloured arrow indicates the first patient scanned with the third ^{18}F-Choline PET/4DCT protocol, where the dose-saving parameter was optimized for arterial phase images.

5.4 Discussion

5.4.1 CT image quality

This pilot study demonstrated differences in image quality metrics between the Siemens Biograph Vision 600 PET/CT and Philips IQon CT scanners, with potential implications for PA localisation. The Siemens Biograph Vision 600 PET/CT scanner yielded a lower median SNR than the Philips IQon CT scanner (5.3 vs 12.0). Although the IQRs were similar, indicating comparable variability in SNR measurements, the lack of overlap in the IQRs suggests a potentially significant difference in SNR between the two imaging systems. In practice, this may indicate that the Philips IQon CT scanner provides images with greater clarity and detail, which may aid in the localisation of PAs.

The Siemens Biograph Vision 600 PET/CT scanner yielded a median CNR_{PA-T} and CNR_{A-NC} closer to zero than the Philips IQon CT scanner (-1.9 and 4.7 vs -2.8 and 6.3). The relatively similar IQRs indicate comparable variability in CNR_{PA-T} and CNR_{A-NC} measurements between the two imaging systems, while the overlap in IQRs suggests that the observed differences in CNR_{PA-T} and CNR_{A-NC} between the two imaging systems are most likely not significant. These results suggest that although the SNR differs between the systems, the CNR remains comparable, implying similar contrast between the parathyroid adenoma and surrounding tissue on the two imaging systems.

The difference in SNR between the two imaging systems was likely influenced by the different iterative reconstruction algorithms and slice thickness parameters used. The Siemens Biograph Vision 600 PET/CT scanner uses the Sinogram-Affirmed Iterative Reconstruction (SAFIRE) method, while the Philips IQon CT scanner uses the Iterative Model Reconstruction (IMR) algorithm. The different iterative reconstruction algorithms may inherently affect noise levels and contrast, thus affecting the SNR and CNR values of the two imaging systems [44]. In addition, the CT images obtained using the Siemens Biograph Vision 600 PET/CT scanner had a slice thickness of 0.75 mm compared to 0.90 mm for the CT images obtained using the Philips IQon CT scanner. In general, thicker slices often result in improved SNR, which may partly explain the higher SNR measurements seen with the Philips IQon CT scanner [45].

5.4.2 Total radiation dose

This pilot study demonstrated a relatively high radiation dose output for the original ^{18}F-Choline PET/4DCT protocol scanned on the Siemens Biograph Vision 600 PET/CT scanner compared to the 4DCT protocol scanned on the Philips IQon CT scanner, with potential implications for the radiation dose received by the patient. This finding contrasted with our initial expectation that the ^{18}F-Choline PET/4DCT protocol would not exceed the total DLP of a four-phase 4DCT scan. For the original ^{18}F-Choline PET/4DCT protocol, the total DLP is approximately the sum of the 4DCT and ^{18}F-Choline PET/CT

protocols. A possible explanation for the higher total DLP is that the non-contrast phase image was acquired at a normal dose from the base of the skull to halfway up the liver, rather than up to the carina. As a result, modifications were made to the original ^{18}F-Choline PET/4DCT protocol to reduce the total DLP.

The first modification successfully reduced the total DLP of the ^{18}F-Choline PET/4DCT protocol, bringing it closer to that of the 4DCT protocol. This second ^{18}F-Choline PET/4DCT protocol includes an additional low-dose non-contrast CT scan from the base of the skull to halfway up the liver, but the contribution of this scan to the total DLP is comparable to, and mostly lower than, the normal-dose non-contrast CT scan from the base of the skull up to the carina. The second modification focused on dose efficiency of the arterial phase, and the results show that the modified protocol achieved comparable $CTDI_{vol}$ values for the non-contrast and arterial phase images within the ^{18}F-Choline PET/4DCT protocol. However, the third ^{18}F-Choline PET/4DCT protocol did not yet provide an additional reduction in total DLP. It is important to note that both $CTDI_{vol}$ and total DLP are strongly influenced by patient characteristics, such as BMI, which affect dose requirements for adequate image quality. Therefore, the limited number of patients scanned with the latest ^{18}F-Choline PET/4DCT protocol, makes it difficult to draw firm conclusions about a reduction in radiation dose output.

It is important to compare the radiation dose output of our latest ^{18}F-Choline PET/4DCT protocol with the radiation dose output of 4DCT protocols from other hospitals, since the radiation dose output of ^{18}F-Choline PET/4DCT protocols from other hospitals could not be found. This comparison highlights the importance of further dose reduction in our ^{18}F-Choline PET/4DCT protocol. Bunch et al. report that the DLP of 4DCT protocols is typically between 400 and 600 mGy*cm per CT phase, which would correspond to a patient effective dose for a four-phase 4DCT protocol between 12 and 18 mSv [5]. According to Raeymaeckers et al, the patient effective dose of 4DCT protocols in the literature ranges from 10.4 to 13.8 mSv, with their own protocol achieving a mean effective dose of 6.7 mSv [46]. On average, the total DLP of our latest ^{18}F-Choline PET/4DCT protocol is approximately 700 mGy*cm. The patient effective dose, expressed in mSv, can be calculated according to the current guidelines of the International Commission on Radiological Protection (ICRP) 103 [27]. A conversion factor of 0.0075 was used, similar to that used by Raeymaeckers et al. This results in a patient effective dose of 5.3 mSv for our latest ^{18}F-Choline PET/4DCT protocol, which is lower than the patient effective dose of 4DCT protocols reported in the literature. This suggests that although it is always recommended to aim for the lowest possible radiation dose, the total radiation dose of our ^{18}F-Choline PET/4DCT protocol is already acceptable.

5.4.3 Recommendations

According to the nuclear medicine physicians at the Rijnstate Hospital, the PA is very easy to localise with the new ^{18}F-Choline PET/4DCT protocol. Although the actual localisation performance with the ^{18}F-Choline PET/4DCT protocol could not be determined in this short time frame, the expectations are very promising. Nevertheless, several recommendations were made that may improve image quality and reduce the total radiation dose of the ^{18}F-Choline PET/4DCT protocol.

Firstly, increasing the slice thickness from 0.75 mm to 1.0 mm may help to reduce image noise, by detecting more photons per slice, resulting in a higher SNR [45]. This modification could bring the image quality of our ^{18}F-Choline PET/4DCT protocol closer to that of the 4DCT protocol, which uses a slice thickness of 0.9 mm. Increasing the slice thickness in a helical CT scan, as in our ^{18}F-Choline PET/4DCT protocol, is unlikely to directly reduce the total radiation dose, since primary dose factors – such as tube current, voltage, scan time, scan range and pitch – remain unchanged [47]. Importantly, increasing the slice thickness to 1.0 mm is unlikely to affect PA localisation, since the smallest PA in the 4DCT database is 5 mm in diameter. Secondly, the low-dose non-contrast CT scan prior to the PET scan may be omitted and replaced by the normal-dose non-contrast CT scan, which can then be used for PET attenuation correction and PA localisation. This modification would make the protocol look similar to the original ^{18}F-Choline PET/4DCT protocol, with the main difference being that the scan would extend only to the carina instead of halfway to the liver. The modification may result in a significant dose reduction, since evaluation of the liver requires a higher mAs value. This modification is not expected to affect PA localisation, since PAs are not located below the carina. Thirdly, it may be valuable to gain a deeper understanding of the CARE Dose kV algorithm (Siemens Healthineers, Erlangen, Germany) and its impact on radiation dose. CARE Dose kV allows for dose reduction by modulating the tube current and automatically selecting the optimal tube voltage according to the size and density of the individual patient [48]. This pilot study showed a relatively large increase in radiation dose output for patients scanned on the Siemens Biograph Vision 600, compared to the Philips IQon CT. Therefore, it may be useful to consult people within Siemens and review the settings in our ^{18}F-Choline PET/4DCT protocol to investigate why patients with a high BMI show such a large increase in radiation dose output.

Once the protocol has been optimised in terms of image quality and radiation dose, the suggestion would be to scan at least thirty patients with the same ^{18}F-Choline PET/4DCT protocol on the Siemens Biograph Vision 600 PET/CT scanner. This will make it easier to compare the ^{18}F-Choline PET/4DCT protocol with the 4DCT protocol on the Philips IQon CT scanner. If the $CTDI_{vol}$ of the CT scans in the ^{18}F-Choline PET/4DCT protocol is still relatively high compared to the $CTDI_{vol}$ of the CT scans in the 4DCT protocol, Siemens should be contacted and asked about the high radiation dose output compared to

the Philips IQon CT scanner. The effective dose to the patient may be acceptable, but the recommended ^{18}F-Choline PET/4DCT protocol, consisting of a normal-dose non-contrast and arterial phase image, should be about half that of a four-phase 4DCT protocol, which is not currently the case. In the future, an MRMC study should be performed to compare PA localisation with the optimised ^{18}F-Choline PET/4DCT protocol with PA localisation with the 4DCT and ^{18}F-Choline PET/CT protocols.

5.5 Conclusion

This pilot study demonstrated that the ^{18}F-Choline PET/4DCT protocol achieved comparable CNR values but lower SNR values than the 4DCT protocol in terms of image quality. The total radiation dose of the ^{18}F-Choline PET/4DCT protocol is currently higher than the 4DCT protocol, but at an acceptable level of patient effective dose. The number of patients scanned with the latest ^{18}F-Choline PET/4DCT protocol is still relatively small, making it difficult to draw firm conclusions. Recommendations were made to further improve the ^{18}F-Choline PET/4DCT protocol in terms of image quality and radiation dose, so that a future MRMC study can determine the performance of PA localisation with the ^{18}F-Choline PET/4DCT protocol with other PA imaging modalities. Overall, the ^{18}F-Choline PET/4DCT protocol has proven to be a promising 'one-stop shop' alternative to the currently used imaging modalities, to the benefit of the patient and the hospital.

6 General discussion & Future perspectives

The goal of this research was to develop the optimal localisation protocol for patients with a suspected parathyroid adenoma (PA) in terms of the number of examinations, the lowest possible total radiation dose and the highest localisation accuracy. The four-dimensional CT (4DCT) multireader, multicase (MRMC) study demonstrated that it is possible to reduce the number of phases in the 4DCT protocol from four to three, while maintaining localisation accuracy. For experienced 4DCT radiologists, the number of phases could be further reduced to a two-phase 4DCT protocol, halving the radiation dose compared to the currently used four-phase 4DCT protocol. The reduced radiation dose makes 4DCT more attractive as a primary imaging modality in any hospital. However, the sensitivity values in the 4DCT MRMC study were relatively low, which may explain why many radiologists at the Rijnstate Hospital usually request a ^{18}F-Choline PET/CT scan to confirm their findings on 4DCT.

The additional ^{18}F-Choline PET/CT scan to confirm the findings of the 4DCT scan, requires an additional hospital visit for the patient and also increases the demands on hospital staff and resources. The nuclear medicine department of the Rijnstate Hospital therefore decided to investigate the combination of 4DCT and ^{18}F-Choline PET/CT into a single ^{18}F-Choline PET/4DCT examination, creating a so-called 'one-stop shop' solution. The pilot study showed that the total radiation dose of the ^{18}F-Choline PET/4DCT protocol is currently higher than the 4DCT protocol, but at an acceptable level of patient effective dose. The ^{18}F-Choline PET/4DCT protocol achieved comparable Contrast-to-Noise Ratio (CNR) values but lower Signal-to-Noise Ratio (SNR) values than the 4DCT protocol in terms of CT image quality. Crucially, according to the nuclear medicine physicians at the Rijnstate Hospital who evaluate these scans, the PA is very easy to localise with the new ^{18}F-Choline PET/4DCT protocol.

The proposed ^{18}F-Choline PET/4DCT protocol consists of non-contrast and arterial phase images, since the 4DCT MRMC study showed that the delayed venous phase could be safely removed without compromising localisation performance. The venous phase was useful for some radiologists, but this information could now be replaced by choline uptake information. The advantage of the ^{18}F-Choline PET/4DCT protocol over ^{18}F-Choline PET/CT is that it provides an arterial phase image, which often eases segmentation of the PA and surrounding structures. This segmentation can be used to construct 3D models to guide the surgeon in the search for the PA, which the surgeons at the Rijnstate Hospital found very useful. In addition, PAs without strong choline uptake may show a rapid wash-in of the iodinated contrast agent, making it still possible to locate the PA.

Magnetic resonance imaging (MRI) is not frequently used as pre-operative imaging modality for PA localisation due to motion artefacts, a low signal-to-noise ratio and suboptimal fat saturation. However, newer MRI technologies and the use of stronger magnets are able to overcome the initial challenges

of PA imaging, resulting in reported sensitivity and specificity values greater than 90% [49], [50], [51]. Diagnostic performance has improved particularly since the introduction of four-dimensional MRI (4DMRI). This technique is similar to 4DCT, in that a contrast agent is used to capture the enhancement kinetics of the PA. Unlike 4DCT, 4DMRI does not involve ionising radiation, which is a clear advantage. The anatomical information and enhancement kinetics of 4DMRI can also be combined with ^{18}F-Choline PET to further increase the sensitivity and specificity of PA localisation. ^{18}F-Choline PET/4DMRI shows promising results as a 'one-stop shop' preoperative imaging modality [52]. However, there are notable drawbacks, including the high cost and limited availability of PET/MR systems, the relatively long scan time and the discomfort that some patients experience with MRI. In addition, the pilot study on ^{18}F-Choline PET/4DCT demonstrated an acceptable patient effective dose, even lower than 4DCT protocols reported in the literature. Therefore, to the best of our knowledge, the benefits of switching to ^{18}F-Choline PET/4DMRI are unlikely to outweigh the challenges.

In the future, the 4DCT and ^{18}F-Choline PET/4DCT protocols may be further optimised to improve PA localisation performance and reduce radiation dose. Further optimisation of the 4DCT protocol could be sought in virtual non-contrast (VNC) imaging by using material decomposition based on more than three materials. VNC images can be reconstructed from a contrast-enhanced image by scanning on dual-energy CT (DECT) scanners. DECT is based on the acquisition or detection of two photon spectra, one high energy and one low energy. This allows material decomposition based on low and high kVp attenuation of two or three materials such as iodine, water and calcium. A study by Leiva-Salinas et al. showed that the performance metrics for PA localisation with VNC images and arterial phase images were comparable to those for the combination of true non-contrast and arterial phase images [53]. A previous study at the Rijnstate Hospital on VNC imaging in PAs offered less perspective due to the almost complete removal of intrinsic iodine in the thyroid gland. Because of this removal, the PA could not be distinguished from the thyroid gland on the VNC image. After presenting these findings to people within Philips, they came up with the idea to investigate whether a four-material decomposition technique would lead to better results from the VNC algorithm. The intrinsic iodine in the thyroid might then be better separated from the extrinsic iodine in the thyroid. Future research could demonstrate whether four-material decomposition preserves the intrinsic iodine in the thyroid, resulting in VNC images that are closer to the true non-contrast images. This would provide opportunities to further reduce the radiation dose in the proposed 4DCT protocols.

Further optimisation of the ^{18}F-Choline PET/4DCT protocol in terms of image quality and radiation dose could be sought by investigating the recommendations suggested in Chapter 5: increasing slice thickness, omitting the low-dose non-contrast CT scan prior to the PET scan and gaining a better understanding of the CARE Dose kV algorithm. The image quality should be comparable to the 4DCT

protocol, while the radiation dose should ideally not exceed that of the 4DCT protocol. Once the ^{18}F-Choline PET/4DCT protocol has been optimised in terms of image quality and radiation dose, it is proposed to scan at least thirty patients to establish a database of patients scanned with the same ^{18}F-Choline PET/4DCT protocol with histopathological confirmation of a PA after surgery. This is necessary for a future MRMC study to compare the ^{18}F-Choline PET/4DCT protocol with the 4DCT and ^{18}F-Choline PET/CT protocols in terms of PA localisation. A cost-effectiveness study can then be conducted to determine whether this 'one-stop shop' examination is cost-effective in clinical practice. The hypothesis is that radiologists and nuclear medicine physicians will locate the PA more quickly and with greater certainty using the ^{18}F-Choline PET/4DCT protocol compared to the 4DCT and ^{18}F-Choline PET/CT protocols, and that it will also be cost-effective because fewer examinations are required to locate the PA with certainty.

In conclusion, the goal of this research was to develop the optimal localisation protocol for patients with a suspected PA in terms of the number of examinations, the lowest possible total radiation dose and the highest localisation accuracy. The 4DCT multireader, multicase (MRMC) study demonstrated that it is possible to reduce the number of phases in the 4DCT protocol from four to three, while maintaining localisation accuracy. For experienced 4DCT radiologists, the number of phases could be further reduced to a two-phase 4DCT protocol, halving the radiation dose compared to the current four-phase 4DCT protocol. 4DCT is widely available and, with the reduction in radiation dose, is a good alternative to cervical ultrasonography (US) and ^{99m}Tc-Sestamibi SPECT (Tc-MIBI) in the first stage of PA localisation. In addition, the pilot study on the ^{18}F-Choline PET/4DCT protocol has shown that it could be a promising 'one-stop shop' alternative for the benefit of the patient and the hospital. While ^{18}F-Choline PET/CT is not available in every hospital, where it is, it could potentially provide even better PA localisation than 4DCT. Future research should determine the performance of PA localisation with the ^{18}F-Choline PET/4DCT protocol, and also investigate its cost-effectiveness. Ultimately, ^{18}F-Choline PET/4DCT has the potential to meet the objectives of this study by providing a highly accurate, low-radiation, and 'one-stop shop' solution for PA localisation, thereby improving patient care and hospital workflow.

References

[1] M. Itani and W. D. Middleton, 'Parathyroid Imaging', *Radiol Clin North Am*, vol. 58, no. 6, pp. 1071–1083, Nov. 2020, doi: 10.1016/J.RCL.2020.07.006.

[2] B. Pokhrel, S. W. Leslie, and S. N. Levine, 'Primary Hyperparathyroidism', *A Case-Based Guide to Clinical Endocrinology, Third Edition*, pp. 201–209, Mar. 2024, doi: 10.1007/978-3-030-84367-0_21.

[3] J. M. Ruda, C. S. Hollenbeak, and B. C. Stack, 'A systematic review of the diagnosis and treatment of primary hyperparathyroidism from 1995 to 2003', *http://dx.doi.org/10.1016/j.otohns.2004.10.005*, vol. 132, no. 3, pp. 359–372, Mar. 2005, doi: 10.1016/J.OTOHNS.2004.10.005.

[4] M. W. Yeh *et al.*, 'Incidence and Prevalence of Primary Hyperparathyroidism in a Racially Mixed Population', *J Clin Endocrinol Metab*, vol. 98, no. 3, p. 1122, Mar. 2013, doi: 10.1210/JC.2012-4022.

[5] P. M. Bunch, G. W. Randolph, J. A. Brooks, V. George, J. Cannon, and H. R. Kelly, 'Parathyroid 4D CT: What the Surgeon Wants to Know', *Radiographics*, vol. 40, no. 5, pp. 1383–1394, Sep. 2020, doi: 10.1148/RG.2020190190.

[6] A. M. Laird and S. K. Libutti, 'Minimally Invasive Parathyroidectomy Versus Bilateral Neck Exploration for Primary Hyperparathyroidism', *Surg Oncol Clin N Am*, vol. 25, no. 1, pp. 103–118, Jan. 2016, doi: 10.1016/J.SOC.2015.08.012.

[7] R. D. Rosen and B. Bordoni, 'Embryology, Parathyroid', *StatPearls*, May 2023, Accessed: Aug. 13, 2024. [Online]. Available: https://www.ncbi.nlm.nih.gov/books/NBK554580/

[8] G. Noussios, P. Anagnostis, and K. Natsis, 'Ectopic parathyroid glands and their anatomical, clinical and surgical implications', *Experimental and Clinical Endocrinology and Diabetes*, vol. 120, no. 10, pp. 604–610, 2012, doi: 10.1055/S-0032-1327628/ID/R01-2012-0037-ENDO-0021/BIB.

[9] R. Phitayakorn and C. R. McHenry, 'Incidence and location of ectopic abnormal parathyroid glands', *The American Journal of Surgery*, vol. 191, no. 3, pp. 418–423, Mar. 2006, doi: 10.1016/J.AMJSURG.2005.10.049.

[10] J. K. Hoang, W. K. Sung, M. Bahl, and C. D. Phillips, 'How to Perform Parathyroid 4D CT: Tips and Traps for Technique and Interpretation', *https://doi.org/10.1148/radiol.13122661*, vol. 270, no. 1, pp. 15–24, Jan. 2014, doi: 10.1148/RADIOL.13122661.

[11] M. A. Morris *et al.*, 'Parathyroid Imaging: Past, Present, and Future', *Front Endocrinol (Lausanne)*, vol. 12, p. 760419, Feb. 2022, doi: 10.3389/FENDO.2021.760419/BIBTEX.

[12] M. Zafereo *et al.*, 'American Head and Neck Society Endocrine Surgery Section update on parathyroid imaging for surgical candidates with primary hyperparathyroidism', *Head Neck*, vol. 41, no. 7, pp. 2398–2409, Jul. 2019, doi: 10.1002/HED.25781.

[13] M. C. de Jong *et al.*, 'The use of computed tomography as a first-line imaging modality in patients with primary hyperparathyroidism', *Hormones*, vol. 20, no. 3, pp. 499–506, Sep. 2021, doi: 10.1007/S42000-020-00205-X/TABLES/3.

[14] W. A. E. Elsayed and R. A. Ali, 'Efficacy of Scintigraphy, Ultrasound and Both Scintigraphy and Ultrasonography in Preoperative Detection and Localization of Primary Hyperparathyroidism', *Cureus*, vol. 11, no. 6, Jun. 2019, doi: 10.7759/CUREUS.4960.

[15] M. J. O'Doherty, A. G. Kettle, P. Wells, R. E. C. Collins, and A. J. Coakley, 'Parathyroid Imaging with Technetium-99m-Sestamibi: Preoperative Localization and Tissue Uptake Studies', *Journal of Nuclear Medicine*, vol. 33, no. 3, pp. 313–318, Mar. 1992, Accessed: Aug. 13, 2024. [Online]. Available: https://jnm.snmjournals.org/content/33/3/313

[16] T. Ekjeen and A. Chaichana, 'Dual-tracer subtraction parathyroid SPECT using Tc-99m pertechnetate and Tc-99m MIBI', *J Phys Conf Ser*, vol. 1248, no. 1, p. 012036, Jun. 2019, doi: 10.1088/1742-6596/1248/1/012036.

[17] J. P. Krol, T. Veerbeek, L. N. Deden, F. B. M. Joosten, C. H. Slump, and W. J. G. Oyen, 'Preoperative imaging in primary hyperparathyroidism patients using 4DCT subtraction maps, a report of three cases.', *Radiol Case Rep*, vol. 18, no. 8, pp. 2814–2822, Jun. 2023, doi: 10.1016/J.RADCR.2023.05.019.

[18] M. Kukar *et al.*, 'The use of modified four-dimensional computed tomography in patients with primary hyperparathyroidism: an argument for the abandonment of routine sestamibi single-positron emission computed tomography (SPECT)', *Ann Surg Oncol*, vol. 22, no. 1, pp. 139–145, 2015, doi: 10.1245/S10434-014-3940-Y.

[19] G. Treglia *et al.*, 'Diagnostic performance of choline PET for detection of hyperfunctioning parathyroid glands in hyperparathyroidism: a systematic review and meta-analysis', *Eur J Nucl Med Mol Imaging*, vol. 46, no. 3, pp. 751–765, Mar. 2019, doi: 10.1007/S00259-018-4123-Z.

[20] T. Ishizuka *et al.*, 'Phospholipid/Ca2+-dependent Protein Kinase Activity in Human Parathyroid Adenoma', vol. 34, no. 6, pp. 965–968, 1987.

[21] W. A. M. Broos, M. Wondergem, R. J. J. Knol, and F. M. van der Zant, 'Parathyroid imaging with 18F-fluorocholine PET/CT as a first-line imaging modality in primary hyperparathyroidism: a retrospective cohort study', *EJNMMI Res*, vol. 9, no. 1, pp. 1–7, Dec. 2019, doi: 10.1186/S13550-019-0544-3/TABLES/2.

[22] E. Ballester Vázquez *et al.*, 'Identification of Occult Adenomas in Primary Hyperparathyroidism With 18F-Fluorocholine PET/CT', *Cirugía Española (English Edition)*, vol. 98, no. 7, pp. 395–402, Aug. 2020, doi: 10.1016/J.CIRENG.2020.07.014.

[23] L. Evangelista *et al.*, '18F-choline PET/CT and PET/MRI in primary and recurrent hyperparathyroidism: a systematic review of the literature', *Ann Nucl Med*, vol. 34, no. 9, pp. 601–619, Sep. 2020, doi: 10.1007/S12149-020-01507-1/TABLES/5.

[24] M. Bahl, A. R. Sepahdari, J. A. Sosa, and J. K. Hoang, 'Parathyroid Adenomas and Hyperplasia on Four-dimensional CT Scans: Three Patterns of Enhancement Relative to the Thyroid Gland Justify a Three-Phase Protocol', *Radiology*, vol. 277, no. 2, pp. 454–462, Nov. 2015, doi: 10.1148/RADIOL.2015142393.

[25] W. P. Kluijfhout *et al.*, 'Diagnostic performance of computed tomography for parathyroid adenoma localization; a systematic review and meta-analysis', *Eur J Radiol*, vol. 88, pp. 117–128, Mar. 2017, doi: 10.1016/J.EJRAD.2017.01.004.

[26] S. E. Rodgers *et al.*, 'Improved preoperative planning for directed parathyroidectomy with 4-dimensional computed tomography', *Surgery*, vol. 140, no. 6, pp. 932–941, Dec. 2006, doi: 10.1016/J.SURG.2006.07.028.

[27] A. Mahajan, L. F. Starker, M. Ghita, R. Udelsman, J. A. Brink, and T. Carling, 'Parathyroid four-dimensional computed tomography: Evaluation of radiation dose exposure during preoperative localization of parathyroid tumors in primary hyperparathyroidism', *World J Surg*, vol. 36, no. 6, pp. 1335–1339, Jun. 2012, doi: 10.1007/S00268-011-1365-3/TABLES/3.

[28] L. Giovanella, L. Bacigalupo, G. Treglia, and A. Piccardo, 'Will 18F-fluorocholine PET/CT replace other methods of preoperative parathyroid imaging?', *Endocrine*, vol. 71, no. 2, pp. 285–297, Feb. 2021, doi: 10.1007/S12020-020-02487-Y.

[29] J. L. Chazen, A. Gupta, A. Dunning, and C. D. Phillips, 'Diagnostic accuracy of 4D-CT for parathyroid adenomas and hyperplasia', *AJNR Am J Neuroradiol*, vol. 33, no. 3, pp. 429–433, Mar. 2012, doi: 10.3174/AJNR.A2805.

[30] P. Raghavan *et al.*, 'Dynamic CT for Parathyroid Disease: Are Multiple Phases Necessary?', *AJNR Am J Neuroradiol*, vol. 35, no. 10, p. 1959, Oct. 2014, doi: 10.3174/AJNR.A3978.

[31] G. J. Hunter, D. T. Ginat, H. R. Kelly, E. F. Halpern, and L. M. Hamberg, 'Discriminating parathyroid adenoma from local mimics by using inherent tissue attenuation and vascular information obtained with four-dimensional CT: Formulation of a multinomial logistic regression model', *Radiology*, vol. 270, no. 1, pp. 168–175, Jan. 2014, doi: 10.1148/RADIOL.13122851/SUPPL_FILE/RADIOL.13122851.SUPPL.

[32] S. Klein, M. Staring, K. Murphy, M. A. Viergever, and J. P. W. Pluim, 'Elastix: A toolbox for intensity-based medical image registration', *IEEE Trans Med Imaging*, vol. 29, no. 1, pp. 196–205, Jan. 2010, doi: 10.1109/TMI.2009.2035616.

[33] C. Boncelet, 'Image Noise Models', *Handbook of Image and Video Processing, Second Edition*, pp. 397–409, Jan. 2005, doi: 10.1016/B978-012119792-6/50087-5.

[34] E. Pessis *et al.*, 'Virtual Monochromatic Spectral Imaging with Fast Kilovoltage Switching: Reduction of Metal Artifacts at CT', *https://doi.org/10.1148/rg.332125124*, vol. 33, no. 2, pp. 573–583, Mar. 2013, doi: 10.1148/RG.332125124.

[35] F. Esmaeili, M. Johari, P. Haddadi, and M. Vatankhah, 'Beam Hardening Artifacts: Comparison between Two Cone Beam Computed Tomography Scanners', *J Dent Res Dent Clin Dent Prospects*, vol. 6, no. 2, p. 49, 2012, doi: 10.5681/JODDD.2012.011.

[36] Y. Nakashima and T. Nakano, 'Optimizing contrast agents with respect to reducing beam hardening in nonmedical X-ray computed tomography experiments', *J Xray Sci Technol*, vol. 22, pp. 91–103, 2014, doi: 10.3233/XST-130411.

[37] M. C. de Jong *et al.*, 'The use of computed tomography as a first-line imaging modality in patients with primary hyperparathyroidism', *Hormones (Athens)*, vol. 20, no. 3, pp. 499–506, Sep. 2021, doi: 10.1007/S42000-020-00205-X.

[38] D. Leong, K. Ng, R. Boeddinghaus, and D. Lisewski, 'Three-phase four-dimensional computed tomography as a first-line investigation in primary hyperparathyroidism', *ANZ J Surg*, vol. 91, no. 9, pp. 1798–1803, Sep. 2021, doi: 10.1111/ANS.16924.

[39] J. P. Krol, F. B. M. Joosten, H. de Boer, M. L. E. Bernsen, C. H. Slump, and W. J. G. Oyen, 'Four-dimensional computed tomography as first-line imaging in primary hyperparathyroidism, a retrospective comparison to conventional imaging in a predominantly single adenoma population', *EJNMMI Reports*, vol. 8, no. 1, May 2024, doi: 10.1186/S41824-024-00198-5.

[40] B. D. Gallas, A. Bandos, F. W. Samuelson, and R. F. Wagner, 'A Framework for Random-Effects ROC Analysis: Biases with the Bootstrap and Other Variance Estimators', *Communications in Statistics—Theory and Methods*, vol. 38, no. 15, pp. 2586–2603, Sep. 2009, doi: 10.1080/03610920802610084.

[41] W. Chen, N. A. Petrick, and B. Sahiner, 'Hypothesis Testing in Noninferiority and Equivalence MRMC ROC Studies', *Acad Radiol*, vol. 19, no. 9, pp. 1158–1165, Sep. 2012, doi: 10.1016/j.acra.2012.04.011.

[42] A. Piccardo *et al.*, 'Head-to-head comparison among 18F-choline PET/CT, 4D contrast-enhanced CT, and 18F-choline PET/4D contrast-enhanced CT in the detection of hyperfunctioning parathyroid glands: a systematic review and meta-analysis', *Endocrine*, vol. 74, no. 2, pp. 404–412, Nov. 2021, doi: 10.1007/S12020-021-02798-8/TABLES/6.

[43] L. Dolenc, B. Petrinjak, N. Mekiš, and D. Škrk, 'The impact of body mass index on patient radiation dose in general radiography', *Journal of Radiological Protection*, vol. 42, no. 4, p. 041505, Nov. 2022, doi: 10.1088/1361-6498/AC9F1F.

[44] B. M. Gramer *et al.*, 'Impact of iterative reconstruction on CNR and SNR in dynamic myocardial perfusion imaging in an animal model', *Eur Radiol*, vol. 22, no. 12, pp. 2654–2661, Dec. 2012, doi: 10.1007/S00330-012-2525-Z.

[45] M. Alshipli and N. A. Kabir, 'Effect of slice thickness on image noise and diagnostic content of single-source-dual energy computed tomography', *J Phys Conf Ser*, vol. 851, no. 1, p. 012005, May 2017, doi: 10.1088/1742-6596/851/1/012005.

[46] S. Raeymaeckers, Y. De Brucker, T. Vanderhasselt, N. Buls, and J. De Mey, 'Detection of parathyroid adenomas with multiphase 4DCT: towards a true four-dimensional technique', *BMC Med Imaging*, vol. 21, no. 1, p. 64, Dec. 2021, doi: 10.1186/S12880-021-00597-1.

[47] L. W. Goldman, 'Principles of CT: Radiation Dose and Image Quality', *J Nucl Med Technol*, vol. 35, no. 4, pp. 213–225, Dec. 2007, doi: 10.2967/JNMT.106.037846.

[48] N. A. Bebbington, T. Jørgensen, E. Dupont, and M. A. Micheelsen, 'Validation of CARE kV automated tube voltage selection for PET-CT: PET quantification and CT radiation dose reduction in phantoms', *EJNMMI Phys*, vol. 8, no. 1, pp. 1–14, Dec. 2021, doi: 10.1186/S40658-021-00373-8/FIGURES/6.

[49] S. Merchavy, J. Luckman, M. Guindy, Y. Segev, and A. Khafif, '4D MRI for the Localization of Parathyroid Adenoma', *Otolaryngology–Head and Neck Surgery*, vol. 154, no. 3, pp. 446–448, Mar. 2016, doi: 10.1177/0194599815618199.

[50] J. L. Becker *et al.*, '4D–Dynamic Contrast-Enhanced MRI for Preoperative Localization in Patients with Primary Hyperparathyroidism', *American Journal of Neuroradiology*, vol. 41, no. 3, pp. 522–528, Mar. 2020, doi: 10.3174/AJNR.A6482.

[51] R. Argirò *et al.*, 'Diagnostic accuracy of 3T magnetic resonance imaging in the preoperative localisation of parathyroid adenomas: comparison with ultrasound and 99mTc-sestamibi scans', *Eur Radiol*, vol. 28, no. 11, pp. 4900–4908, Nov. 2018, doi: 10.1007/S00330-018-5437-8/FIGURES/4.

[52] W. P. Kluijfhout *et al.*, '18F Fluorocholine PET/MR Imaging in Patients with Primary Hyperparathyroidism and Inconclusive Conventional Imaging: A Prospective Pilot Study', *Radiology*, vol. 284, no. 2, pp. 460–467, Aug. 2017, doi: 10.1148/RADIOL.2016160768.

[53] C. Leiva-Salinas *et al.*, 'Detection of parathyroid adenomas using a monophasic dual-energy computed tomography acquisition: diagnostic performance and potential radiation dose reduction', *Neuroradiology*, vol. 58, no. 11, pp. 1135–1141, Nov. 2016, doi: 10.1007/S00234-016-1736-4/FIGURES/3.

Appendices

Appendix A

Table 7: Analysis of the contrast between the PA and thyroid tissue on the subtraction map and the contrast on the enhancement map for each included patient.

Patient	PA (mean HU)		Thyroid (mean HU)		Contrast on subtraction map	Contrast on enhancement map
	Non-contrast	Arterial	Non-contrast	Arterial		
1	38	122	70	125	29	142
2	39	118	110	188	1	132
3	48	206	87	168	77	236
4	56	203	108	268	-13	114
5	56	110	99	226	-73	-32
6	17	50	98	160	-29	131
7	35	132	50	140	7	97
8	9	53	43	136	-49	273
9	66	156	94	151	33	76
10	64	112	84	198	-66	-61
11	32	87	68	186	-63	-2
12	34	62	160	234	-46	36
13	75	192	115	230	2	56
14	49	175	100	195	31	162
15	40	160	121	193	48	240
16	79	200	100	220	1	33
17	65	185	75	237	-42	-31
18	29	189	81	210	31	392
19	57	222	103	249	19	148
20	66	187	96	199	18	76
21	69	123	136	240	-50	2
22	44	148	84	243	-55	47
23	10	165	76	231	0	1346
24	43	185	85	230	-3	160
25	79	150	91	213	-51	-44
26	16	73	89	227	-81	201
27	24	169	93	237	1	449

Appendix B

Table 8: Baseline characteristics of the data.

Patient	Gender	Age	Weight	Nr. of adenomas	Adenoma location	Adenoma size (mm)	PTH (pre-op – post-op)
1	V	60	72	1	Bottom left	6	12.4 – 2.2
2	M	53	88	1	Bottom left	9	15.1 – 2.2
3	M	54	67	2	Upper left & bottom right	5 & 20	52.1 – 8.4
4	V	60	66	2	Bottom left & bottom right	9 & 11	11.8 – 4.9
5	V	24	118	1	Upper right	7	21.8 – 1.9
6	V	76	75	1	Bottom left	14	19.3 – 2.9
7	V	58	126	1	Bottom left	8	23.8 – 3.6
8	V	46	80	1	Bottom left	13	8.1 – 3.4
9	V	61	62	1	Bottom right	6	17.7 – 3.0
10	V	47	80	1	Bottom right	13	9.6 – 2.8
11	V	60	69	1	Bottom right	15	72.8 – 27.2
12	M	74	90	1	Bottom right	30	81.0 – 16.4
13	V	57	69	1	Bottom right	7	14.7 – 2.4
14	V	76	55	1	Bottom left	18	15.7 – 2.9
15	V	75	53	1	Upper left	13	15.3 – 5.5
16	M	51	84	1	Bottom left	5	16.8 – 1.5
17	V	69	62	1	Bottom left	5	23.9 – 3.3
18	V	66	59	1	Bottom left	16	9.7 – 2.3
19	V	63	44	1	Upper left	13	37.5 – 4.0
20	V	67	77	1	Ectopic	9	7.0 – 4.1
21	M	53	76	2	Bottom left & bottom right	11 & 13	65.5 – 8.8
22	V	58	68	1	Bottom left	45	41.5 – 6.6
23	V	67	90	1	Bottom right	6	17.0 – 3.2
24	V	67	68	1	Bottom right	6	17.5 – 2.3
25	V	46	64	1	Upper left	10	15.3 – 1.8
26	V	76	47	1	Ectopic	5	29.7 – 4.9
27	V	69	67	1	Ectopic	30	16.4 – 3.5
28	V	56	71	0			
29	V	69	73	0			
30	V	70	55	0			

Appendix C

These tables show the sensitivity, specificity and AUC of each reader in each round. The colours next to the readers indicate to which group they belong. A blue colour indicates that this reader belongs to the experienced 4DCT group, whereas a red colour indicates that this reader had little to no experience with 4DCT. There is also a figure showing the mean sensitivity, specificity and AUC in each round, together with the sensitivity, specificity and AUC for each reader.

Table 9: Empirical AUC values of individual readers in every round. The 95% CI is shown in brackets.

		Round 1	Round 2	Round 3	Round 4	Round 5
	Reader 01	0.87	0.85	0.81	0.79	0.81
	Reader 02	0.78	0.75	0.77	0.80	0.74
	Reader 03	0.88	0.85	0.90	0.95	0.86
	Reader 04	0.78	0.75	0.78	0.82	0.81
	Reader 05	0.78	0.72	0.78	0.71	0.68
	Reader 06	0.71	0.80	0.66	0.85	0.67
	Reader 07	0.83	0.80	0.78	0.80	0.80
	Reader 08	0.90	0.81	0.82	0.81	0.83
	Reader 09	0.85	0.86	0.87	0.89	0.85
	Reader 10	0.76	0.79	0.81	0.84	0.89
	Reader 11	0.86	0.85	0.75	0.87	0.80
	Reader 12	0.94	0.92	0.90	0.94	0.93
	Reader 13	0.73	0.73	0.78	0.84	0.82
	Mean	**0.82** (0.76, 0.88)	**0.81** (0.74, 0.87)	**0.80** (0.73, 0.86)	**0.84** (0.78, 0.90)	**0.81** (0.75, 0.87)

		Sensitivity					Specificity				
		Round 1	Round 2	Round 3	Round 4	Round 5	Round 1	Round 2	Round 3	Round 4	Round 5
	Reader 01	0.77 (0.58, 0.90)	0.73 (0.54, 0.88)	0.67 (0.47, 0.83)	0.60 (0.41, 0.77)	0.63 (0.44, 0.80)	0.96 (0.91, 0.99)	0.95 (0.89, 0.98)	0.94 (0.88, 0.98)	0.97 (0.93, 0.99)	0.99 (0.95, 1.00)
	Reader 02	0.60 (0.41, 0.77)	0.53 (0.34, 0.72)	0.60 (0.41, 0.77)	0.63 (0.44, 0.80)	0.50 (0.31, 0.69)	0.93 (0.87, 0.97)	0.96 (0.91, 0.99)	0.93 (0.87, 0.97)	0.97 (0.92, 0.99)	0.97 (0.92, 0.99)
	Reader 03	0.77 (0.58, 0.90)	0.73 (0.54, 0.88)	0.80 (0.61, 0.92)	0.90 (0.73, 0.98)	0.73 (0.54, 0.88)	0.95 (0.89, 0.98)	0.95 (0.89, 0.98)	0.99 (0.95, 1.00)	0.98 (0.94, 1.00)	0.97 (0.92, 0.99)
	Reader 04	0.67 (0.47, 0.83)	0.53 (0.34, 0.72)	0.63 (0.44, 0.80)	0.67 (0.47, 0.83)	0.63 (0.44, 0.80)	0.88 (0.81, 0.93)	0.97 (0.92, 0.99)	0.93 (0.87, 0.97)	0.97 (0.93, 0.99)	0.97 (0.92, 0.99)
	Reader 05	0.67 (0.47, 0.83)	0.47 (0.28, 0.66)	0.60 (0.41, 0.77)	0.43 (0.25, 0.63)	0.37 (0.20, 0.56)	0.85 (0.77, 0.91)	0.97 (0.92, 0.99)	0.95 (0.89, 0.98)	0.97 (0.93, 0.99)	0.99 (0.95, 1.00)
	Reader 06	0.47 (0.28, 0.66)	0.63 (0.44, 0.80)	0.40 (0.23, 0.59)	0.73 (0.54, 0.88)	0.43 (0.25, 0.63)	0.92 (0.86, 0.97)	0.95 (0.89, 0.98)	0.88 (0.81, 0.93)	0.96 (0.91, 0.99)	0.90 (0.83, 0.95)
	Reader 07	0.67 (0.47, 0.83)	0.63 (0.44, 0.80)	0.60 (0.41, 0.77)	0.63 (0.44, 0.80)	0.63 (0.44, 0.80)	0.97 (0.93, 0.99)	0.97 (0.93, 0.99)	0.94 (0.88, 0.98)	0.97 (0.92, 0.99)	0.97 (0.92, 0.99)
	Reader 08	0.80 (0.61, 0.92)	0.63 (0.44, 0.80)	0.67 (0.47, 0.83)	0.63 (0.44, 0.80)	0.67 (0.47, 0.83)	0.97 (0.93, 0.99)	0.97 (0.93, 0.99)	0.95 (0.89, 0.98)	0.97 (0.93, 0.99)	0.99 (0.95, 1.00)
	Reader 09	0.73 (0.54, 0.88)	0.73 (0.54, 0.88)	0.80 (0.61, 0.92)	0.80 (0.61, 0.92)	0.73 (0.54, 0.88)	0.94 (0.88, 0.98)	0.98 (0.94, 1.00)	0.91 (0.84, 0.95)	0.98 (0.94, 1.00)	0.96 (0.91, 0.99)
	Reader 10	0.53 (0.34, 0.72)	0.60 (0.41, 0.77)	0.67 (0.47, 0.83)	0.70 (0.51, 0.85)	0.80 (0.61, 0.92)	0.95 (0.89, 0.98)	0.98 (0.94, 1.00)	0.94 (0.88, 0.98)	0.97 (0.93, 0.99)	0.97 (0.92, 0.99)
	Reader 11	0.77 (0.58, 0.90)	0.73 (0.54, 0.88)	0.53 (0.34, 0.72)	0.77 (0.58, 0.90)	0.63 (0.44, 0.80)	0.94 (0.88, 0.98)	0.94 (0.88, 0.98)	0.94 (0.88, 0.98)	0.96 (0.91, 0.99)	0.94 (0.88, 0.98)
	Reader 12	0.90 (0.73, 0.98)	0.87 (0.69, 0.96)	0.83 (0.65, 0.94)	0.90 (0.73, 0.98)	0.87 (0.69, 0.96)	0.92 (0.86, 0.97)	0.97 (0.92, 0.99)	0.93 (0.87, 0.97)	0.96 (0.91, 0.99)	0.97 (0.92, 0.99)
	Reader 13	0.50 (0.31, 0.69)	0.50 (0.31, 0.69)	0.57 (0.37, 0.75)	0.70 (0.51, 0.85)	0.67 (0.47, 0.83)	0.96 (0.91, 0.99)	0.96 (0.91, 0.99)	0.98 (0.94, 1.00)	0.98 (0.94, 1.00)	0.96 (0.91, 0.99)
	Mean	**0.68** (0.63, 0.73)	**0.64** (0.59, 0.69)	**0.64** (0.59, 0.69)	**0.70** (0.65, 0.75)	**0.64** (0.59, 0.69)	**0.94** (0.92, 0.95)	**0.96** (0.95, 0.97)	**0.94** (0.93, 0.95)	**0.97** (0.96, 0.98)	**0.96** (0.95, 0.97)

Table 10: Sensitivity and specificity of each reader in every round. The 95% CI is shown in brackets.

Figure 24: Mean sensitivity, specificity and AUC with 95% CI in every round. Sensitivity and specificity of individual readers are also shown to the right of the mean values. (A) Sensitivity over all radiologists, (B) Sensitivity for both groups, (C) Specificity over all radiologists, (D) Specificity for both groups, (E) AUC over all radiologists and (F) AUC for both groups.

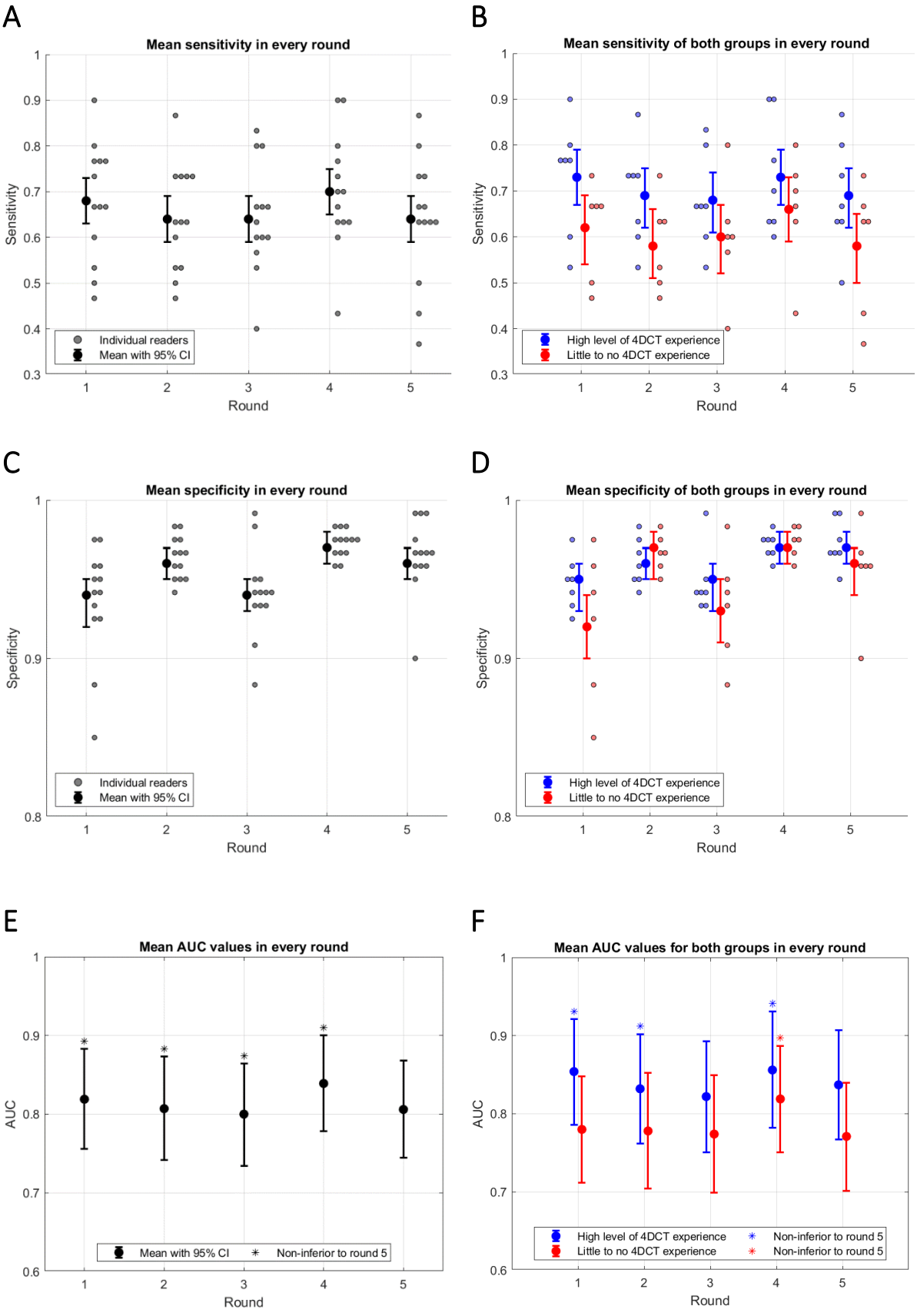

Appendix D

Table 11: Test for equality to see if both groups achieve significantly different scores in AUC, for each round.

	Round 1	Round 2	Round 3	Round 4	Round 5
AUC of experienced 4DCT group	0.85 (0.79, 0.92)	0.83 (0.76, 0.90)	0.82 (0.75, 0.89)	0.86 (0.78, 0.93)	0.84 (0.77, 0.91)
AUC of less experienced 4DCT group	0.78 (0.71, 0.85)	0.78 (0.70, 0.85)	0.77 (0.70, 0.85)	0.82 (0.75, 0.89)	0.77 (0.70, 0.84)
ΔAUC	0.07 (0.00, 0.15)	0.05 (-0.01, 0.12)	0.05 (-0.03, 0.13)	0.04 (-0.04, 0.12)	0.07 (-0.02, 0.15)
P value	0.048	0.095	0.211	0.317	0.122
Outcome	Difference	No difference	No difference	No difference	No difference

Appendix E

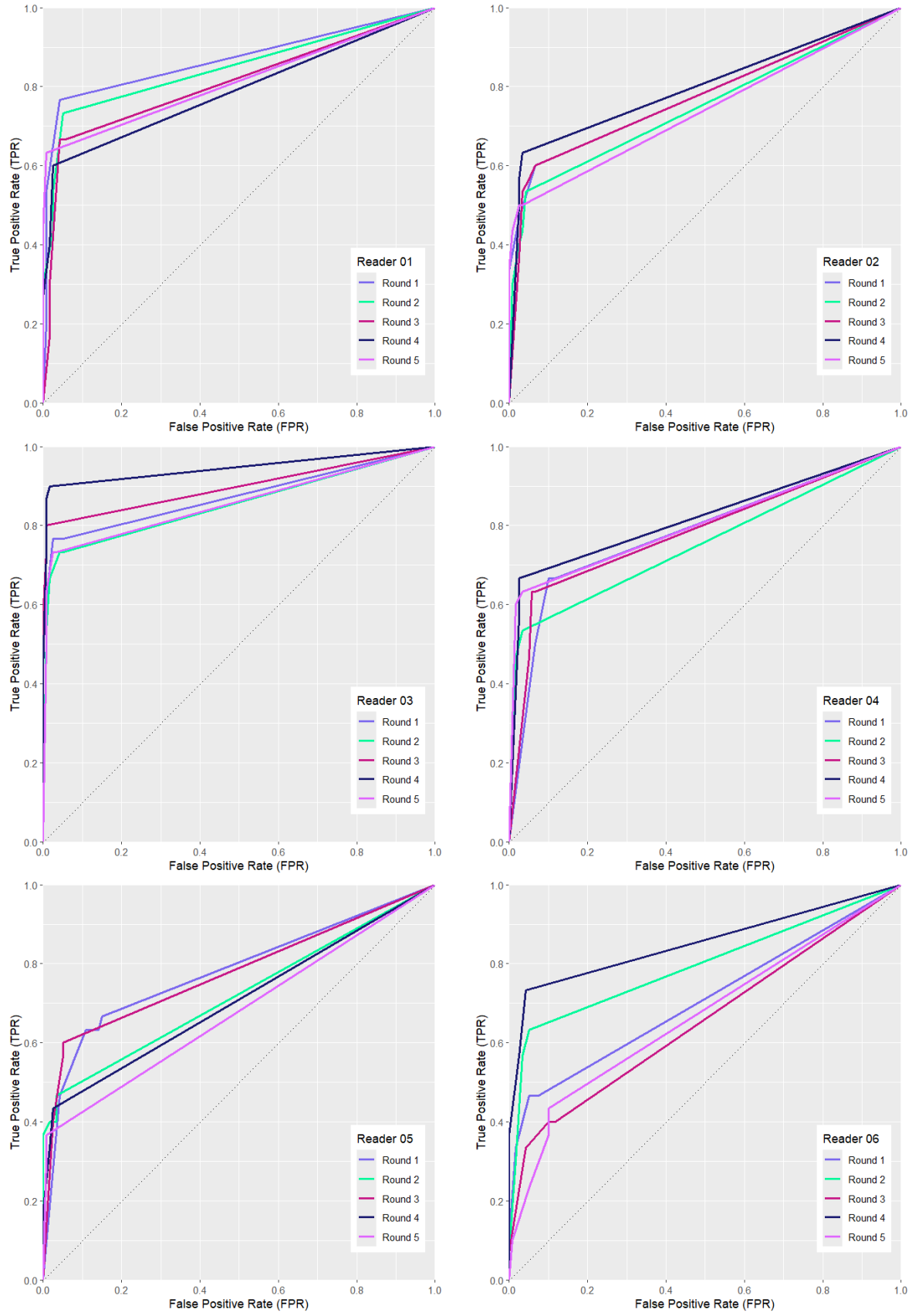
True Positive Rate (TPR)
False Positive Rate (FPR)
0.0
0.2
0.4
0.6
0.8
1.0
Reader 01
Round 1
Round 2
Round 3
Round 4
Round 5
Reader 02
Reader 03
Reader 04
Reader 05
Reader 06

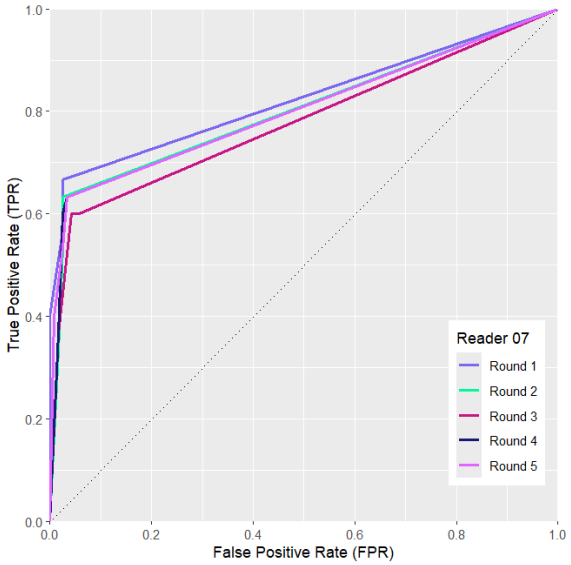
True Positive Rate (TPR)
False Positive Rate (FPR)
Reader 07
Round 1
Round 2
Round 3
Round 4
Round 5

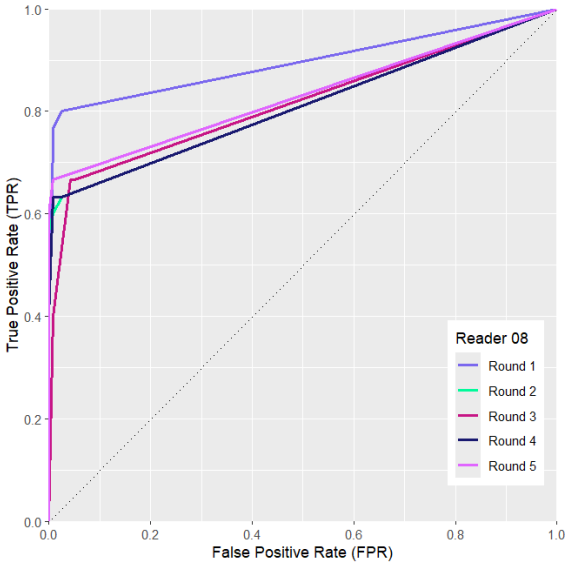
True Positive Rate (TPR)
False Positive Rate (FPR)
Reader 08
Round 1
Round 2
Round 3
Round 4
Round 5

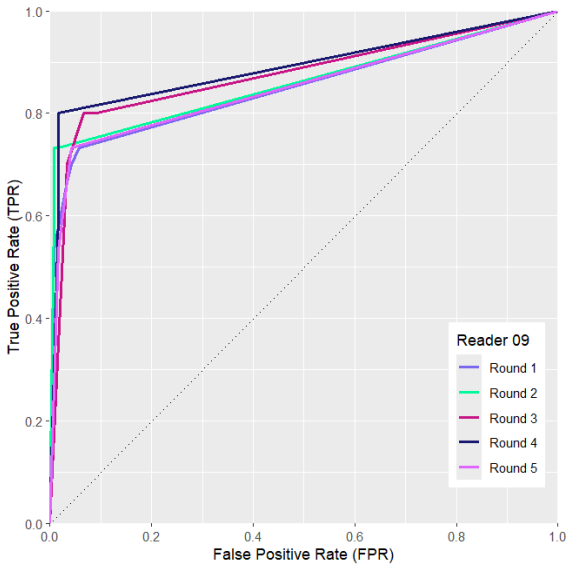
True Positive Rate (TPR)
False Positive Rate (FPR)
Reader 09
Round 1
Round 2
Round 3
Round 4
Round 5

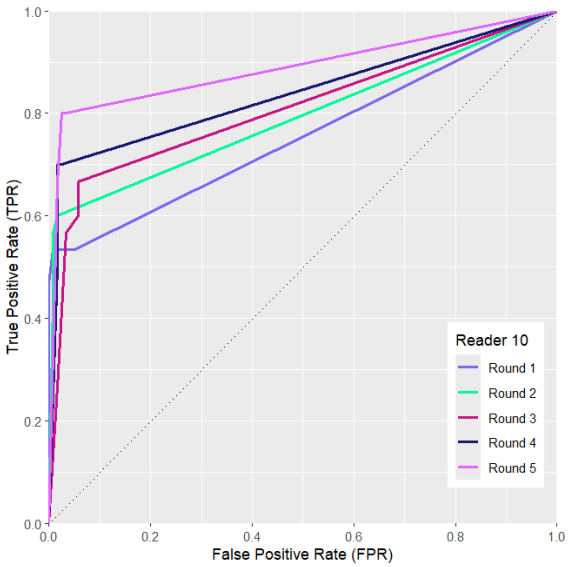
True Positive Rate (TPR)
False Positive Rate (FPR)
Reader 10
Round 1
Round 2
Round 3
Round 4
Round 5

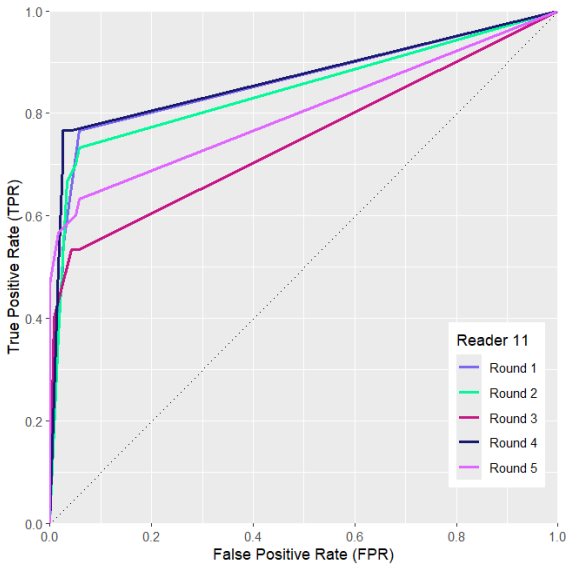
True Positive Rate (TPR)
False Positive Rate (FPR)
Reader 11
Round 1
Round 2
Round 3
Round 4
Round 5

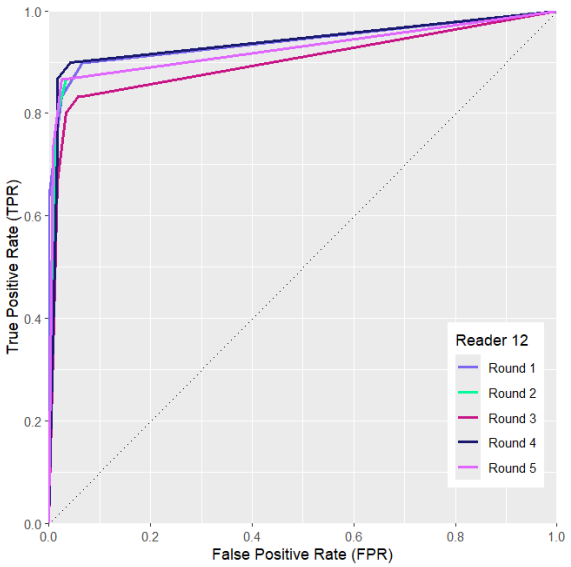
True Positive Rate (TPR)
False Positive Rate (FPR)
Reader 12
Round 1
Round 2
Round 3
Round 4
Round 5

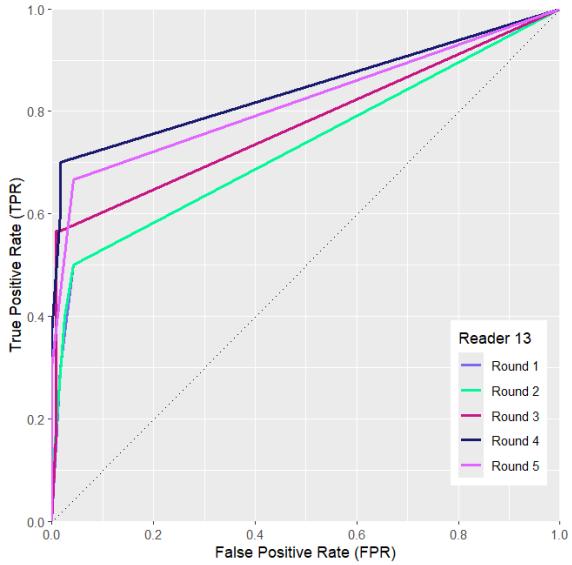
True Positive Rate (TPR)
False Positive Rate (FPR)
0.0
0.2
0.4
0.6
0.8
1.0
Reader 13
Round 1
Round 2
Round 3
Round 4
Round 5

Appendix F

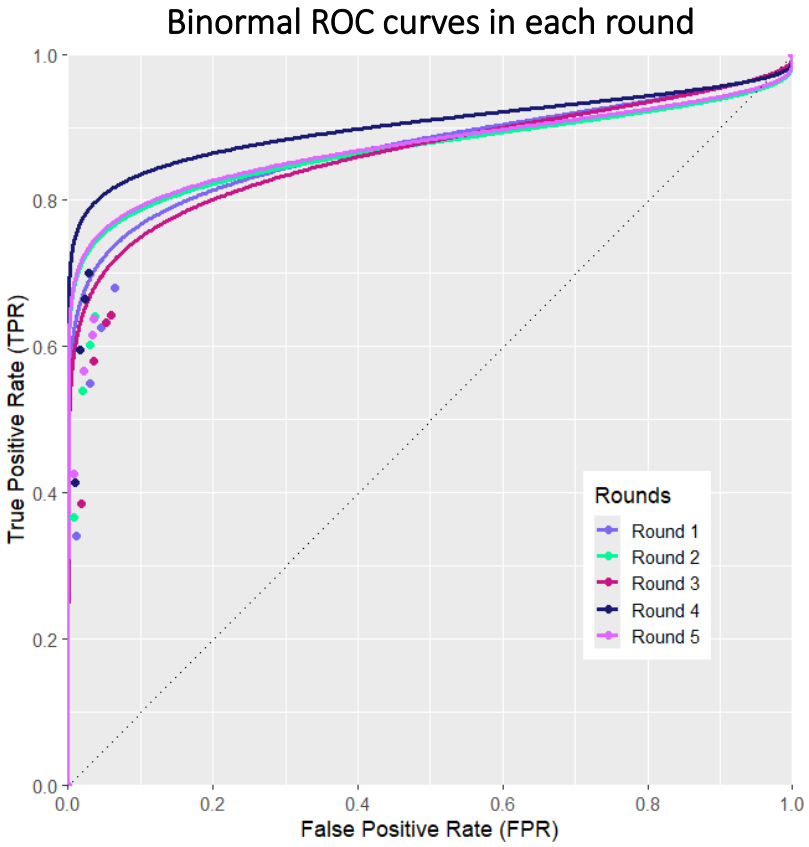
Binormal ROC curves in each round
True Positive Rate (TPR)
False Positive Rate (FPR)
0.0
0.2
0.4
0.6
0.8
1.0
Rounds
Round 1
Round 2
Round 3
Round 4
Round 5

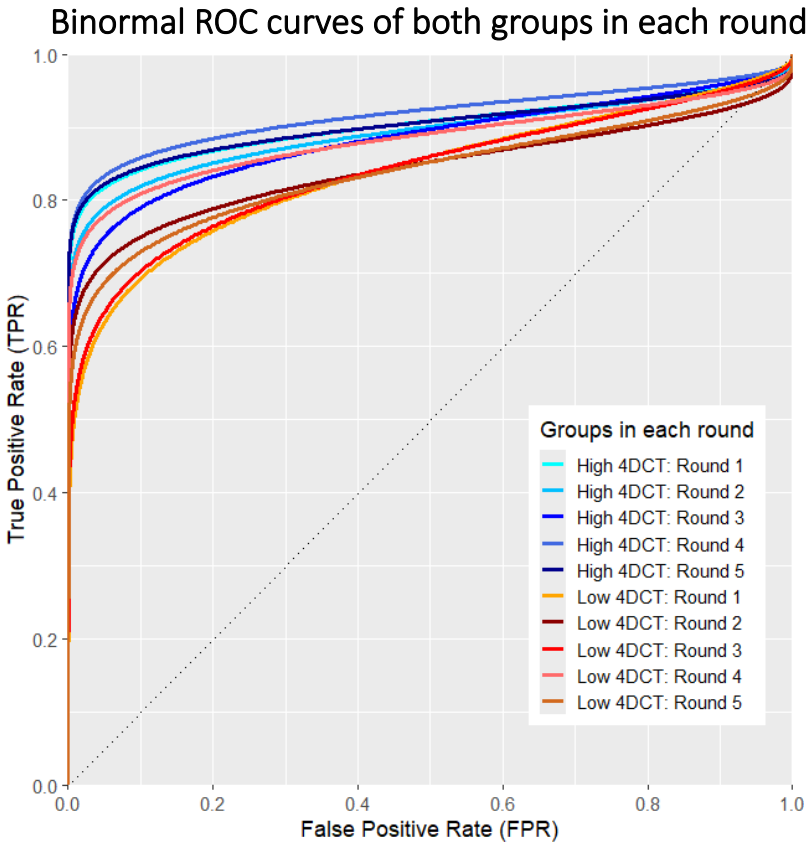
Binormal ROC curves of both groups in each round
True Positive Rate (TPR)
False Positive Rate (FPR)
0.0
0.2
0.4
0.6
0.8
1.0
Groups in each round
High 4DCT: Round 1
High 4DCT: Round 2
High 4DCT: Round 3
High 4DCT: Round 4
High 4DCT: Round 5
Low 4DCT: Round 1
Low 4DCT: Round 2
Low 4DCT: Round 3
Low 4DCT: Round 4
Low 4DCT: Round 5

Binormal ROC curves of each radiologist in round 1

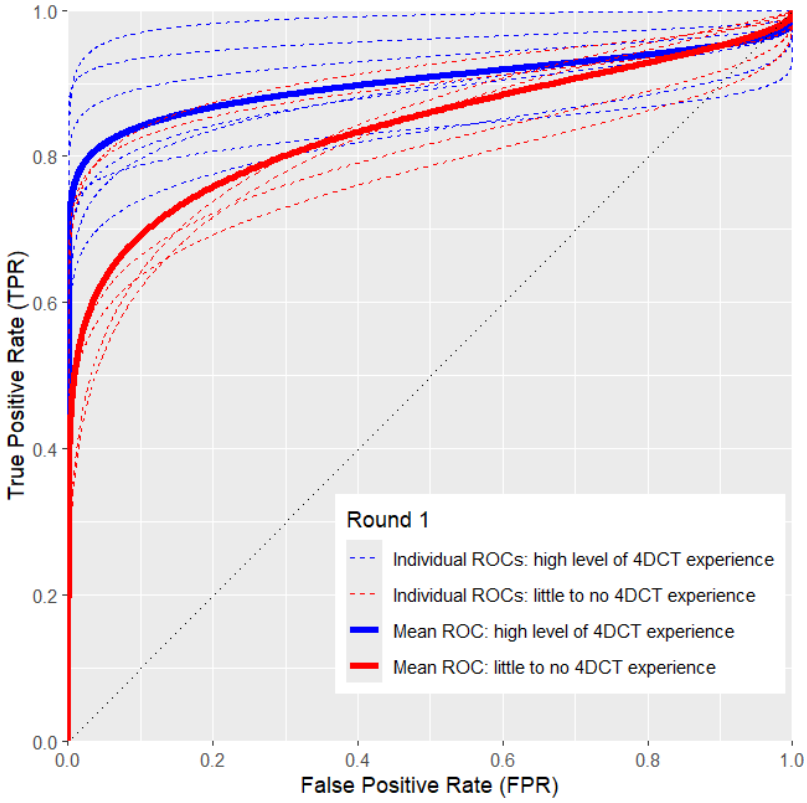

Binormal ROC curves of each radiologist in round 2

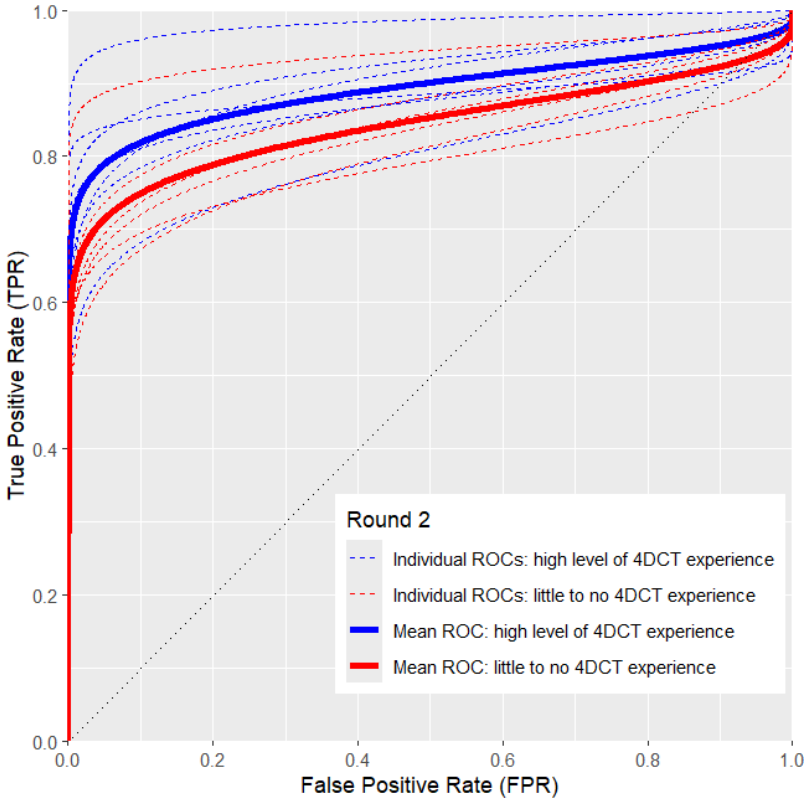

Binormal ROC curves of each radiologist in round 3

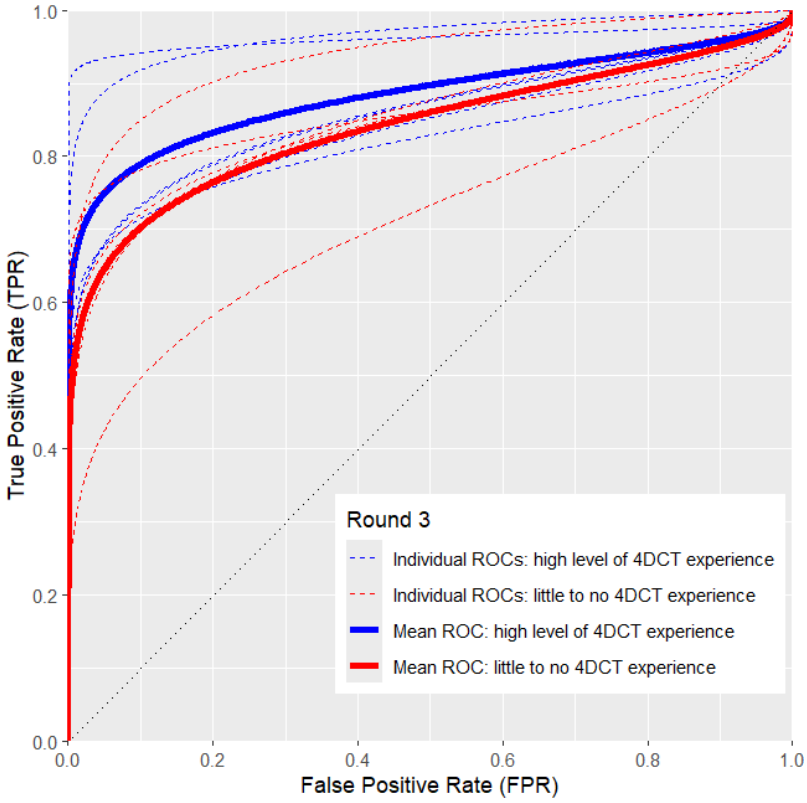

Binormal ROC curves of each radiologist in round 4

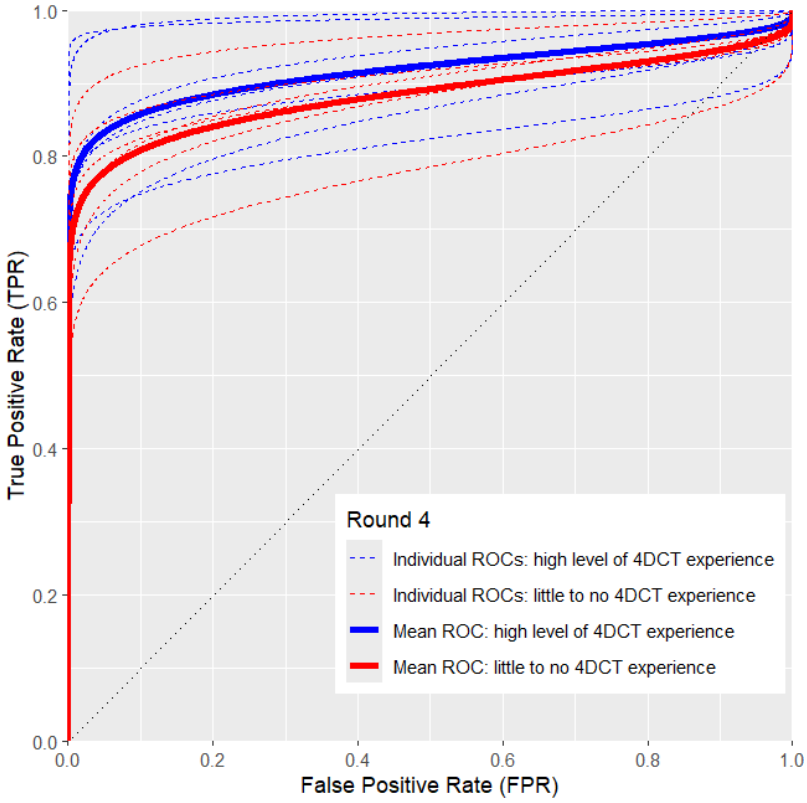

Binormal ROC curves of each radiologist in round 5

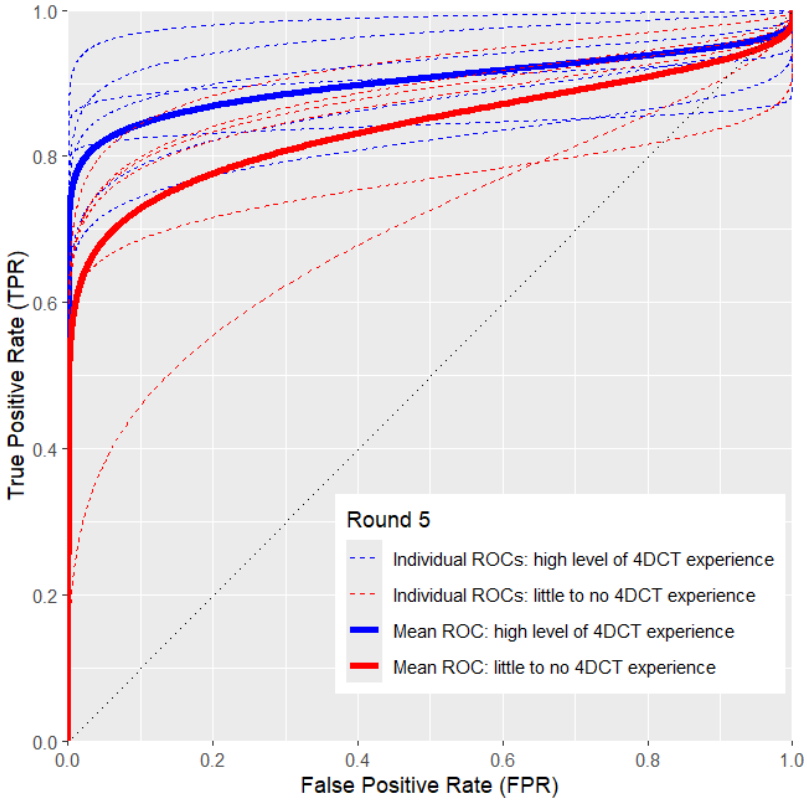

Appendix G

BMI 18.5 – 24.9 BMI 25.0 – 34.9 BMI > 35.0

^{18}F-Choline PET/4DCT

	Scan 1	Scan 2	Scan 3
Protocol 1 (PT01 – PT06)	Normal-dose, non-contrast CT scan (base of skull – mid-liver)	Normal-dose, arterial CT scan (base of skull – carina)	
Protocol 2 (PT07 – PT15)	Low-dose, non-contrast CT scan (base of skull – mid-liver)	Normal-dose, non-contrast CT scan (base of skull – carina)	Normal-dose, arterial CT scan (base of skull – carina)
Protocol 3 (PT16 – PT22)	Low-dose, non-contrast CT scan (base of skull – mid-liver)	Normal-dose, non-contrast CT scan (base of skull – carina)	Normal-dose (dose saving optimised for CTA), arterial CT scan (base of skull – carina)

Non-contrast phase CT scan before PET scan (for PET attenuation correction)

Patient	Gender	BMI	kV	mAs / ref	CTDIvol (mGy)	DLP (mGy*cm)
01	Male	26.9	120	154 / 116	11.77	513.5
02	Female	32.0	120	150 / 116	17.53	780.7
03	Female	23.5	100	115 / 201	5.15	209.4
04	Male	22.2	140	73 / 80	8.57	475.2
05	Female	29.3	140	92 / 80	10.80	531.0
06	Female	28.0	140	119 / 80	13.90	816.3
07	Male	24.9	120	26 / 37	2.03	122.6
08	Female	25.6	120	39 / 37	2.98	154.6
09	Female	26.3	120	37 / 37	2.82	150.8
10	Female	25.7	120	25 / 37	1.97	94.7
11	Male	45.3	140	57 / 26	6.73	359.5
12	Male	28.1	120	50 / 37	3.87	199.1
13	Female	20.5	120	23 / 37	1.78	94.9
14	Female	28.3	140	37 / 26	4.41	181.8
15	Female	28.3	120	37 / 37	2.89	116.2
16	Male	29.6	140	44 / 26	5.13	260.9
17	Male	34.4	140	40 / 26	4.65	219.5
18	Male	21.4	120	37 / 37	2.92	160.9
19	Female	39.0	140	43 / 26	5.04	239.4
20	Female	28.1	120	53 / 37	4.09	203.8
21	Female	32.1	140	45 / 26	5.23	262.6
22	Female	27.8	120	48 / 37	3.71	198.3

Non-contrast phase CT scan after PET scan (for PA localisation)

Patient	Gender	BMI	kV	mAs / ref	CTDIvol (mGy)	DLP (mGy*cm)
07	Male	24.9	120	62 / 116	4.76	105.7
08	Female	25.6	120	67 / 116	5.14	102.1
09	Female	26.3	120	68 / 116	5.20	147.0
10	Female	25.7	120	50 / 116	3.87	107.3
11	Male	45.3	140	120 / 80	14.04	438.5
12	Male	28.1	120	122 / 116	9.30	267.6
13	Female	20.5	100	78 / 201	3.49	101.7
14	Female	28.3	120	127 / 116	9.68	288.5
15	Female	28.3	120	77 / 116	5.87	172.7
16	Male	29.6	140	104 / 80	12.15	425.1
17	Male	34.4	120	134 / 116	10.25	293.5
18	Male	21.4	120	92 / 116	7.01	242.5
19	Female	39.0	140	90 / 80	10.55	337.9
20	Female	28.1	120	83 / 116	6.90	172.4
21	Female	32.1	120	138 / 116	10.53	270.4
22	Female	27.8	120	76 / 116	5.84	148.0

Arterial phase CT scan after PET scan (for PA localisation)

Patient	Gender	BMI	kV	mAs / ref	CTDIvol (mGy)	DLP (mGy*cm)
01	Male	26.9	100	196 / 150	8.75	251.2
02	Female	32.0	100	228 / 150	10.20	254.1
03	Female	23.5	100	140 / 150	6.24	168.0
04	Male	22.2	100	157 / 150	7.02	136.1
05	Female	29.3	100	164 / 150	7.31	198.3
06	Female	28.0	100	190 / 150	8.47	257.9
07	Male	24.9	100	176 / 150	7.86	177.2
08	Female	25.6	100	183 / 150	8.18	163.1
09	Female	26.3	100	180 / 150	8.03	227.4
10	Female	25.7	100	162 / 150	7.23	200.3
11	Male	45.3	120	182 / 116	13.93	430.5
12	Male	28.1	120	151 / 116	11.52	329.1
13	Female	20.5	100	150 / 150	6.71	195.4
14	Female	28.3	120	156 / 116	11.93	351.8
15	Female	28.3	100	190 / 150	8.49	251.9
16	Male	29.6	120	165 / 116	12.63	443.9
17	Male	34.4	100	183 / 125	8.18	234.8
18	Male	21.4	100	165 / 125	7.34	252.4
19	Female	39.0	120	155 / 116	11.83	377.9
20	Female	28.1	100	155 / 125	6.90	188.4
21	Female	32.1	100	188 / 125	8.40	217.5
22	Female	27.8	100	146 / 125	6.53	163.9

Total DLP of ^{18}F-Choline PET/4DCT protocol

Patient	Gender	BMI	Total DLP (mGy*cm)
01	Male	26.9	775
02	Female	32.0	1049
03	Female	23.5	386
04	Male	22.2	621
05	Female	29.3	737
06	Female	28.0	1083
07	Male	24.9	416
08	Female	25.6	425
09	Female	26.3	534
10	Female	25.7	408
11	Male	45.3	1239
12	Male	28.1	804
13	Female	20.5	400
14	Female	28.3	829
15	Female	28.3	550
16	Male	29.6	1142
17	Male	34.4	754
18	Male	21.4	665
19	Female	39.0	960
20	Female	28.1	571
21	Female	32.1	758
22	Female	27.8	517

4DCT

Non-contrast phase CT scan (same applies to the (delayed) venous CT scan)

Patient	Gender	BMI	kV	mAs / ref	CTDIvol (mGy)	DLP (mGy*cm)
01	Female	21.0	120	29 / 83	2.7	92.6
02	Male	23.0	120	39 / 83	3.6	133.1
03	Female	24.6	120	33 / 83	3.0	100.7
04	Female	25.3	120	41 / 83	3.8	129.4
05	Male	33.5	120	69 / 83	6.4	203.3
06	Female	29.2	120	43 / 83	4.0	139.5
07	Male	21.9	120	36 / 83	3.3	92.9
08	Female	22.0	120	35 / 83	3.2	86.8
09	Female	21.0	120	30 / 83	2.8	96.9
10	Female	36.5	120	70 / 83	6.5	212.9
11	Female	26.7	120	42 / 83	3.9	110.9
12	Female	26.0	120	38 / 83	3.5	123.9
13	Female	22.5	120	37 / 83	2.9	97.8
14	Female	27.7	120	47 / 83	3.6	112.0
15	Female	20.0	120	48 / 83	3.6	125.0
16	Female	46.4	120	89 / 83	6.8	210.0
17	Female	28.7	120	39 / 83	3.0	108.0
18	Female	21.1	120	31 / 83	2.4	86.2
19	Female	28.3	120	44 / 83	3.4	120.0
20	Female	34.6	120	61 / 83	4.7	135.0
21	Female	22.1	120	29 / 83	2.2	78.1
22	Female	20.3	120	29 / 83	2.3	72.0
23	Female	24.2	120	37 / 83	2.8	103.0
24	Female	22.2	120	34 / 83	2.6	88.7
25	Male	33.8	120	70 / 83	5.4	191.0
26	Male	24.7	120	45 / 83	3.6	110.0
27	Female	29.3	120	49 / 83	3.8	118.0
28	Female	26.1	120	39 / 83	3.1	123.0
29	Female	18.9	120	27 / 83	2.1	72.1
30	Female	26.7	120	34 / 83	2.7	91.4

Arterial phase CT scan

Patient	Gender	BMI	kV	mAs / ref	CTDIvol (mGy)	DLP (mGy*cm)
01	Female	21.0	120	19 / 53	1.7	58.3
02	Male	23.0	120	25 / 53	2.3	85.0
03	Female	24.6	120	21 / 53	1.9	63.8
04	Female	25.3	120	26 / 53	2.4	81.7
05	Male	33.5	120	45 / 53	4.1	135.4
06	Female	29.2	120	27 / 53	2.5	87.2
07	Male	21.9	120	23 / 53	2.1	59.1
08	Female	22.0	120	22 / 53	2.1	56.9
09	Female	21.0	120	19 / 53	1.8	62.3
10	Female	36.5	120	44 / 53	4.2	140.0
11	Female	26.7	120	27 / 53	2.5	71.1
12	Female	26.0	120	24 / 53	2.2	77.9
13	Female	22.5	120	23 / 53	1.8	60.7
14	Female	27.7	120	30 / 53	2.3	71.5
15	Female	20.0	120	31 / 53	2.3	80.2
16	Female	46.4	120	56 / 53	4.4	139.0
17	Female	28.7	120	26 / 53	2.0	75.3
18	Female	21.1	120	20 / 53	1.5	53.9
19	Female	28.3	120	28 / 53	2.2	77.7
20	Female	34.6	120	39 / 53	3.0	86.4
21	Female	22.1	120	18 / 53	1.4	49.7
22	Female	20.3	120	19 / 53	1.5	48.2
23	Female	24.2	120	23 / 53	1.8	66.5
24	Female	22.2	120	22 / 53	1.7	58.0
25	Male	33.8	120	44 / 53	3.4	121.0
26	Male	24.7	120	29 / 53	2.3	70.3
27	Female	29.3	120	31 / 53	2.5	77.7
28	Female	26.1	120	25 / 53	1.9	75.5
29	Female	18.9	120	17 / 53	1.3	44.6
30	Female	26.7	120	22 / 53	1.7	57.6

Total DLP of 4DCT protocol

Patient	Gender	BMI	Total DLP (mGy*cm)
01	Female	21.0	366
02	Male	23.0	511
03	Female	24.6	396
04	Female	25.3	493
05	Male	33.5	788
06	Female	29.2	529
07	Male	21.9	360
08	Female	22.0	335
09	Female	21.0	375
10	Female	36.5	793
11	Female	26.7	429
12	Female	26.0	469
13	Female	22.5	371
14	Female	27.7	437
15	Female	20.0	468
16	Female	46.4	790
17	Female	28.7	437
18	Female	21.1	326
19	Female	28.3	454
20	Female	34.6	507
21	Female	22.1	299
22	Female	20.3	289
23	Female	24.2	394
24	Female	22.2	349
25	Male	33.8	721
26	Male	24.7	428
27	Female	29.3	451
28	Female	26.1	468
29	Female	18.9	277
30	Female	26.7	361

^{18}F-Choline PET/CT

Non-contrast CT scan before PET scan

Patient	Gender	BMI	kV	mAs / ref	CTDIvol (mGy)	DLP (mGy*cm)
01	Female	27.5	120	37 / 58	2.8	151.9
02	Female	23.7	120	38 / 58	2.9	141.7
03	Female	23.3	120	35 / 58	2.7	129.9
04	Female	21.3	120	32 / 58	2.5	118.3
05	Female	30.9	140	45 / 40	5.3	216.1
06	Male	26.3	120	53 / 58	4.1	189.0
07	Female	30.5	120	58 / 58	4.4	170.2
08	Female	30.1	140	49 / 40	5.8	281.0
09	Female	23.2	120	42 / 58	3.2	137.9
10	Female	20.7	120	35 / 58	2.7	144.0
11	Female	26.1	120	52 / 58	4.0	213.5
12	Female	24.6	120	50 / 58	3.9	159.7
13	Male	28.2	140	45 / 40	5.3	281.8
14	Female	37.0	140	50 / 40	5.9	271.0
15	Male	29.7	140	51 / 40	6.0	280.7
16	Male	27.1	120	58 / 58	4.4	233.8
17	Female	45.4	140	75 / 40	8.8	424.2
18	Male	28.8	140	44 / 40	5.2	237.7
19	Female	26.0	120	66 / 58	5.0	241.3
20	Male	24.3	120	48 / 58	3.7	198.2
21	Female	30.8	140	40 / 40	4.7	219.2
22	Female	34.7	140	78 / 40	9.1	351.2
23	Female	30.6	140	52 / 40	6.2	247.4
24	Female	37.2	140	72 / 40	8.4	343.0
25	Female	23.6	120	45 / 58	3.5	151.9
26	Female	31.4	140	48 / 40	5.7	205.7
27	Male	27.7	140	65 / 40	7.6	400.9
28	Female	22.5	120	39 / 58	3.0	101.4
29	Female	45.7	140	66 / 40	7.8	352.4
30	Female	32.0	140	40 / 40	4.7	193.8

UNIVERSITY OF TWENTE.

Rijnstate